TECHNICAL MEMORANDUM

288

The importance of the Earth Radiation Mission for numerical weather prediction

J-F. Mahfouf, A. Beljaars, F. Chevallier,
D. Gregory, C. Jokob, M. Janisková,
J-J. Morcrette, T. Teixeira and P. Viterbo

Research Department

September 1999

European Centre for Medium-Range Weather Forecasts
Europäisches Zentrum für mittelfristige Wettervorhersage
Centre européen pour les prévisions météorologiques à moyen

Contents

Abstract

This reports presents a number of results from the ECMWF forecasting system showing that satellite data from the Earth Radiation Mission should be useful for improving the quality of operational forecasts. Information on vertical profiles of cloud cover together with radiation fluxes and hydrometeors concentrations (particularly on ice contents) should lead to a better representation of the sub-grid scale processes describing cloud-radiation interactions in the forecast model. It is shown that the ECMWF 4D-Var assimilation is in principle capable of including any type of observation provided observation operators are defined. Developments required to assimilate satellite data from the Earth Radiation Mission are explained.

1 Introduction

Clouds are known to play a major role in the water and energy budgets of the Earth's atmosphere. Their description in General Circulation Models (GCMs) remains difficult because they encompass a broad spectrum of scales from very small ones describing microphysical processes to planetary scales describing cloud organization in large systems (frontal bands, ITCZ, easterly waves, ...). GCMs can explicitly describe atmospheric motions having horizontal scales larger than few hundred of kilometers. Therefore, important physical processes describing the formation and dissipation of clouds cannot be explicitly resolved by global numerical models. These processes are implicitly accounted for through *parametrization* schemes, which represent the effects of sub-grid scale processes on resolved model scales. The parametrization of sub-grid scale processes is a key issue of both climate and Numerical Weather Prediction (NWP) models. The reason is that they describe phenomena that are not properly sampled by conventional observations. As a consequence, they are not sufficiently understood to be accurately modelled.

During the last decade the parametrization of clouds in climate GCMs has greatly improved (Heise and Roekner,1990 ; Ricard and Royer, 1993; Fowler et al., 1996). Such effort was stimulated by the fact that the response of GCMs to climate changes is extremely sensitive to cloud description. This has been demonstrated in various intercomparison studies (Cess et al., 1990; Cess et al., 1996) and recognized by the Intergovernemental Panel on Climatic Change (Houghton et al., 1995). Both cloud type, fractional coverage and optical properties play a role in determining feedback mechanisms that will amplify or reduce an initial external radiative forcing (Senior and Mitchell, 1993). Early descriptions of clouds using empirical dependencies with relative humidity and other quantities (Slingo, 1987) are now progressively replaced by prognostic cloud schemes. The emergence of such schemes has been made possible by the availability of new data sets from field experiments, satellite observations and also from cloud resolving models.

The Earth Radiation Mission (ERM) is one of the Earth Explorer Missions candidates proposed by ESA (Ingmann, 1997). The main objective of ERM is to document the vertical structure of cloud and aerosol fields over all climatic zones together with the components of the radiation budget at the top of the atmosphere. From ERM measurements, geophysical parameters should be derived such as vertical profiles of cloud ice water content, cloud liquid water content and aerosol optical thickness.

Instruments embarked on ERM will include :

- a broadband radiometer to provide measurements of the shortwave (0.2 to 4.0 μm) and longwave (4.0 to 50 μm) radiances at the top of the atmosphere. The instantaneous field of view should be 50 x 50 km^2.
- a cloud profiling radar to provide backscattered signals of the atmosphere along track. The instrument should allow the detection or retrieval of cloud tops, cloud bases and

vertical distribution of thick clouds. The footprint diameter will be less than 1 km and the vertical sampling interval about 250 m.

- a backscattered lidar to detect cloud top and cloud base of thin clouds and aerosol layers, and derive cloud optical depth. The footprint will be less than 200 m and the vertical sampling interval about 100 m.

- a visible/infrared imager to validate the representativity of measured cloud fields by active instruments. The field of view should be about 100 km.

Measurements from the Earth Radiation Mission should help to define methodologies for achieving improvements in the description of cloud-radiation interactions both for climate models and for NWP models. NWP models aim at providing a description of the atmospheric fluid over periods of time ranging from a few hours to 10 days or more, starting from the best possible knowledge of the present state of the atmosphere. The initial state of NWP models, the *analysis*, is obtained by combining in an optimal way all the possible sources of information on the atmosphere (observations of various types, climatology, atmospheric equilibriums, short-range forecasts) into a consistent picture. This complex process is achieved within a *data assimilation system* maintained and developed by the main operational weather centres such as ECMWF.

Currently, operational data assimilation systems only include conventional and satellite observations of pressure, temperature, wind and water vapour. They do not explicitly include any quantity related to the condensed phase of water (cloud water, cloud ice, rain, ...). Cloud properties given as a by-product of operational analyses are currently the only way to obtain a tri-dimensional coherent description. The strong coupling between clouds and dynamical processes (explicitly described for the large scales by data assimilation systems) and recent improvements in the description of cloud processes in the ECMWF model (Tiedtke, 1993) have demonstrated significant skill in analysis and forecast products when compared to radar and lidar observations from field experiments (Mace et al., 1998; Miller et al., 1999). Data from ERM should provide a unique set of observations that could be used for improving the quality of operational products in various ways. A better description of cloud-radiation interactions will lead to improved forecasts in the medium-range (two-metre temperature, cloudiness, precipitation, ...) and also to a more reliable seasonal forecasting system since the ocean-atmosphere coupling in the tropics is strongly driven by the energy and water fluxes between the two systems. The inclusion of cloud observations in the ECMWF data assimilation system should lead to an improved initial state of the prognostic variables of the cloud scheme and also of the dynamical and thermodynamical variables linked to the generation and dissipation of clouds.

In this report some evidence on the importance of ERM for NWP is described.

The description of cloud and radiation parametrizations in the ECMWF model are summarized in Section 2. Large uncertainties concern the description of optical properties for ice particules as well as the associated microphysics. Quantitative information on ice water content for various types of clouds could help to reduce the level of uncertainty on the ice phase in the ECMWF

model.

The new data assimilation system known as 4D-Var (four-dimensional variational) and implemented at ECMWF in November 1997 is described in Section 3. This data assimilation system is flexible enough to allow the inclusion of new types of observations. Some work has already started at ECMWF to assimilate rainfall rate products from the Tropical Rainfall Measuring Mission (Mahfouf et al., 1998).

Section 4 explains that the assimilation of cloud properties and top of atmosphere fluxes requires the development of linearized versions of a radiative transfer model and of a cloud scheme. These linearized operators are required to get model counterparts of observations in order to solve the minimization problem of 4D-Var. Preliminary results in clear-sky conditions are presented with a one-column version of the ECMWF model to demonstrate the usefulness of a linearized radiative transfer model for the assimilation of longwave fluxes. The validity of the tangent-linear approximation for the radiative transfer model is also examined in the presence of cloud cover.

The importance of data sets providing information on the vertical structure of clouds is emphasized through various field experiments (LITE, ARM,...) where the ECMWF model has shown skill in simulating the observations but also where some weaknesses in the representation of clouds have been identified (Section 5). In this section standard evaluations of cloudiness and TOA radiation budget using ISCCP and ERBE satellite climatologies are presented. The incomplete picture they provide demonstrates the necessity of a synergy between instruments measuring TOA radiative fluxes and cloud properties. For example, the agreement of model radiative fluxes should not compensate for an incorrect specification of cloud cover or of cloud water/ice path. A more detailled evaluation of the performance of the cloud and radiation schemes is undertaken using ISCCP data and simple weather regimes classifications.

Currently, the vertical structure of observed global cloud distribution is only known very crudely through three main layers derived from ISCCP satellite data. How cloud overlap in the vertical is of crucial importance for a number of physical processes such as radiative fluxes, evaporation of rainfall or ice sedimentation. Various sensitivity studies are presented in Section 6 to both cloud overlap assumption and ice sedimentation on the climate simulated by the ECMWF model. Finally, the influence of analyses and forecasts to the initialisation of cloud variables is examined over a one-week assimilation of 4D-Var.

2 Cloud and radiation processes in the ECMWF forecast model

2.1 The radiation scheme

2.1.1 General features

The radiation scheme solves the radiative transfer equation in two distinct spectral regions. The longwave (LW) spectrum from 0 to 2820 cm^{-1} is divided into six spectral regions and the integration over wavenumber is performed using a band emissivity method (Morcrette, 1990). The transmission functions for water vapour and carbon dioxide over the six spectral intervals of the scheme are fitted using Padé approximants on narrow-band transmissions obtained with statistical band models (Morcrette et al., 1986).

The shortwave (SW) part of the scheme integrates the fluxes over the whole shortwave spectrum between 0.2 and 4.0 μm. It uses the photon path distribution method to separate the parametrization of scattering processes from that of molecular absorption. To perform the spectral integration, it is convenient to discretize the solar spectral interval into subintervals in which the surface reflectance can be considered as constant. Since the main cause of important spectral variation of the surface albedo is the sharp increase of reflectivity of the vegetation in the near-infrared, and since water vapour does not absorb below 0.68 μm, the shortwave scheme considers two spectral intervals, one for the visible (0.2-0.68 μm), one for the near-infrared (0.68-4.0 μm) parts of the spectrum.

To save time in the rather expensive radiation computations, the full radiation part of the scheme is currently called every three hours in the operational ECMWF forecast model (Morcrette, 1999). Shortwave transmissivities and longwave fluxes are computed using values of temperature, specific humidity, liquid/ice water and cloud fraction. The computation of the fluxes is not done at every-grid point but is performed at sample points, using a sampling algorithm that is latitude dependent. The results are then interpolated back to the original grid using a cubic interpolation algorithm. The shortwave fluxes are updated every time-step using current values of the solar zenith angle.

2.1.2 The incorporation of clouds

The incorporation of the effects of clouds on the longwave fluxes follows the treatment discussed by Washington and Williamson (1977). The scheme calculates first upward and downward fluxes corresponding to a clear-sky atmosphere : $F_0^{\uparrow}(i)$ and $F_0^{\downarrow}(i)$. The scheme then evaluates in any cloudy layer the fluxes assuming a unique overcast cloud of emissivity unity : $F_n^{\uparrow}(i)$ and

$F_n^{\downarrow}(i)$ (for a cloud present in the nth layer of the atmosphere). Then, the fluxes for the actual atmosphere are derived from a linear combination of the fluxes calculated in the previous steps with some cloud overlap assumption in the case of cloud present in several layers. Let N be the number of model layers, C_i the fractional cloud cover in layer i, the cloudy upward $F^{\uparrow}$ and downward $F^{\downarrow}$ fluxes are expressed as:

$$F^{\uparrow}(z_i) = (1 - CC_{i,0})F_0^{\uparrow}(z_i) + \sum_{k=1}^{i}(CC_{i,k-1} - CC_{i,k})F_k^{\uparrow}(z_i) \tag{1}$$

$$F^{\downarrow}(z_i) = (1 - CC_{i,0})F_0^{\downarrow}(z_i) + \sum_{k=i}^{N-1}(CC_{i,k+1} - CC_{i,k})F_k^{\downarrow}(z_i) \tag{2}$$

where $CC_{i,j}$ is the cloudiness encountered between any two levels i and j in the atmosphere expressed using a maximum-random cloud overlap assumption as follows :

$$CC_{i,j} = 1 - \prod_{k=1}^{j-1}\left[\frac{1 - \max(C_k, C_{k-1})}{1 - C_{k-1}}\right] \tag{3}$$

In the case of semi-transparent clouds, the fractional cloudiness entering the calculations is an effective cloud cover equal to the product of the emissivity due to the condensed water and the gases in the layer by the horizontal coverage of the cloud cover, with the emissivity, ε_{cld}, related to the condensed water amount by:

$$\varepsilon_{cld} = 1 - \exp(-K_{abs}u_{LWP}) \tag{4}$$

where K_{abs} is the condensed water mass absorption coefficient following Ebert and Curry (1992) and u_{LWP} the condensed water path. K_{abs} depends upon the water phase (ice or water) and upon temperature. A spectral dependency can also be included.

In the shortwave part of the spectrum, reflectance at the top and transmittance at the bottom of a cloudy layer are calculated with the Delta-Eddington approximation. These two quantities are calculated as functions of the total optical thickness δ, the total single scattering albedo ω and the total asymmetry factor g. These optical properties for clouds are derived from Fouquart (1987) and Ebert and Curry (1992). δ is related to the cloud liquid/ice water amount u_{LWP} by :

$$\delta = u_{LWP}\left(a_i + \frac{b_i}{r_e}\right) \tag{5}$$

where a_i and b_i are defined from Ebert and Curry (1992) for ice particles and are set to respectively 0 and 3/2 for water particles. The mean effective radius of the size distribution of the cloud water droplets is defined by r_e. For water clouds, r_e is set to 13 μm over oceans and to 10 μm over continents. When ice cloud optical properties were initially introduced in the radiation code, the effective radius was set to 40 μm. However, observations indicate that the effective radius of ice crystals increases with temperature, usually attributed to accretion from falling crystals. In the current scheme, account is taken of this by using the diagnostic formulation of Ou and Liou (1995):

$$r_e = 326.3 + 12.42 \times T_i + 0.197 \times T_i^2 + 0.0012 \times T_i^3 \tag{6}$$

where $T_i = \min(T, -23°C)$.

In the two spectral intervals of the shortwave scheme, the asymmetry factor g_c is fixed to 0.865 and 0.910, repectively and ω_c is given as a function of δ_c following Fouquart (1987):

$$\omega_{c1} = 0.9999 - 5 \times 10^{-4} \exp(-0.5\delta_c) \tag{7}$$

$$\omega_{c2} = 0.9988 - 2.5 \times 10^{-3} \exp(-0.05\delta_c) \tag{8}$$

These cloud shortwave radiative parameters have been fitted to in-situ measurements of stratocumulus clouds (Bonnel et al., 1983).

The optical properties of ice clouds are expressed as:

$$\omega_i = c_i - d_i r_e \tag{9}$$

$$g_i = e_i + f_i r_e \tag{10}$$

where the coefficients are derived from Ebert and Curry (1992).

Considering an atmosphere where a fraction C_{tot} (as seen from the surface or the top of the atmosphere) is covered by clouds (the fraction C_{tot} depends on which cloud-overlap assumption is assumed for the calculations), the final fluxes are given as weighted average of the fluxes in the clear sky and in the cloudy fractions of the column.

2.2 The prognostic cloud scheme

The ECMWF prognostic cloud scheme developed by Tiedtke (1993) has been put in the operational model in April 1995. This scheme includes prognostic equations for cloud fraction and liquid/ice water content and has been shown to provide a much more realistic description of the cloud cover than the previous diagnostic scheme described by Slingo (1987). The inclusion of cloud fraction as a prognostic variable is an original feature of this scheme since most of the prognostic cloud schemes treat cloud fraction by means of diagnostic relations (e.g. Sundqvist, 1988, Smith,1990).

The prognostic scheme consists of two prognostic equations, one for liquid/ice water l and one for cloud fraction a:

$$\frac{\partial l}{\partial t} = A(l) + S^l_{conv} + S^l_{bl} + C^l - E - P - D_{entr} \tag{11}$$

$$\frac{\partial a}{\partial t} = A(a) + S^a_{conv} + S^a_{bl} + C^a - D_{evap} \tag{12}$$

where $A(l)$ and $A(a)$ represent the advection of liquid/ice water and cloud fraction, S^l_{conv} and S^a_{conv} represent the source terms of liquid/ice water and cloud fraction from moist convection

processes, S_{bl}^{l} and S_{bl}^{a} represent the source terms of liquid/ice water and cloud fraction due to boundary layer turbulence, C^{l} and C^{a} are the formation of liquid/ice water and cloud fraction by stratiform condensation processes, E is the evaporation rate, P is the precipitation rate, D_{entr} is the destruction of liquid/ice water due to cloud top entrainment and D_{evap} is the reduction of cloud fraction by evaporation. Figure 1 summarizes the various contributions to the production and destruction of cloud fraction and cloud condensate.

The prognostic cloud scheme allows the ice and liquid water to co-exist (mixed phase) based on a simple quadratic temperature dependence between 0°C and -23°C (see Jakob, 1995).

This scheme accounts explicitly for the physical sources and sinks leading to the production and dissipation of clouds. It is therefore strongly coupled to the other physical parametrizations described in the ECMWF model (radiation, turbulence, deep and shallow convection). Clouds formed by convective processes are parametrized by considering them to be condensates produced by cumulus updrafts and detrained in the environmental air. Clouds are also assumed to be formed by non-convective processes (e.g. large-scale lifting of moist air, radiative cooling, etc). Evaporation of clouds is described by two processes in connection with large-scale and cumulus-induced descent and diabatic heating and by turbulent mixing of cloud air with unsaturated environmental air. Precipitation processes are represented differently for pure ice clouds and for mixed phase and pure water clouds. The rain and snow formed are removed from the atmospheric column immediately but can evaporate and interact with the cloud water in the layers it passes through. The precipitation process in ice clouds is treated as a sedimentation of the ice particles with a terminal fall speed of :

$$w_{ice} = 3.29(\rho l/a)^{0.16} \tag{13}$$

based on Heymsfield and Donner (1990), where ρ is the air density.

The precipitation from pure ice can then be written as:

$$P = \frac{1}{\rho}\frac{\partial}{\partial z}(\rho w_{ice} l) \tag{14}$$

Ice settling into cloudy areas is treated as source for cloud ice in the layer below, whereas ice settling into clear-sky is converted into snowfall. For mixed phase and pure water clouds a parametrization describing the conversion of cloud droplets into raindrops is taken from Sundqvist (1978). It represents both the collision process and the Bergeron-Findeisen mechanism. Evaporation of rain/snow is described by a scheme following Kessler (1969) and only takes place when the grid mean relative humidity is below a threshold value.

3 The ECMWF 4D-Var data assimilation system

The general problem of assimilation of observations in NWP consists in defining the initial conditions of a forecast model using all the available information on the atmospheric state in

an optimal way. Since November 1997 the operational data assimilation system at ECMWF is a four-dimensional variational (4D-Var) system.

3.1 General formalism

4D-Var seeks an optimal balance between observations and the dynamics of the atmosphere by finding a model trajectory $x(t)$ which is as close as possible, in a least-square sense, to the observations available during a given time period $[t_0,\ t_n]$. The model trajectory $x(t)$ is completely defined by the initial state x_0 at time t_0.

The misfit to given observations y^o and to an *a-priori* model state x^b called background and usually provided by a short-range forecast is measured by an objective cost-function defined as follows:

$$J(x_0) = \frac{1}{2}(x_0 - x_0^b)^T \mathbf{B}^{-1}(x_0 - x_0^b) + \frac{1}{2}\sum_{i=0}^{n}(H_i[x(t_i)] - y_i^0)^T \mathbf{R_i}^{-1}(H_i[x(t_i)] - y_i^0) \qquad (15)$$

where at any time t_i, y_i^0 is the vector of observations, H_i is the operator providing the equivalent of the data from the model variable $x(t_i)$, $\mathbf{R_i}$ the observation error covariance matrix (including measurement and representativeness errors), and $\mathbf{B}$ the background error covariance matrix of the state x^b. The *observation operator* H_i describes the spatial interpolations to the observation locations, the calculation of the observation variables (for example, a radiative transfer model is used to compute radiances) and also the action of the forecast model to propagate the initial state x_0 to the time of observation. The background information valid at time t_0 summarizes all information used before that time. Superscripts -1 and T denote respectively matrix inverse and transpose. The subscript i denotes the time index.

The model state $x(t_i)$ is defined as :

$$x(t_i) = M(t_i, t_0)[x_0] \qquad (16)$$

where M is the non-linear forecast model integrated from time t_0 to time t_i. The control vector x_0 includes the prognostic variables to be initialised in the forecast model : vorticity, divergence, temperature, specific humidity and surface pressure. The prognostic cloud variables previously defined are not yet part of the control vector (more will be said about the initialisation of these quantities in the next chapter). The minimization of the cost-function J is performed in spectral space, since it allows an easier specification of the balance constraints between wind and mass imposed in the background error covariance matrix (Bouttier et al., 1997). The minimization uses a descent algorithm which requires several computations of the gradient of J with respect to the initial state x_0. Given the dimension of the state vector the adjoint technique is used to provide an efficient estimate of ∇J (Le Dimet and Talagrand, 1986) :

$$\nabla J(x_0) = \mathbf{B}^{-1}(x_0 - x_0^b) + \sum_{i=0}^{n} \mathbf{H_i^T R_i}^{-1}(H_i[x(t_i)] - y_i^0) \qquad (17)$$

The numerical coding of the transpose of tangent-linear versions of both the forecast model and of the observation operators $\mathbf{H_i}$ is required for such an efficient computation. Moreover the trajectory of the non-linear model around which the linearization is performed needs to be stored.

3.2 The incremental approach

The current operational model describes the state of the atmosphere in spectral space up to the wavenumber 319 corresponding to a physical resolution of about 60 km and the vertical is discretized in 50 layers. As a consequence the dimension of the control variable (about 10^7) is such that the full 4D-Var problem cannot be solved on present-day computers. Moreover only part of the forecast model has been linearized (the dynamics and a set of simplified physical parametrizations). Courtier et al. (1994) have proposed an incremental approach in order to reduce significantly the computational cost of 4D-Var. The incremental 4D-Var consists of computing the background trajectory and the departures (observations minus model) using the full non-linear model at high resolution including a full set of physical parametrizations, and minimizing the cost-function in a low resolution space for the increments at initial time using a tangent-linear model $\mathbf{M}$ and its adjoint with a limited set of physical parametrizations.

Writing:

$$x_0 = x_0^b + \delta x_0 \tag{18}$$

and

$$H_i[x(t_i)] = H_i[x^b(t_i)] + \mathbf{H_i}\delta x(t_i) \tag{19}$$

with $\mathbf{H_i}$ the linearization of the observation operator H_i in the vicinity of the background x^b and :

$$\delta x(t_i) = \mathbf{M}(t_i, t_0)[\delta x_0] \tag{20}$$

the new cost-function becomes:

$$J(\delta x) = \frac{1}{2}(\delta x_0)^T \mathbf{B}^{-1}(\delta x_0) + \frac{1}{2}\sum_{i=0}^{n}(\mathbf{H_i}\delta x(t_i) - d_i)^T \mathbf{R_i}^{-1}(\mathbf{H_i}\delta x(t_i) - d_i) \tag{21}$$

where $d_i = y_i^o - H_i[x^b(t_i)]$ the innovation vector.

The optimum δx^a is added to the background x^b in order to provide the analysis x^a:

$$x^a = x^b + \delta x^a \tag{22}$$

It is possible to take into account the non-linearities introduced by the physical processes by updating iteratively the trajectory in the vicinity of which the model is linearized. In the current ECMWF operational 4D-Var the increments are computed at T63 resolution (about 200 km) and two external updates of the trajectory are performed (Rabier et al., 1999). The first inner-loop minimization is performed through 50 iterations with an adiabatic tangent-linear

model. The second minimization consists of 20 iterations with a set of linear physical processes (Mahfouf and Rabier, 1999). The time window of the observations is currently 6 hours but it should be extended in the near future to 12 and 24 hours. The development of the adjoint of the semi-lagrangian integration scheme will allow very soon to compute higher resolution increments at a reasonable computing cost. In two-years, increments should be computed at 80 km (T_L255) resolution with a non-linear trajectory computed at 40 km (T_L511).

4 Towards the assimilation of cloud and radiation observations

4.1 Results from an empirical approach

The variational approach, as developed in the previous section, is not straightforward for the assimilation of cloud properties in NWP models. A much simpler assimilation would consist in setting cloud model variables equal to observed values in the vicinity of available observations, and to the previous forecast otherwise. This approach has been tested for cloud cover observations using a single-column version of the ECMWF model.

The context of this test is the Atmospheric Radiation Measurement (ARM) program to be more extensively developed in the next sections. For the present study, three selected days of ECMWF short-range forecasts (from 20/09/1997 onwards) over the ARM North Central Oklahoma site have been compared with cloud cover measurements derived from millimetric radar observations by Mace et al. (1998). Figure 2 shows cloud cover estimations from both the radar and the model. They agree in the general shape of the cloudiness, even though the cloud top and base may vary by a few atmospheric layers from one estimation to the other.

The assimilation experiment conducted here consists in adding cloud layers where the radar detects one that has not been forecasted, and to suppress cloud layers where forecasted cloud layers are not confirmed by the radar. Cloud amounts added in the model layers are set to the radar-derived value. The corresponding liquid and ice water contents are prescribed from the temperature and water vapour contents as in the previous ECMWF diagnostic cloud scheme (Morcrette, 1990).

As shown on Figure 3, this crude assimilation of cloud cover observations allows a better fit of the model short-range forecast to the surface downward SW flux observations (also performed on the ARM site). On the other hand, the comparison with surface downward LW flux observations brings ambiguous results, with a better agreement of the analysis in some cases, and a worse one in other cases (Figure 4). As a conclusion, modifying the cloud cover without changing other atmospheric variables appears rather incomplete. Observations of other cloud variables, like liquid and ice water contents, are also needed. A variational approach allows a consistency in

the analysis between the variables that are observed and the ones that are not (like temperature here). The first steps towards the development of a variational assimilation of cloudiness at ECMWF are described in the following sections.

4.2 Development of linear physical parameterizations

The variational approach has been exposed in section 3. In order to enable the assimilation of cloud properties derived from the Earth Radiation Mission, important adaptations and improvements to the current 4D-Var system are required. Linearized versions of physical parametrization schemes need to describe the main aspects of cloud processes and of their interactions with other processes. They should be included in the tangent-linear model $\mathbf{M}$ (Equation 20) for the propagation in time of analysis increments and in its adjoint version $\mathbf{M}^{\mathbf{T}}$ for the estimation of the gradient of the cost-function. However, such linearization is not straightforward. since the on/off nature of clouds can make the tangent-linear approximation questionable. Janisková et al. (1999) reported results on the linearization of a simple diagnostic cloud scheme for use in a global atmospheric model. They noticed important noise in the solution due to the presence of thresholds in the cloud scheme and decided for their study to neglect perturbations in cloud cover. More encouraging results were obtained at smaller scale where linearized versions of cloud resolving models have been developed with some success for radar retrievals applications (Verlinde and Cotton, 1993; Park and Droegemeier, 1997). The development of linearized observation operators ($\mathbf{H_i}$ in Equation 17) including cloud description are needed in order to compare the satellite products with model counterparts. Satellite radiances from polar orbiting satellites (TOVS-SSM/I) are already assimilated in the operational 4D-Var system but they are either decontaminated from clouds (Level 1b) or rejected when clouds are detected (Level 1c). Therefore these data only provide information on atmospheric temperature and water vapour vertical profiles.

In the following (sections 4.2.1, 4.2.2 and 4.2.3), various ideas on these matters are proposed, both for the cloud processes and for the radiation processes. They will be explored more extensively during the course of the project.

4.2.1 The cloud scheme

The use of a prognostic cloud scheme poses the problem of the initialisation of cloud fraction and cloud condensate. The need for an explicit initialisation of these quantities has to be assessed. Indeed it poses difficulties for the inclusion grid-point control variables in the current 4D-Var system, and for the specification of statistics of background errors. If the response of cloud variables to dynamical and physical forcings is fast enough (less than 6 hours), it may be possible to develop a diagnostic approach in which cloud variables will be modified by an adjustment of the control variables in the minimization problem (e.g. temperature, humidity,

vertical velocity, ...).

Some simplifications of the prognostic cloud scheme are possible in order to get a diagnostic relation for cloud fraction. Teixeira (1998) has shown that for boundary layer clouds in the trades, the cloud fraction prognostic equation presented above is dominated by two terms:

$$\frac{\partial a}{\partial t} = \frac{D_u}{\rho}(1-a) - \frac{a^2}{l}K(q-q_s) \tag{23}$$

where a is the cloud fraction, D_u is the detrainment rate, l is the liquid water, q is the specific humidity, q_s is the saturation specific humidity, ρ is the air density and K is an erosion coefficient. The first term on the right hand side represents the production of clouds by detrainment from shallow convection and the second term represents the erosion of cloud by turbulent mixing with the environment.

It was verified that in some typical shallow convective regimes the two terms on the right hand side of Equation (23)are of similar magnitude and the cloud fraction tendency is small compared to them. In this case we get an equilibrium solution:

$$\frac{D_u}{\rho}(1-a) - \frac{a^2}{l}Kq_s(1-RH) = 0 \tag{24}$$

where RH is the relative humidity. This equation can be seen as a quadratic equation in the unknown a. Solving it (and neglecting one of the roots) a diagnostic relation gives a as a function of RH, l, q_s and D_u:

$$a = \frac{D_u l}{2\rho K q_s(1-RH)}\left(-1+\sqrt{1+\frac{4\rho K q_s(1-RH)}{D_u l}}\right) \tag{25}$$

Teixeira (1998) has shown that the behaviour of the cloud fraction as function of RH for fixed values of D_u and q_s/l can reproduce some of the main properties found in Saito and Baba (1988) and Walcek (1994).

4.2.2 Generalities on the shortwave and the longwave radiation schemes

Even though some saturation effects can take place in water vapour absorption bands, radiative transfer models in clear-sky do not describe strong non-linear processes. Thus linearized cloud-free radiation codes have been used successfully for a variational assimilation of clear-sky radiances in NWP models (see for example Eyre, 1995). The non-linearities in the description of cloud-radiation interactions mainly come from on/off switches in cloud formation and dissipation and from the non-linear behaviour of cloud optical properties with liquid and ice water contents.

The linearized shortwave part of the radiation is not included in the current operational 4D-Var system. However, the tangent-linear and adjoint versions of the ECMWF shortwave code have

been developed and are currently under evaluation. Results will be provided in the following of the project.

Important developments will concern the longwave part of the spectrum because, in addition to the cloud non-linearities shared with the shortwave part, its complexity makes accurate computations expensive. Therefore, its adaptation to the assimilation framework requires simplifications. A tangent-linear code is usually twice as expensive in computing time as the corresponding non-linear code, whereas an adjoint code is three times more expensive. A very simplified linearized longwave code is currently introduced in the 4D-Var. Variations of the radiative tendencies only depend on atmospheric temperature perturbations (Mahfouf and Rabier, 1999). Several options for improving the linearized longwave scheme at a reasonable cost have been studied at ECMWF and are described in the following section.

4.2.3 The longwave scheme

As shown in Equations (1) and (2), the upward and downward longwave fluxes at height z_i can be expressed by the following equation:

$$F(z_i) = \sum_k a_k(z_i) F_k(z_i) \tag{26}$$

where the coefficients a_k are function of the cloudiness matrices $CC_{i,k}$.

From a differentiation of the above equation, it comes:

$$dF(z_i) = \sum_k [a_k(z_i) dF_k(z_i) + F_k(z_i)_k da_k(z_i)] \tag{27}$$

Because of the weak non-linearities in the variations of the radiative fluxes F_k with respect to temperature and water vapour (see for instance Chou and Neelin, 1996), the tangent-linear approximation can be used to compute accurately finite-size perturbations ΔF_k from the Jacobian matrices $(\partial F_k/\partial x)$ where x are the atmospheric temperature and humidity profiles:

$$\Delta F_k(z_i) \simeq \sum_x \sum_j \frac{\partial F_k(z_i)}{\partial x_j} \Delta x_j \tag{28}$$

where j represents the summation over the vertical layers.

As illustrated on Figure 5, this not the case for finite amplitude variations Δa_k of the coefficients a_k where strong linearities can be seen. In particular, the strong gradient for small liquid water contents limits the validity of the tangent-linear approximation to infinitesimal perturbations of the cloud properties.

A mixed approach is being investigated, where Equation (27) is approximated by:

$$\Delta F(z_i) \simeq \sum_k [a_k(z_i) \Delta F_k(z_i) + F_k(z_i) \Delta a_k(z_i)] \tag{29}$$

In this approach, flux perturbations $\Delta F_k(z_i)$ are estimated using the tangent-linear approximation (Equation 28), whereas Δa_k is computed exactly from $a_k(y + \Delta y) - a_k(y)$, where y represents cloud fraction and cloud ice/water profiles [1]. The estimation of Δa_k in finite differences does not require significant additional computing time. The exact computation of Δa_k implies that the operator providing flux perturbations ΔF from perturbations of the input variables Δy is not linear, therefore its adjoint does not exists. This can create problems in the minimization of the cost function (Equation 21) and also prevents from computing singular vectors.

In Equation (29), the fluxes F_k from the basic state are also needed. This implies either significant extra memory storage or important recomputations. However, is possible to make benefit of a neural network version (called NeuroFlux) of the ECMWF longwave radiative transfer model, that has been developed following an initial study at Laboratoire de Météorologie Dynamique (France). The basic principles of this new method can be found in Chéruy et al. (1996) and Chevallier et al. (1998). It combines an artificial neural network technique, the multilayer perceptron (MLP) as defined by Rumelhart *et al.* (1986), with the cloud description used by the ECMWF operational LW radiative transfer code, which insures the coherence between the two codes. All the parameters in NeuroFlux - several tens of thousands - are inferred from a series of learning databanks during a supervised training phase. The various validations of the method in the framework of the ECMWF GCM have showed that NeuroFlux is about 8 times faster than the operational LW code with a comparable accuracy (Chevallier *et al.*, 1999a; Chevallier *et al.*, 1999b). This may enable NeuroFlux to replace the current operational LW scheme, as well as to solve some of the problems related to the assimilation of cloud and radiation observations within the 4D-Var system.

The accuracy of the above approach to estimate perturbations of radiative fluxes has been evaluated in the following experiment. Differences between two short-range forecasts 12h and 6h valid for the same date were chosen to generate finite size perturbations of cloud cover, cloud condensate, temperature and specific humidity (similar to those generated in 4D-Var assimilations). For the whole globe description, at resolution 2.5°×2.5°, perturbations in cooling rates obtained with the above approach are compared to the differences between cooling rates obtained from the two sets of forecasts. Doing so, the validity of the following approximation is being evaluated:

$$\left(\frac{\partial T}{\partial t}\right)'_{LW} \simeq \left(\frac{\partial T}{\partial t}\right)^1_{LW} - \left(\frac{\partial T}{\partial t}\right)^2_{LW} \tag{30}$$

where X' is the perturbation of a quantity X, X^i represents the value of X produced by the forecast i. Profiles presented in Figure 6 show an example of cloudiness profiles from the two sets of forecasts and the perturbations in cooling rates (i.e. the derivative of the net fluxes) obtained in finite differences (considered as the truth) and from the tangent-linear approximation. Cloud modifications are large (up to 100 %), leading to significant changes in cooling rates profiles particularly at cloud interfaces. However, the approximated computation looks reasonable for

[1] The variational problem can be solved for the full control variable $z = (x, y)$ or only for the control variable x if a diagnostic cloud scheme $y = y(x)$ is defined with its linearization $\partial y / \partial x$.

finite size perturbations.

Error statistics for the whole globe are presented both in Table 1 and on Figures 7 and 8. The difference between the two figures comes from the Jacobian matrices used in the tangent-linear approximation for the ΔF_k computations. These Jacobian matrices (which are computed by a perturbation method) are either defined as global mean values (Figure 7) or set to zero (Figure 8). Figure 9 shows the reference values (right hand side of Equation 30). This comparison illustrates the dominance of clouds perturbations (computed exactly in the present approach) to the total variations in the longwave fluxes. The introduction of Jacobians mainly improves the cooling rates close to the surface, marked by strong variations of the surface temperature. The use of the operational non-linear LW scheme instead of the neural network version of it does not significantly change the results (not shown). The use of different Jacobians for every grid point (computationally expensive) does not significantly improve the results except in polar regions (not shown). This indicates that the remaining differences stem from the limitation of the tangent-linear approximation and encourages to use of mean Jacobians to save computational time.

As a conclusion, the approach developed for computing LW flux perturbations appears to be both accurate and fast. Future work on this subject will involve the study of its interaction with the adjoint model in the 4D-Var system.

4.2.4 Preliminary results from 1D-Var assimilation experiments

Previous sections emphasized the importance of an improved linearized physics for the assimilation of ERM products. A complementary study concerns the development of observation operators. It is related to the future broad-band longwave radiometer from ERM and makes use of data collected during the Atmospheric Radiation Measurement (ARM) program.

The ARM program run by the United States Department of Energy (Stokes and Schwartz, 1994) has undertaken to collect time series of ground-based measurements from active and passive remote sensors. By the combination of passive radiometers, lidar, millimeter-wave cloud radar together with conventional observations, the ARM program has produced very valuable datasets to evaluate cloud and radiation description in atmospheric models.

In this section we present preliminary results from a feasibility study performed at the ARM Central Oklahoma site during December 1997. A series of 5 clear-sky days was selected to evaluate a one-dimensional variational assimilation (1D-Var) of surface downward longwave fluxes together with additional observations of total column water vapour from a microwave radiometer. Observations were processed to get hourly averages and ECMWF atmospheric profiles for temperature and specific humidity were taken from short-range forecasts.

The principle of the 1D-Var is to modify atmospheric profiles from the ECMWF model to

produce surface longwave fluxes closer to the observed ones. A cost-function J, similar to the one presented in the 4D-Var context, is minimized:

$$J(x) = \frac{1}{2}(x - x^b)^T \mathbf{B}^{-1}(x - x^b) + \frac{1}{2}\left[\frac{LW(x) - LW_o}{\sigma_o}\right]^2 \tag{31}$$

where the control vector x contains vertical profiles of temperature T, specific humidity q as well as the surface pressure p_s. An observation error σ_o of the longwave flux has to be specified. The statistics of background errors described in the matrix $\mathbf{B}$ are imposed from the ECMWF operational 4D-Var system.

The gradient of the cost-function writes:

$$\nabla J(x) = \mathbf{B}^{-1}(x - x^b) + \mathbf{LW}^T\left[\frac{LW(x) - LW_o}{\sigma_o^2}\right] \tag{32}$$

where the operator $\mathbf{LW}^T$ is the adjoint of the tangent-linear version of the longwave radiative transfer parametrization scheme.

Given the low dimension of the control vector (63 variables for a 31-level grid) it is possible to compute explicitly the Jacobian elements of the adjoint operator, by a perturbation method requiring 64 calls (63 perturbations and one reference) to the non-linear radiative transfer model to estimate the following quantities:

$$\left(\frac{\partial LW}{\partial x}\right)_i \simeq \frac{LW(x + \delta x_i) - LW(x)}{\delta x_i} \tag{33}$$

Neural networks allows a more efficient computation of these partial derivatives. We show in this study that they are accurate enough to provide a solution of the minimization problem similar to the finite difference computations.

The Jacobian vector of the surface longwave radiation with respect to temperature $\partial LW/\partial T$ and specific humidity $\partial LW/\partial q$ is presented on Figure 10 for a typical mid-latitude atmospheric profile. All the Jacobian elements are positive which means that an increase in water vapour or temperature will increase the surface downward longwave radiation. Sensitivity of LW to temperature is only significant near the surface and then decreases exponentially with height. Sensitivity of LW to specific humidity is important over a deeper layer of the lower troposphere up to 600 hPa. The decrease of the Jacobian near the surface comes from the dominance of water vapour absorption.

For the selected five days, large differences between model surface longwave radiation fluxes and corresponding ARM measurements are noticed (Figure 11). Model values are hourly outputs from short-range forecasts (12 to 35 hours) and are updated every 24 hours (leading sometimes to discontinuities between 35-hour on day D and 12-hour forecasts on day D+1). Observations obtained every 2 min are hourly averaged. There is a systematic underestimation by the radiation code of the surface longwave fluxes up to 20 Wm^{-2}. These differences cannot entirely come

from deficiencies in the radiation code. Indeed, J.-J. Morcrette (personal communication) perfomed a number of simulations with different versions of the ECMWF radiative transfer scheme and also with an alternative radiation code RRTM (Mlawer et al., 1997) and significant biases persist. Part of the errors may come from the measurements themselves (representativeness problem of a point-station to describe the average behaviour within the model grid box) and from the radiative transfer scheme. These errors are taken into account in the minimization through the specification of σ_o which is set to 5 Wm^{-2}. Another source of errors comes from the atmospheric profiles in temperature and humidity from the ECMWF model. The 1D-Var modifies these profiles in order to better match the observed surface fluxes within a range of background errors given by the covariance matrix $\mathbf{B}$ computed from the ECMWF background statistics defined for the operational 3D/4D-Var system by Rabier et al. (1997) and Bouttier et al. (1997).

The result of the 1D-Var assimilation produces a series of longwave fluxes in much better agreement with the observations as expected (Figure 11). As also expected from the examination of the Jacobians profiles $\partial LW/\partial X$, the increase in longwave flux has been done mostly through an increase of water vapour in the atmospheric column. The total column water vapour resulting from the 1D-Var can be compared to an independent measurement from a microwave radiometer (its quality was checked using radiosoundings and the agreement was good). It appears (Figure 11) that for three of the 5 days (the first two days and the last one), the atmosphere is indeed too dry and that the moistening produced by the assimilation is producing a total column water vapour closer to the microwave estimate. However, for the two remaining days the agreement of the initial forecast in terms of water vapour was already very good. Therefore, the discrepancy of the surface longwave flux during this period with measurements is not likely to come from a too dry atmosphere and the moistening produced by the 1D-Var is not pertinent.

It is possible to reduce humidity corrections during these two days by adding a new observation term in the cost-function, measuring the departure of the model from the observed total column water vapour provided by the microwave radiometer. By setting an empirical observation error proposed by Phalippou and Gérard (1996) for the radiometer SSM/I, a 1D-Var assimilation was run with this new constraint on the minimization. Results presented on Figure 12 show much reduced water vapour corrections during the period where the model forecast was already in agreement with the observations. In consequence, the fit to the downward longwave flux observations is slightly worse. The specification of both background and observation errors has to be revised, but such development is out of the scope of the present report.

Results presented above were obtained using Jacobians computed in finite differences (which is an expensive method but affordable in a one-dimensional context). Similar results were also obtained using Jacobians explicitly derived from a neural network. Differences of the analysed quantities (longwave flux and total column water vapour) with corresponding observations are shown for both approaches on Figure 13 to summarize the behaviour of the two sets of 1D-Var assimilations. Results between the two approaches are very similar. It is a first demonstration that the neural network is accurate enough for solving variational problems with a gain in

computing time by a factor of three.

This 1D-Var study stresses the necessity of having collocated data of various types in order to better constraint the minimization problem and/or to provide independent sets of validation. This example also shows how linearized physical parametrizations (here the clear-sky longwave radiation code) can be used to solve the 1D-Var problem. Cloudy situations could be examined with the same methodology provided suitable observations and a linearized cloud scheme parametrization are available.

5 Validation studies on clouds and radiative fluxes at ECMWF

5.1 Comparisons with satellite data

In this section we illustrate how model changes related to clouds and radiation are currently evaluated in the ECMWF forecasting system in order to emphasize the need for complementary datasets such as those proposed by ERM.

In December 1997, important changes to the physics were introduced in the operational ECMWF model. The water vapour absorption continuum formulation was changed according to Zhong and Haigh (1995) from tests with line-by-line models. The longwave properties of ice clouds were modified using the formulation of Ebert and Curry (1992) instead of Smith and Shi (1992). The effective radius of ice particles was changed from a constant value of 40 μm to a dependency with temperature previously described (see Equation (6)). A treatment of cloud inhomogeneities following Tiedtke (1996) was introduced in the shortwave radiation scheme, where cloud water path is multiplied by 0.7. The numerical treatment of ice fallout in the cloud scheme was improved and the closure assumption of the moist convection scheme was changed.

Seasonal forecasts were run at low resolution (T63) from which three month averages of various fields were compared with associated satellite climatologies. Some illustrative results are presented for the winter period of 1987/1988 (December/January/February).

The patterns of upper cloudiness in the model are significantly affected by the above changes. Cloud amount (Figure 14) increases in the upper troposphere with the revised physics as also do cloud water/ice contents (Figure 15). In mid-latitudes this is mainly due to the revised ice fallout, although in the tropics the revised convection scheme also contributes. These zonal means describing the vertical structure of clouds can only be partially evaluated through satellite climatologies.

The spatial pattern of cloudiness can be compared with ISCCP estimates (Figure 16). The

revised physics increases cloud cover in many regions in the tropics. In the storm tracks region of the Northern hemisphere the area covered by cloud amounts greater than 80 % is increased, in better agreement with observations. The extent of regions with cloudiness above 80 % in the Equatorial Pacific is too large with the revised physics compared to ISCCP estimates. In the sub-tropical regions over the Pacific and Atlantic total cloud amount is slightly increased although still strongly underestimated by the model.

When compared with ERBE data, the increased cloud fraction with the revised physics lead to reduced errors in top of atmosphere (TOA) radiative fluxes. Overestimates of OLR (Figure 17) seen in the control simulation over Indonesia and northern South America are greatly reduced with the revised physics leading to better comparison with ERBE OLR estimates. However, over some regions (for example along the Pacific ITCZ) OLR is underestimated with the revised physics, providing some evidence that tropical high cloud amounts may be too large in these regions as also indicated by comparison with ISCCP. However, it is important to stress that radiative optical properties and cloud water/ice content may also play a role. Measurements from ERM should be able to provide additional information to better understand the source of model errors. Biases in the Southern Hemisphere of the control simulation (Figure 17) are also reduced by the revised physics as a consequence of the revisions to the longwave radiation scheme.

Errors in the estimation of TOA absorbed shortwave radiation in the tropics and sub-tropics (Figure 18 - negative values indicating an overestimation of albedo) are slightly reduced by the revised physics, specifically along the Pacific ITCZ and the sub-tropics of the Pacific and Atlantic oceans. A treatment of the inhomogeneity of clouds tends to reduce excessive albedos seen in the control simulation but this is counter balanced to a great extent by increased high level cloudiness. In southern mid-latitudes, the revised physics produces too large an TOA absorbed shortwave flux compared to ERBE. Although high cloud cover is increased in these regions by the revised physics, the inclusion of an effective radius which increases with temperature reduces the albedo of these mid-latitude clouds.

Clouds have strong influence of the surface energy balance and therefore an accurate description is of paramount importance for seasonal forecasting where atmospheric NWP models are coupled to ocean models. With the revised physics more heat goes into the ocean. Coupled ocean-atmosphere simulations indicate that the sea surface temperature (SST) bias over a large part of the tropics is reduced with the revised physics. Figure 19 shows the annual mean drift in SST after 6 months for an ensemble of forecasts obtained using the ECMWF coupled ocean-atmosphere model. Errors are substantially reduced in the tropical Indian, Pacific and Atlantic oceans, although warm biases have increased in the vicinity of stratocumulus sheets and in the southern hemisphere depression tracks due to remaining deficiencies in cloud amounts in these regions. The ability of the coupled model with revised physics to predict SST anomalies appears to be slightly increased.

A one-dimensional variational assimilation of brightness temperatures from the imager SSM/I has been developed by Phalippou (1996) and Phalippou and Gérard (1997) in order to retrieve

total column water vapour, surface wind speed and cloud liquid water path through a minimization process using ECMWF background profiles as an a-priori information. Total column water vapour from the 1D-Var is assimilated operationally in the 4D-Var system since June 1998. The assimilation of surface wind speed in under progress for near future operational implementation. Cloud liquid water path retrievals from the 1D-Var are not used in the operational assimilation system but are monitored to evaluate the model first-guess. Figure 20 presents a monthly average of cloud liquid water path produced by the ECMWF model first-guess, from the 1D-Var retrieval and from an independent statistical regression (Weng and Grody, 1994). Although the 1D-Var retrieval is not totally independent from the model first-guess, the large background error imposed on liquid water path from the model (0.2 kgm^{-2}) means that it represents a weak constraint in the minimization and therefore large modifications of the initial profiles are possible in order to match observed brightness temperatures. Global values from the model are almost twice as large as the 1D-Var estimate. Values from the regression are even smaller particularly over tropical oceans. There is a reasonable agreement between the three types of estimation along the mid-latitude storm tracks. The ECMWF cloud scheme produces much higher contents than the 1D-Var along the ITCZ whereas smaller amounts are simulated in the sub-tropical subsidence regions, off the west coast of South America and South Africa. In equatorial regions, the outgoing longwave radiation is controled to a large extent by ice water content in cirrus anvils generated from deep cumulus convection than by underneath water content. Such large differences between model products and satellite retrievals in terms of cloud liquid water path are certainly reduced in the comparison of OLR with ERBE data. However, it is also probable that the rather low spatial resolution of the SSM/I brightness temperatures used in the 1D-Var and in the statistical regression (125 km instead of 25 km for the original dataset) contributes to an undersampling of tropical convective systems.

This comparison with SSM/I products underlines the importance for future cloud satellite missions to generate consistent measurements of radiative fluxes, cloud fractional coverage and cloud water/ice contents to allow more comprehensive evaluations of cloud-radiation interactions in NWP models.

Although the types of comparison illustrated above provide useful general information on the model's performance in the representation of clouds it is obvious that they are insufficient to uncover the reasons for model errors. One approach to improve our understanding of model deficiencies is to link them to dynamical regimes. Tselioudis et al. (1999) have analysed ISCCP data in different pressure regimes defined by the local sea level pressure anomaly and derived frequency distributions of satellite-derived cloud top pressure versus cloud optical thickness for each regime. Figure 21 shows an example of a comparison of ECMWF model output against their data for the ocean areas in the latitude belt 30° to 60°N. The distributions are derived twice a day for the month of April 1992 from both the data (left panels) and short-range forecasts with a T106L31 version of the ECMWF model (middle panels). The right panels show the difference between model and observation. The top three panels show data including only cases with a negative anomaly of -5 hPa or more, the bottom three those with a positive anomaly of 5 hPa or more. The total cloud cover for each of the cases is indicated at the top of each panel. It is obvious from the data (left) that the two pressure regimes are connected with

two different cloud regimes. In the negative anomaly cases the distribution exhibits 3 peaks: at high-top clouds of large-optical thickness, at thin middle-level top clouds and medium thick low-top clouds. During periods of positive pressure anomaly the thick high top clouds do not occur and the amount of low-top medium thick clouds is increased. This is consistent with the predominant occurence of deep precipitating clouds connected to baroclinic systems versus a maximum occurence of clouds at the boundary layer top in the subsiding regions between those systems. Although the model is able to capture some of these differences the comparison within each of the pressure anomaly regimes reveals various shortcomings.

In the negative pressure anomaly regime the model underestimates the cloud cover by 14 %. However, when clouds are present they appear to be optically too thick in comparison with the data. The thin mid-level top clouds observed are not present in the model simulations at all and the tops of the low clouds are at lower levels than in the observation although the choice of 800 hPa as a threshold might influence that result. The underestimation of total cloudiness is even more severe (21 %) under positive pressure anomalies. The optical thickness of the clouds when present is again overestimated.

A step further in linking dynamical regime and cloud properties is illustrated in Figure 22. This figure is taken from the work of Klein and Jakob (1999). It shows the geographical distribution of clouds within a composite cyclone build from about 1200 individual cases following a technique developed by Lau and Crane (1995). The clouds are grouped by cloud top pressure and optical thickness. The top panel shows the cloud distribution derived from the ISCCP data overlayed with the sea level pressure anomaly showing the location of the composite low pressure centre. The expected cloud distribution in an extra-tropical cyclone is evident in Figure 22. High top medium-thick to thick clouds are found to the northeast of the low pressure center whereas medium-thick low clouds are found in the positive pressure anomaly ahead of the system as well as in the cold air flow behind the cyclone. The middle panel shows the cloud distribution for the same composite derived from short-range forecasts run from the ECMWF reanalysis (T106L31 resolution). It is evident that the model is able to reproduce the general cloud structure in the cyclones very well. However, a number of shortcomings are also apparent. The low-top clouds ahead and behind the system appear to be too thick, a band of low to medium top cloud extending from the low pressure anomaly centre to the southwest of the domain is entirely absent, and most prominently, the high top clouds appear to be optically too thin. This becomes even more apparent in the lowest panel. Instead of using the physical cloud top found in the model, as was done in the middle panel, an attempt to account for the difficulties the satellite has too detect very thin ice clouds is made (see Klein and Jakob (1999) for details). In that case the model cloud tops as seen by the satellite move further down indicating that a large number of high-top clouds in the model are very thin.

The two model validation studies summarized above show the potential of combining satellite data with information about the large-scale flow, an approach intrinsic in 4D-Var assimilation when applied to cloud fields.

Another new approach to the validation of cloud parametrization is made possible by the use

of new advanced active instruments, as they are planned for the Earth Radiation Mission. As a feasability study for a lidar in space the Lidar In-space Technology Experiment (LITE) was carried out aboard the space shuttle Discovery. Miller et al. (1999) examined the performance of the ECMWF prognostic cloud scheme against data from LITE during September 1994. Details on atmospheric profiles of cloud cover are available from this active sensor. Short-range (24 to 30 hours) forecasts were run for validation purposes over 15 different LITE orbit overpasses. ECMWF grid boxes along the flight tracks were identified and the resultant profiles were comprised of adjacent grid boxes with a variable amount of lidar information contained in each. The LITE data were binned to both the vertical and horizontal of the model grid. A pseudo-cloud fraction for the LITE data was computed for each level by normalizing the number of cloud profiles found by the number of total profiles in the grid box. An example of the ECMWF/LITE comparisons is shown for LITE Orbit 124 in Figure 23. Qualitatively, the vertical extent and placement of deep convection in the ITCZ, migratory mid-latitude disturbances, and large-scale subsidence zones appear to be in good agreement with the observations for this case. Some limitations of LITE data must also be taken into consideration. Some observations may possess an overestimate of the true cloud base altitude due to complete attenuation of the lidar pulse in the presence of optically-thick clouds. Further, all clouds below the level of attenuation are unreported. This is certainly the case for optically-thick stratus and deep convective clouds. The cloud base altitude may also be underestimated by pulse stretching produced by in-cloud multiple scattering of lidar photons. The analysis of the 15 orbits indicates possible underestimation of the frequency of high-altitude cirrus and overestimation of lower tropospheric clouds (subject to the caveats mentioned above) by the ECMWF model.

5.2 Comparisons with field experiments datasets

As shown in the previous section one difficulty of the validation of the cloud parametrizations in global circulation models comes from the fact that current satellites only provide TOA fluxes, total cloud cover and optical thickness which are insufficient to precisely identify the origin of deficiencies in cloud and radiation schemes.

However, for specific field experiment datasets, the vertical structure of observed clouds is available and comparisons with clouds described by the ECWMF forecast model have started.

A preliminary comparison between model profiles of clouds and precipitation and active sensor has been performed by Mace et al. (1998) using data from a vertically pointing millimeter wave radar (35 GHz) at a research site in North Central Oklahoma during three months (December 1996, January and February 1997). ECWMF data used for the comparison are derived from a special diagnostic tool run operationally. They are averaged over 4 grid points surrounding the radar location and correspond to short-range forecasts between 12 and 35 hours. Since the radar is unable to distinguish between clouds and precipitation, both cloud water and ice as well as precipitation from the model were considered as radar targets. Radar data have been subsampled both temporally and vertically for model comparisons. Figure 24 shows a

comparison of the model and radar cloud boundaries for the three-month period. December 1996 is characterized by an infrequent occurence of cirrus with no major deep cloud systems. In January and February 1997, however, several periods of extensive cloudiness are observed that resulted from migratory low pressure systems. The ECMWF model shows very good skill overall at predicting the vertical frequency distribution of clouds and precipitation that occured over this site during this period. There is, however, an indication that isolated cirrus events like on the 6 and 7 December are frequently missed by the model. It is also evident from Figure 24 that the model has a tendency to predict the onset of cloudiness too early, predict too great a layer depth and predict the dissipation of the layer too late. However, most of the false alarms occur in the vicinity (either in time or space) of observed cloud events, pointing to timing and vertical misplacement problems in the model. There are only few false alarms, like that on the 13/14 January, that occur in isolation. The occurence of false alarms only in the lowest 200 m is due to the fact that the lowest radar range gate occurs above this level.

This work shows that the ECMWF model is sufficiently skillful to allow for more in depth analysis of individual cases where the macroscale and microphysical properties of the predicted clouds can be evaluated.

Although of obvious importance the correct simulation of cloud occurence is only a necessary but not sufficient condition for capturing the main hydrological and radiative effects of clouds in GCMs. A further requirement is to correctly simulate the amount of condensate present in the cloud. Mace et al. (1997) have recently derived ice contents for isolated cirrus clouds from combined radar reflectivity and infrared interferometer data. Figure 25 shows an attempt to use this information for a first evaluation of the ECMWF model performance in simulating the ice content in those clouds. This figure shows the frequency distribution of ice content for clouds at temperatures lower than 219 K and higher than 227 K (note that all clouds in this study need to be colder than 250 K to be ice clouds) derived from observations and two versions of the ECMWF model. The bounding temperatures were chosen because they represent the 33 % and 67 % percentiles of the observed cloud distribution with respect to temperature. The observations were gathered between November 1996 and December 1997. The model data represents the periods November 1996 to October 1997 (Mod97) and January to July 1998 (Mod98). Although the time periods over which the comparison is made are not identical, enough cases are used in all samples to allow at least a qualitative comparison.

It is evident that a marked difference in the shape of the observed distributions exists for the two temperature regimes. At low temperatures the distribution is fairly narrow and exhibits a large peak at low ice contents. Although similar in shape the distribution at high temperatures is much broader and the peak at low ice contents is less pronounced. Large ice contents are encountered more frequently at high temperatures. The difference in the distributions is captured to a fair degree by the two model versions. Both do however severely overestimate the frequency of very low ice contents and underestimate the number of events with intermediate values. It is evident that despite those problems the 1998-version of the model, which incorporates a change to the numerical treatment of falling cloud ice, constitutes an improvement over the 1997-version. Although only qualitative in its nature the comparison shown is a major

step forward in model evaluation. For the first time long time series of observations of cloud ice exist and can be compared to GCM results at least in a statistical way.

Another crucially important parameter in the simulation of clouds and their radiative effects is the cloud fraction and its vertical distribution. Figure 26 shows a comparison of cloud cover derived from a 94 GHz radar during the Cloud Lidar And Radar Experiment (CLARE) over Chilbolton (U.K.) from 24 October to 8 November 1998 with those from ECMWF short-range forecasts. It is evident that the model is able to correctly capture the major cloud events in that period although errors in the details are clearly visible. This figure shows the potential of the use of space-borne radar to derive vertical cloud fraction distributions for model comparison.

The model to data comparisons presented above are far from comprehensive. They can and should only be considered as an example of the possibilities that both the new remotely sensed data and the short-range forecast approach to evaluation of model clouds provide. This approach will gain importance with the use of data provided by space-borne radar systems which form part of ERM.

5.3 Evaluation of weather parameters

Clouds are known to affect significantly the Earth's climate but they can also influence the atmosphere on shorter time scales. The skill of short and medium range forecasts of weather parameters such as precipitation, air temperature and cloudiness is strongly determined by the ability of a NWP model to correctly describe cloud elements. Moreover, feedback mechanisms can take place to enhance the sensitivity to cloud description. Figures 27 and 28 show monthly errors (forecast minus observation) at day 3 of the forecast for 2m temperature and cloud cover averaged over the European area from 1988 to 1999. Each curve represents a weekly average, top curves show the standard deviation, bottom curves show the bias. Cloud cover was characterized by a negative bias between 1 and 2 octas until the introduction of the prognostic cloud scheme in the operational model in April 1995. By then the systematic biases are strongly reduced. Comparison with SYNOP observations shows a slight underestimation by 0.5 octa during daytime and almost no biases during the night. Differences between daytime and nighttime could come from the difficulty in performing visual observations of cloudiness during nighttime. Before the introduction of the prognostic cloud scheme gross errors in the model were large enough for such comparisons to be useful. The differences currently noticed are certainly within the range of observational errors and more accurate measurements on cloud cover are required to identify remaining model errors.

Biases in 2m temperature correlate rather well with biases in cloud cover. Indeed, temperature biases were much larger before the implementation of the prognostic cloud scheme. The systematic underestimation of cloudiness was producing too cold nocturnal temperatures whereas in summer the overestimation of the downward solar radiation was leading to a positive bias in near surface temperature. Such positive bias was maximum in spring 1994 when a new soil-

vegetation scheme was introduced in the operational model. The temperature drift observed during that period was caused mainly by deficiencies in the cloud cover. The negative bias in cloud cover translates into excessive shortwave radiation at the surface of the order of 100 Wm^{-2}; the excessive energy available at the surface causes too much evaporation early in spring, drying the surface soil water reservoir too rapidly, too early in the year. Summer (convective) precipitation being tightly connected to local evaporation, a positive feedback was enhanced especially in areas of comparatively large recirculation of moisture in summer. This problem was less pronounced during previous years because soil moisture was restored to climatological values in the old land surface scheme, thereby avoiding large drifts from the climate. Such example illustrates how important the description of clouds is on the forecast skill of weather parameters.

6 Influence of cloud and radiative processes on NWP products

6.1 Sensitivity to cloud overlap assumptions

Cloud overlap assumptions must be made in atmospheric models in order to organize the cloud distribution used for radiation and precipitation/evaporation computations. Indeed, given the grid size of global NWP models (10^4 km^2) cloudiness cannot be considered as an all or nothing process. A cloud overlap assumption of some sort appears to be necessary to account for the fact that clouds are likely not to fill the whole grid box, particularly when the radiative transfer is not computed at every time-step of the model. However, little is known about the actual vertical distribution of clouds and results described in this section show that radiation fields are sensitive to the cloud overlap assumption. One of the original features of the ERM mission would be to provide some description of the vertical structure of cloud layers that could help to better define cloud overlap assumptions in NWP and climate models.

6.1.1 Cloud overlap assumptions

The most common cloud overlap assumptions in radiation schemes presently used in global atmospheric models are the random (RAN), the maximum-random (MRN) and the maximum (MAX) overlap assumptions, neither of which is completely justifiable on a global scale from limited observations of the actual atmosphere. The definition of cloud overlap assumptions is given from the point of view of cloudiness $CC_{i,j}$ encountered between any two levels i and j in the atmosphere. Let C_k by the cloud fraction of layer k located between levels k and $k+1$.

The maximum overlap assumption gives:

$$CC_{i,j} = \max(C_i, C_{i+1}, ..., C_{j-1}) \tag{34}$$

The random overlap assumption gives:

$$CC_{i,j} = 1 - \prod_{k=1}^{j-1}(1 - C_k) \tag{35}$$

The maximum-random overlap assumption gives:

$$CC_{i,j} = 1 - \prod_{k=1}^{j-1}\left[\frac{1 - \max(C_k, C_{k-1})}{1 - C_{k-1}}\right] \tag{36}$$

These three different overlap assumptions are illustrated in Figure 29.

Tian and Curry (1989) have tested the previous cloud overlap assumptions by applying them to the U.S. Air Force three dimensional nephanalysis in January 1979 over the North Atlantic Ocean. This data set is believed to be the best available information on the vertical distribution of clouds since it integrates both satellite and conventional observations over an area with relatively good data coverage. They compared the observed total cloud amount to the computed total cloudiness obtained with the three different assumptions. Their conclusion is somewhat in favour of the maximum-random overlap assumption first proposed by Geleyn and Hollingsworth (1979) : adjacent layers containing cloud are combined by using maximum overlap to form a contiguous cloud and discrete layers separated by clear-sky are combined randomly. Charlock et al. (1994) applied different interpretation for cloud overlap and cloud thickness to the ISCCP data and computed the resulting distribution of longwave radiative fluxes and cooling rates. With their top of the atmosphere radiation constrained by the data, they showed the high sensitivity of atmospheric and surface longwave radiation to the choice of cloud interpretation.

6.1.2 Sensitivity experiments with the ECMWF model

We present a number of results from Morcrette and Jacob (1999) who examined the impact of changing cloud overlap assumptions on the radiation and precipitation/evaporation schemes of the ECMWF model. Different sets of low resolution experiments (T_L95L31) were run over November 1987 to February 1988. Each set includes seven simulations starting 24 hours apart from 26 November to 1 December 1987 and all finishing on 1 March 1988. The first set (RAD) has the various cloud overlap assumptions used only in the radiation scheme. The second set (EPR) has the various overlap assumptions implemented in both the radiation and the prognostic cloud schemes, so that their effect is also felt in the computations of the large-scale precipitation and evaporation. The third set (EP) only considers the effects of cloud overlap assumptions within the prognostic cloud scheme, but has the radiation computations assuming the operational maximum-random overlap assumption.

Figure 30 presents the total cloudiness for the EPR simulations. Not surprisingly, the set of MAX simulations displays the minimum cloud cover at 0.609, followed by the MRN at 0.639, whereas the RAN simulations have a much larger total cloud cover at 0.714. The increase of MRN to RAN and the decrease from MRN to MAX are apparent over most of the globe, but are more pronounced over the sub-tropics, particularly those of the Southern Hemisphere. Most of the effect on cloudiness is linked to the vertical arrangement of clouds within the radiation scheme rather than to the effects of the arrangement for the precipitation/evaporation processes.

Longwave emissivity and shortwave optical thickness obviously depend on the amount of condensed water in the clouds, and on the radiative properties (longwave absorption coefficient, short wave single scattering albedo, asymmetry factor, extinction coefficient). Figures 31 and 32 present the outgoing longwave radiation (OLR) and the absorbed shortwave radiation (ASW) for the EPR simulations. While the global means presented in Table 2 all appear reasonable, the geographical distribution clearly shows a large impact of clouds in the ITCZ when the RAN assumption is used in the radiation scheme. Over the ITCZ, both the OLR and ASW go down with the RAN assumption to too low values, with averaged OLR over the three months period reaching 160 Wm^{-2} around 150 °E, and averaged ASW reaching 200 Wm^{-2}. However, at least for the ECMWF model with its prognostic description of clouds, it would be rather artificical to decrease the volume of clouds to ensure a smaller total cloud cover in the ITCZ, which would lead to OLR and ASW closer to observations.

Due to the lack of available observations on cloud overlap, this study is based only on model simulations. Observational data to be provided by the Earth Radiation Mission will provide essentially sub-grid scale quantities with respect to the current climate and NWP model grids. How these measurements should be aggregated both horizontally and vertically for meaningful comparisons with models is a challenge for the years to come. Given the large sensitivity of both the model total cloud cover and the radiation fields to cloud overlap assumptions used in the radiation scheme, it is very important to validate these quantities simultaneously. With that respect ERM is very valuable since it should sample both the cloud and radiative properties of a given atmospheric volume.

6.2 Sensitivity to ice formulation

In this section the sensitivity of the model climate of the ECMWF global model to the value of the fall speed of ice is investigated. The operational version formulates ice settling from Equation (14) The fall speed w_{ice} is a function of the ice content proposed by Heymsfield and Donner (1990). The integration of the model at T63L31 resolution with that version will be referred to as CONTROL simulation. Six more model integrations were carried out each using a fixed value of fall speed of 0.1, 0.3, 0.5, 1, 1.5 and 2 ms^{-1} respectively.

Figure 33 shows three-month averages (JJA 1987) of global means of for Ice Water Path (IWP) (a), radiative flux divergence (b) and precipitation (c) as a function of ice fall speed. The

horizontal lines represent the results of the CONTROL experiment. It is evident that with the reduction of fall speed the IWP averaged over the globe increases from values around 40 gm^{-2} for the largest assumed fall speed (2 ms^{-1}) to 140 gm^{-2} for the smallest (0.1 ms^{-1}). This leads to a reduction of the global mean radiative flux divergence from 110 Wm^{-2} to 90 Wm^{-2}. This decrease is achieved mainly through a decrease in outgoing longwave radiation (OLR). The flux divergence of the solar component and the net surface longwave radiation change only by small amounts (not shown). The reduction in the radiative cooling has an immediate effect on the atmosphere's response through latent heat release, which becomes obvious in Figure 33c. The global mean precipitation is reduced from 3.25 mm d^{-1} to 2.7mm d^{-1}. The main reduction is in convective precipitation, pointing to a much lower level of convective activity when using small ice fall speeds.

The geographical distribution of the changes outlined is shown in Figure 34 for the most extreme case of fall speed $w_{ice} = 0.1$ ms^{-1}. The figure shows the change in IWP (Fig. 34a), OLR (Fig. 34b) and convective precipitation (Fig. 34c) with respect to the CONTROL simulation. It is evident that the largest changes occur in the tropics. This is not surprising since it has been identified as the region of maximum ice production in the model. It is however noteworthy that the regions of maximum change in OLR do not coincide with the region of minimum OLR in the ITCZ but occur downwind to both sides of the minimum value. This is most likely due to the fact that by decreasing the fall speed of the ice particles, their residence time in the atmosphere is increasing. Hence, the advection process is able to transport ice further away from its source before it falls out.

It has been shown that through the modification of assumed fall speed of ice particles, the climate of the ECMWF model, in particular that of the tropics, can be changed dramatically. It is obvious from the slope of the curves in Figures 33a to 33c that the CONTROL model results are situated in a quite sensitive part of the parameter space although not the most sensitive one. Hence, small changes to the fall speed parametrization will substantially modify the model climate. Unfortunately the accuracy of the available global observations is not sufficient to draw firm conclusions about the right value of IWP in the sensitivity experiments.

6.3 Accuracy of ERM products

The above sensitivity experiments have shown that large uncertainties exist in the description of cloud properties in atmospheric models. The detection of cloud top and cloud base with an accuracy of 500 m is compatible with the vertical resolution currently used in NWP models. However, the boundary layer will be resolved with a better accuracy (about 150 m) in the near future at ECMWF (Teixeira, 1999). An accuracy in 5 % of the fractional cloud cover is certainly sufficient to address the cloud overlap problem. Accurate measurements of ice water contents about 40 % would help to improve the description of ice microphysics in NWP models since this quantity is particularly sensitive to ice fall speed specification.

6.4 Initialisation of cloud variables

The easiest way to initialise cloud variables in a prognostic scheme is to start the forecast with no clouds at all. However, this leads to a significant spin-up as clouds slowly build up during the forecast. Jakob (1995) showed that it takes up to ten hours for the top of the atmosphere radiation fields to reach an equilibrium state. In the ECMWF data assimilation system initial cloud variables are set to their values provided by a 6-hour forecast (first-guess). In this section, the impact of cloud spin-up on data assimilation and medium range forecasts experiments is revisited using the current ECMWF system.

A one-week assimilation of 4D-Var (11/04/1999 - 17/04/1999) is performed with a configuration similar to the operational one (Cycle 19R2). A series of seven 10-day forecasts was run from the analyses at 1200 Z. A set of experiments was run with initial cloud variables taken from the first-guess (*Control*) and another set was run with cloud variables set to zero initially in the forecast model (*Nocli*).

Within a data assimilation cycling, the length of the forecasts (6 hours) is too short to allow a complete build-up of the three-dimensional cloud field when it is initialized to zero. Therefore, there is a systematic deficit of clouds when the model first-guess is compared with observations to construct the analysis. Even though clouds observations are not used in the ECMWF data assimilation system, the reduction in cloud cover in the *Nocli* experiments has a non negligible impact on the temperature field. The influence of low level clouds is more pronounced in the shortwave part of the spectrum, whereas high clouds have more an effect on the longwave radiation. The reduction in low-level clouds produces lower albedos and therefore reduces the shortwave cooling. This leads to a warming of the lower troposphere. This effect is important in the sub-tropics, at mid-latitudes and over polar regions. The reduction in high clouds decreases the warming produced by greenhouse effect. This leads to a cooling the mid and high troposphere, which predominantly takes place along the ITCZ. These initial biases can be seen on the evolution of the mean temperature error in the tropical belt at 850 hPa and 300 hPa averaged over seven forecasts (Figure 35). There is a positive bias at 850 hPa of 0.3 K and a negative bias of 0.2 K at 300 hPa.

The fit of the model first-guess to radiosonde data averaged over one-week is significantly different between the two sets of experiments. The model is characterized by a warm bias in the troposphere and a cold bias higher up. In the Northern Hemisphere, the warming at low levels produces a negative bias in the *Nocli* experiment whereas the *Control* experiment has no significant bias up to 500 hPa (Figure 36). The cooling at higher levels has a slight beneficial impact on the bias between 400 hPa and 200 hPa. This effect is more pronounced in the tropics eventhough the amount of data is much less than in the Northern Hemisphere mid-latitudes (Figure 36).

10-day forecasts run from these analyses show a small but systematic degradation of the objective scores for geopotential, wind and temperature. As an example the anomaly correlation

of the geopotential at 1000 hPa is shown on Figure 37 for the Northern and Southern Hemispheres. The evolution of the mean temperature error at 850 hPa and 300 hPa in the tropics shows that three days are necessary to remove the initial bias imposed by the lack of clouds (Figure 35).

Table 3 summarizes the quality of the short-range forecasts (from 24 hour to 72 hours) for cloud cover and 2m-temperature as compared to SYNOP observations over Europe. Results show no significant differences between the *Control* and the *Nocli* experiments which indicates that clouds build-up rapidly enough in forecast mode so that the quality of weather parameters is unchanged.

Results presented above can be considered as an extreme sensitivity study to cloud initialisation. A significant impact is noticed on the fit of the first-guess to observations since cloud spin-up is of the order of 10 hours. The deficit of clouds in the 6-hour forecast has a significant impact on the temperature field. Even though the quality of medium-range forecasts is improved with a more realistic cloud initialisation, the impact on weather parameters is negligible. Additional studies will to be performed in order to examine more precisely how to improve the initialisation of cloud variables in the ECMWF integrated forecasting system.

Acknowledgements

We are grateful to Robin Hogan from the University of Reading for providing the CLARE radar comparison. We also thank Anna Ghelli from the Operation Department for providing the comparison with SYNOP observations. This work was funded by grants from ESA/ESTEC Contract 13151/98/NL/GD.

References

Bonnel, B., Y. Fouquart, J.-C. Vanhoutte, C. Fravalo and R. Rosset, 1983: Radiative properties of some African and mid-latitude stratocumulus. *Beitr. Phys. Atmos.*, **56**, 409-428

Bouttier, F., J. Derber and M. Fisher, 1997 : The 1997 revision of the J_b term in 3D/4D-Var. *ECMWF Technical Memorandum No 238*

Cess, R.D., G.L. Potter, J.-P. Blanchet, G.J Boer, A.D. DelGenio, M. Déqué, V. Dymnikov, V. Galin., W.L. Gates, S.J. Ghan, J.T. Kiehl, A.A. Lacis, H. Le Treut, Z.-X. Li, Z.-X. Liang, B.J. McAvaney, V.P. Meleshko, J.F.B. Mitchell, J.-J. Morcrette, D.A. Randall, L. Rikus, E. Roekner, J.-F. Royer, U. Schlese, D.A. Scheinin, A. Slingo, A.P. Sokolov, K.E. Taylor, W.M. Washington, R.T. Wetherald, I. Yagai, and M.-H. Zhang, 1990 : Intercomparison and interpretation of climate feedback processes in 19 general circulation models. *J. Geophys. Res.*, **95**, 16601-16615

Cess, R.D., M.H. Zhang, W.J. Ingram, G.L. Potter, V. Alekseev, H.W. Barker, E. Cohen-Solal, R.A. Colman, D.A. Dazlich, A.D. Del Genio, M.R. Dix, V. Dymnikov, M. Esch, L.D. Fowler, J.R. Fraser, V. Galin, W.L. Gates, J.J. Jack, J.T. Kiehl, H. Le Treut, K. K.-W. Lo, B.J. McAvaney, V.P. Meleshko, J.-J. Morcrette, D.A. Randall, E. Roeckner, J.-F. Royer, M.E. Schlesinger, P.V. Sporyshev, B. Timbal, E.M. Volodin, K.E. Taylor, W. Wang, and R.T. Wetherald, 1996: Cloud feedback in atmospheric general circulation models: An update. *J. Geophys. Res.*, **101D**, 12791-12794.

Charlock, T., F Rose, T. Alberta, G.L. Smith, D. Rutan, N. Manalo-Smith, P. Minnis and B. Wielicki, 1994 : Cloud profiling radar requirements : Perspectives from retrievals of the surface and atmospheric radiation budget and studies of atmospheric energetics. Report of GEWEX Topical Workshop on Utility and Feasibility of a Cloud Profiling Radar. WRCP-84, IGPO Publication Series No 10, B10-21

Chéruy, F., F. Chevallier, J.-J. Morcrette, N.A. Scott, and A. Chédin, 1996: Une méthode utilisant les techniques neuronales pour le calcul rapide de la distribution verticale du bilan radiatif thermique terrestre. *C. R. Acad. Sci. Paris*, **322:IIb**, 665-672.

Chevallier, F., F. Chéruy, N. A. Scott, and A. Chédin, 1998: A neural network approach for a fast and accurate computation of longwave radiative budget. *J. Appl. Meteor.*, **37**, 1385-1397.

Chevallier, F., A. Chédin, F. Chéruy, J.-J. Morcrette, and N. A. Scott, 1999a: A TIGR-like atmospheric profile database for accurate radiative flux computation. Submitted to *Quart. J. Roy. Meteor. Soc.*.

Chevallier, F., J.-J Morcrette, F. Chéruy, and N. A. Scott, 1999b: Use of a neural network-based longwave radiative transfer scheme in the ECMWF atmospheric model. Submitted to *Quart. J. Roy. Meteor. Soc.*.

Chou, C. and J.D. Neelin, 1996: Linearization of a longwave radiation scheme for intermediate tropical atmospheric model. *J. Geophys. Res.*, **101D**, 15129-15146

Courtier, P., J.-N. Thépaut, and A. Hollingsworth, 1994 : A strategy for operational implementation of 4D-Var using an incremental approach. *Quart. J. Roy. Meteor. Soc.*, **120**, 1367-1388

Ebert, E.E. and J.A. Curry, 1992 : A parameterization of ice optical properties for climate models. *J. Geophys. Res.*, **97D**, 3831-3836

Eyre, J.R., 1995 : Variational assimilation of remotely-sensed observation of the atmosphere. *ECMWF Technical Memorandum No 221*, 14pp.

Fouquart, Y., 1987 : Radiative transfer in climate models. *Physically Based Modelling and Simulation of Climate and Climatic Changes*, M.E. Schlesinger, Ed., Kluwer Acad. Publ., 223-284

Fowler, L.D., D.A. Randall and S.A. Rutledge, 1996: Liquid and ice cloud microphysics in the CSU general circulation model. Part I : Model description and simulated microphysical processes. *J. Climate*, **6**, 498-529

Geleyn, J.-F. and A. Hollingsworth, 1979 : An economical analytical method for the computation of the interaction between scattering and line absorption in radiation. *Beitr. Phys. Atmos.*, **52**, 1-16

Gregory, D., J.-J. Morcrette, C. Jakob, and A. Beljaars, 1998: Introduction of revised radiation, convection, cloud and vertical diffusion schemes into cy18r3 of the ECMWF integrated forecasting system. *ECMWF Technical Memorandum No 254*, 39 pp.

Heise, E. and E. Roekner, 1990 : The performance of physically based cloud schemes in general circulation models. *Beitr. Phys. Atmos.*, **93**, 1-14

Heymsfield, A.J. And L.J. Donner, 1990 : A scheme for parameterising ice cloud water content in general circulation models. *J. Atmos. Sci.*,**47**, 1865-1877

Houghton J.T., L.G. Meira Filho, B.A. Callander, N. Harris, A. Kattenberg and K., Maskel, 1995 : Climate change 1995. The science of climate change. Cambridge University Press, 572pp.

Ingmann, P., 1998 : The Earth Radiation Mission, Proceedings of the Workshop on Synergy of Active Instruments in the Earth Radiation Mission, 12-14 November 1997, GKSS, Geesthacht, Germany, 47-50

Jakob, C., 1995 : The impact of the new cloud scheme on ECMWF's Integrated Forecasting System (IFS). Proceedings of ECMWF/GEWEX Wokshop on Modelling, Validation and Assimilation of clouds, November 1994, ECMWF, Reading, United Kingdom, 277-294

Janisková, M., J.-N. Thépaut and J.-F. Geleyn, 1999: Simplified and regular physical parameterizations for incremental four-dimensional variational assimilation. *Mon. Wea. Rev.*, **127**, 26-45

Kessler, E., 1969 : On the distribution and continuity of water substance in atmospheric circulation. *Meteorol. Monog.*, **10**, American Meteor. Soc., Boston, Mass.

Klein, S. A., and C. Jakob, 1999: Validation and sensitivities of frontal clouds simulated by the ECMWF model. *Mon. Wea. Rev.* in press.

Le Dimet, F.-X. and O. Talagrand, 1986 : Variational algorithms for analysis and assimilation of meteorological observations. *Tellus*, **38A**, 97-110

Tselioudis, G., Y. Zhang and W. Rossow, 1999: Cloud and Radiation Variations Associated with Northern Midlatitude Low and High Sea Level Pressure Regimes, *J. Climate*, (in press)

Lau, N.-C., and M.W. Crane, 1995: A satellite view of the synoptic- scale organization of cloud properties in Midlatitude and Tropical circulation systems. *Mon. Wea. Rev.*, **7**, 1984-2006.

Mace, G.G., T.P. Ackermann, and E.E. Clothiaux, 1997: A study of composite cirrus morphology using data from a 94-Ghz radar and correlations with temperature and large-scale vertical motion. *J. Geophys. Res.*, **D12**, 13581-13593

Mace, G.G., C. Jakob and K.P. Monan, 1998 : Validation of hydrometeor prediction from the ECMWF model during the winter season 1997 using millimeter wave radar data, *Geophys. Res. Lett.*, **25**, 1645-1648

Mahfouf, J.-F. and F. Rabier, 1999 : The ECMWF operational implementation of four dimensional variational assimilation. Part II Experimental results with improved physics. *Quart. J. Roy. Meteor. Soc.*, (submitted)

Mahfouf, J.-F., E. Gérard, V. Marécal, M. Miller and R. Saunders, 1998 : User requirements for the assimilation of TRMM products in the ECMWF 4D-Var system. *ECMWF Technical Memorandum No 264*, 31pp.

Miller, S.D., G.L. Stephens, and A.C.M. Beljaars, 1999 : A validation survey of the ECMWF prognostic cloud scheme using LITE, *Geophys. Res. Lett.*, (in press)

Mlawer, E.J., S.J. Taubman, P.D. Brown, M.J. Iacono and S.A. Clough, 1997: Radiative transfer for inhomogeneous atmospheres: RRTM, a validated correlated k-model for the longwave. *J. Geophys. Res.*, **102D**, 16663-16682

Morcrette, J.-J., L. Smith and Y. Fouquart, 1986: Pressure and temperature dependence of absorption in longwave radiation parameterizations. *Beitr. Phys. Atmos.*, **59**, 455-469

Morcrette, J.-J., 1990: Impact of changes in the radiation transfer parametrization plus cloud optical properties in the ECMWF model. *Mon. Wea. Rev.*, **113**, 847-873

Morcrette, J.-J., 1999: On the effects of the temporal and spatial sampling of radiation fields on the ECMWF forecasts and analyses. *ECMWF Technical Memorandum No 277*

Morcrette,J.-J. and C. Jakob, 1999: The response of the ECMWF model to changes in cloud overlap assumption. *Mon. Wea. Rev.*, (submitted)

Ou, S.C. and K.-N. Liou, 1995: Ice microphysics and climate temperature feedback. *Atmosph. Research*, **35**, 127-138

Phalippou, L., 1996: Variational retrieval of humidity profile, wind speed and cloud liquid water path with the SSM/I : Potential for numerical weather prediction. *Quart. J. Roy. Meteor. Soc.*, **122**, 327-355

Phalippou, L. and E. Gérard, 1996: Use of precise microwave imagery in Numerical Weather Prediction. *Study report to the European Space Agency*, 70 pp.

Park, S.K. and K.K. Droegemeier, 1997: Validity of the tangent linear approximation in a moist convective cloud model. *Mon. Wea. Rev.*, **125**, 3320-3340

Rabier, F., A. McNally, E. Andersson, P. Courtier, P. Unden, J. Eyre, A. Hollingsworth and F. Bouttier, 1997 : The ECMWF implementation of three dimensional variational assimilation (3D-Var). Part II : Structure functions. *ECMWF Technical Memorandum No 242*

Rabier, F., H. Järvinen, E. Klinker, J.-F. Mahfouf and A. Simmons, 1999 : The ECMWF operational implementation of four dimensional variational assimilation. Part I : Experimental results with simplified physics. *Quart. J. Roy. Meteor. Soc.*, (accepted for publication)

Ricard, J.-L. and J.-F. Royer, 1993: A statistical cloud scheme for use in an AGCM. *Ann. Geophysicae*, **11**, 1095-1115

Rumelhart, D.E., Hinton, G.E., Williams, R.J., 1986 : Learning internal representations by error propagation, Parallel distributed processing: Explorations in the macrostructure of cognition 1, Rumelhart and McClelland eds, MIT Press.

Saito, K. and A. Baba, 1988 : A statistical relation between relative humidity and the GMS observed cloud amount. *J. Meteor. Soc. Japan*, **66**, 187-192

Senior, C. A. and J.F.B. Mitchell, 1993 : Carbon dioxide and climate : the impact of cloud parameterization. *J. Climate*, **6**, 393-418

Slingo, J.M., 1987 : The developement and verification of cloud prediction scheme in the ECMWF model, *Quart. J. Roy. Meteor. Soc.*, **113**, 899-927

Smith, E.A., and L. Shi, 1992 : Surface forcing of the infrared cooling profile over the Tibetan plateau. Part I: Influence of the relative longwave radiative heating at high altitude. *J. Atmos. Sci.*, **49**, 805-822

Smith, R.N.B., 1990 : A scheme for predicting layer clouds and their water content in a general circulation model. *Quart. J. Roy. Meteor. Soc.*, **116**, 435-460

Stokes, G.M. and S.E. Schwartz, 1994 : The Atmospheric Radiation Measurement (ARM) Program: Programmatic background and design of the cloud and radiation test bed. *Bull. Amer. Meteor. Soc.*, **75**, 1201-1221

Sundqvist, H., 1978 : A parameterisation scheme for non-convective condensation including prediction of cloud water content. *Quart. J. Roy. Meteor. Soc.*, **104**, 677-690

Sundqvist, H., 1988 : Parameterization of condensation and associated clouds in models for weather prediction and general circulation simulation. *Physically-Based Modelling and Simulation of Climate Change*, M.E. Schlesinger, Ed. Kluwer, 433-461.

Teixeira, J., 1998 : A prognostic cloud fraction scheme and the representation of boundary layer clouds. Proceedings of the 4th International Cloud Modelling Workshop. Clermont-Ferrand, France, WMP Report No 29, WMO, 31-36.

Teixeira, J., 1999 : The impact of increased boundary layer vertical resolution on the ECMWF forecast system. *ECMWF Technical Memorandum No 268*, 55pp.

Tiedtke, M., 1993 : Representation of clouds in large-scale models. *Mon. Wea. Rev.*,**121**, 3040-3061.

Tiedtke, M., 1996 : An extension of cloud-radiation parameterization in the ECMWF model : The representation of sub-grid scale variations of optical depth. *Mon. Wea. Rev.*, **124**, 745-750

Tian, L. and J. Curry, 1989 : Cloud overlap statistics. *J. Geophys. Res.*, **94D**, 9925-9936

Verlinde, J. and W.R. Cotton, 1993: Fitting microphysical observations of nonsteady convective clouds to an numerical model: An application of the adjoint technique of data assimilation to a kinematic model. *Mon. Wea. Rev.*, **121**, 2776-2793

Walcek, C.J., 1994 : Cloud cover and its relationship to relative humidity during a springtime midlatitude cyclone. *Mon. Wea. Rev.*, **122**, 1021-1035

Washington, W.M., and D.L. Williamson, 1977: A description of the NCAR GCMs. "GCMs of the atmosphere". J. Chang, Ed., Methods in computational physics, Vol. 17, Academic Press, 111-172.

Wend, F. and N..C. Grody, 1994 : Retrieval of cloud liquid water using the specilal sensor microwave imager (SSM/I). *J. Geophys. Res.*, **99**, 25535-25551

Zhong, W. and J.D. Haigh, 1995 : Improved broadband emissivity parameterization for water vapor cooling rate calculations. *J. Atmos. Sci.*, **52**, 124-138

(a)

	polar			mid-latitude			tropical		
	m	σ	M	m	σ	M	m	σ	M
(FC-06) - (FC-12)	0.0	5.7	69.0	0.4	11.8	96.1	-0.5	17.3	145.2
Approx. error (mean Jac.)	0.0	0.6	4.9	0.0	1.1	7.8	0.1	1.2	10.8
Approx. error (no Jac.)	-0.1	1.4	8.6	-0.1	2.2	21.0	0.1	2.5	17.8

(b)

	polar			mid-latitude			tropical		
	m	σ	M	m	σ	M	m	σ	M
(FC-06) - (FC-12)	-1.3	10.5	82.1	-0.4	13.7	80.8	-0.4	9.5	68.4
Approx. error (mean Jac.)	0.0	1.7	16.8	0.0	0.6	9.2	-0.1	0.7	5.9
Approx. error (no Jac.)	0.1	2.8	28.9	-0.2	4.3	49.6	-0.5	3.5	27.6

Table 1: Global statistics on the longwave flux perturbation computation. Top line of the arrays: mean (m), standard deviation (σ) and maximum absolute error (M) of the comparisons between the 6-hour forecast and the 12-hour forecast for the computation of the OLR (a), and the net LW flux at the surface (b). Middle line: same statistics for the error introduced by the approximation including a mean Jacobian matrix (see text). Lower line: same statistics for the error introduced by the approximation using no Jacobian matrix (see text). 1^{st} July 1998, 00 UTC. 2.5° × 2.5° horizontal resolution. Fluxes in W/m^2. Results are shown by latitude class.

	EPR			RAD		EP	
	MRN	MAX	RAN	MAX	RAN	MAX	RAN
TCC (%)	63.9	60.9	71.4	61.1	70.8	63.8	64.4
OLR (Wm^{-2})	241.2	242.8	234.5	243.1	234.7	241.6	241.6
ASW (Wm^{-2})	247.1	248.4	245.1	249.6	247.0	247.0	246.2

Table 2: Global mean (3-month average for December-January-February) of total cloudiness (TCC), outgoing longwave radiation (OLR) and absorbed shorwave radiation (ASW) for various cloud overlap assumptions applied to radiation processes (RAD), precipitation/evaporation fluxes due to the cloud processes (EP) and both (EPR).

	Cloud cover [octa]			2m Temperature [deg C]		
Exp (Step)	Bias	StDev	Mae	Bias	StDev	Mae
Control (24h)	-0.11	2.22	1.49	0.32	2.28	1.70
Nocli (24h)	-0.09	2.25	1.52	0.34	2.27	1.70
Control (48h)	0.13	2.37	1.65	0.38	2.42	1.83
Nocli (48h)	0.10	2.39	1.65	0.39	2.46	1.85
Control (72h)	0.16	2.70	1.91	0.44	2.88	2.19
Nocli (72h)	0.16	2.69	1.91	0.40	2.88	2.18

Table 3: Forecast errors in total cloud cover and 2m-temperature with respect to SYNOP observations over Europe for *Control* experiments and experiments with zero initial clouds *Nocli*. Results are presented for three forecast ranges (24, 48 and 72 hours) in terms of bias (Bias), standard deviation (Stdev) and mean absolute error (Mae) and are averaged over 7 cases.

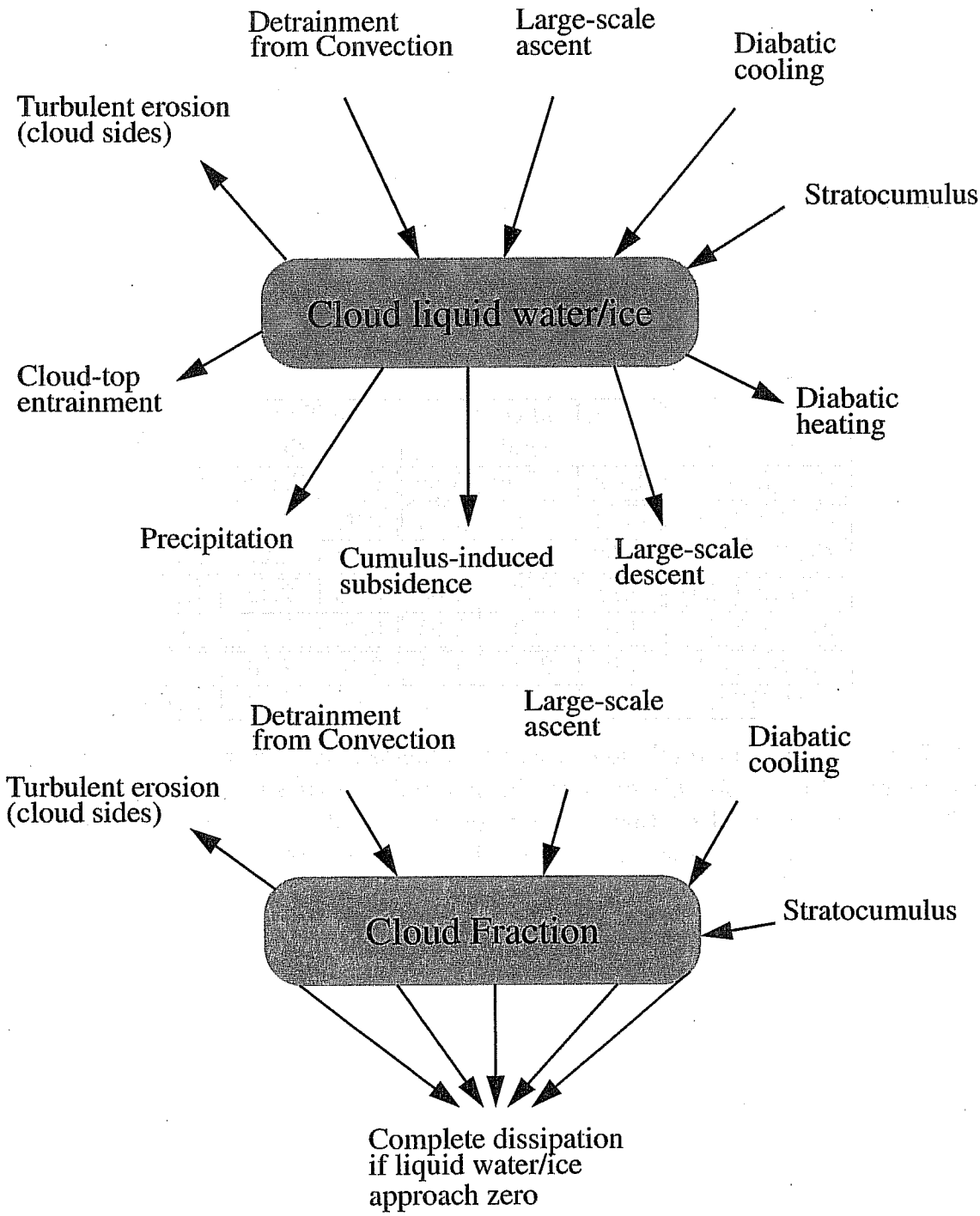

Figure 1: Schematic description of the production and dissipation terms for cloud fraction and cloud condensate in the ECMWF prognostic cloud scheme

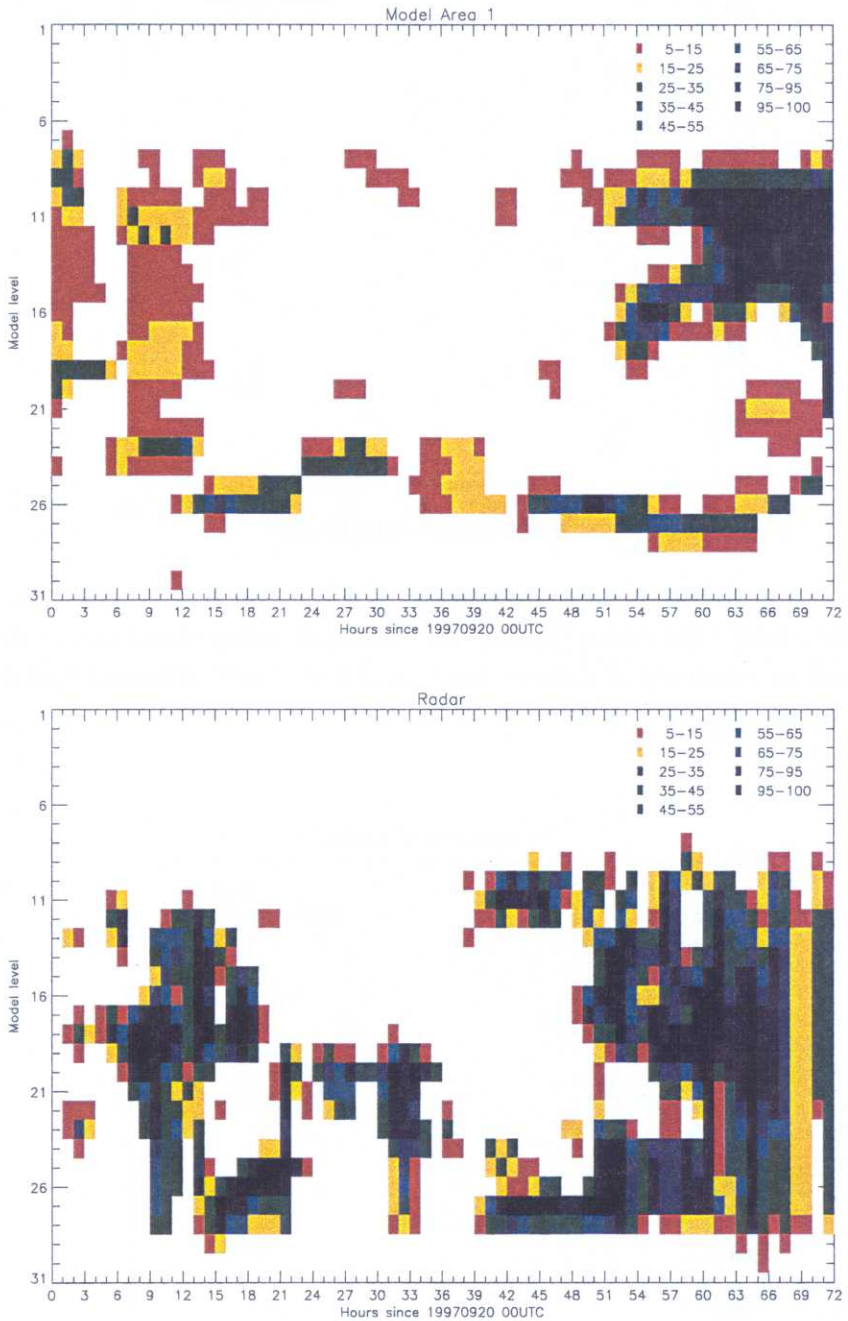

Figure 2: Comparison of ECMWF short-range forecast of cloud cover with radar-derived observations at ARM North Central Oklahoma site, from 20/09/1997 to 23/09/1997.

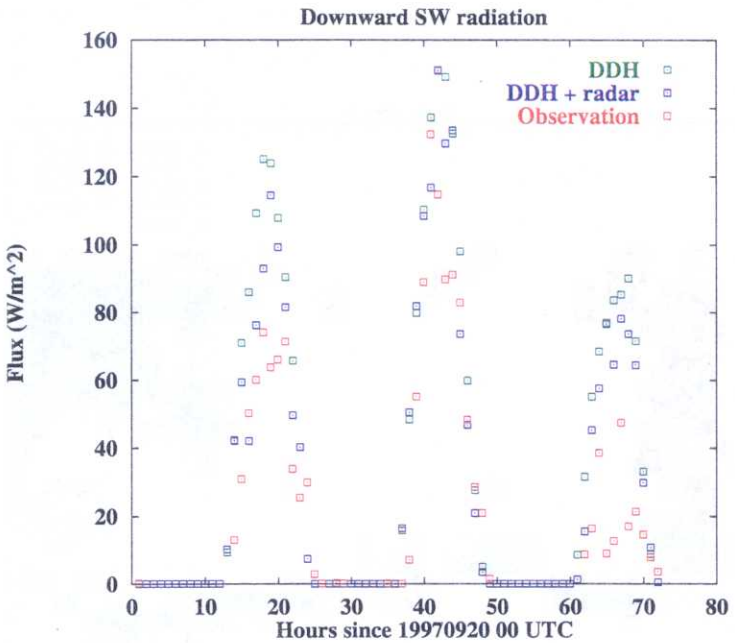

Figure 3: Comparison between the downward surface shortwave flux as estimated from ECMWF short-range forecasts (DDH), as corrected using cloud cover observations (DDH+radar), and as observed (Observation) at ARM North Central Oklahoma site, from 20/09/1997 to 23/09/1997. Fluxes in $W.m^{-2}$.

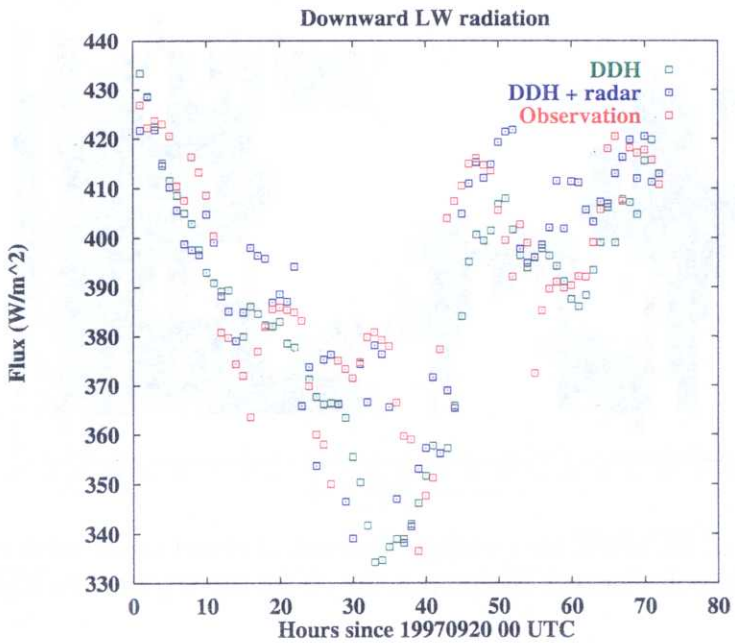

Figure 4: As figure above, but for the downward surface longwave flux. in $W.m^{-2}$.

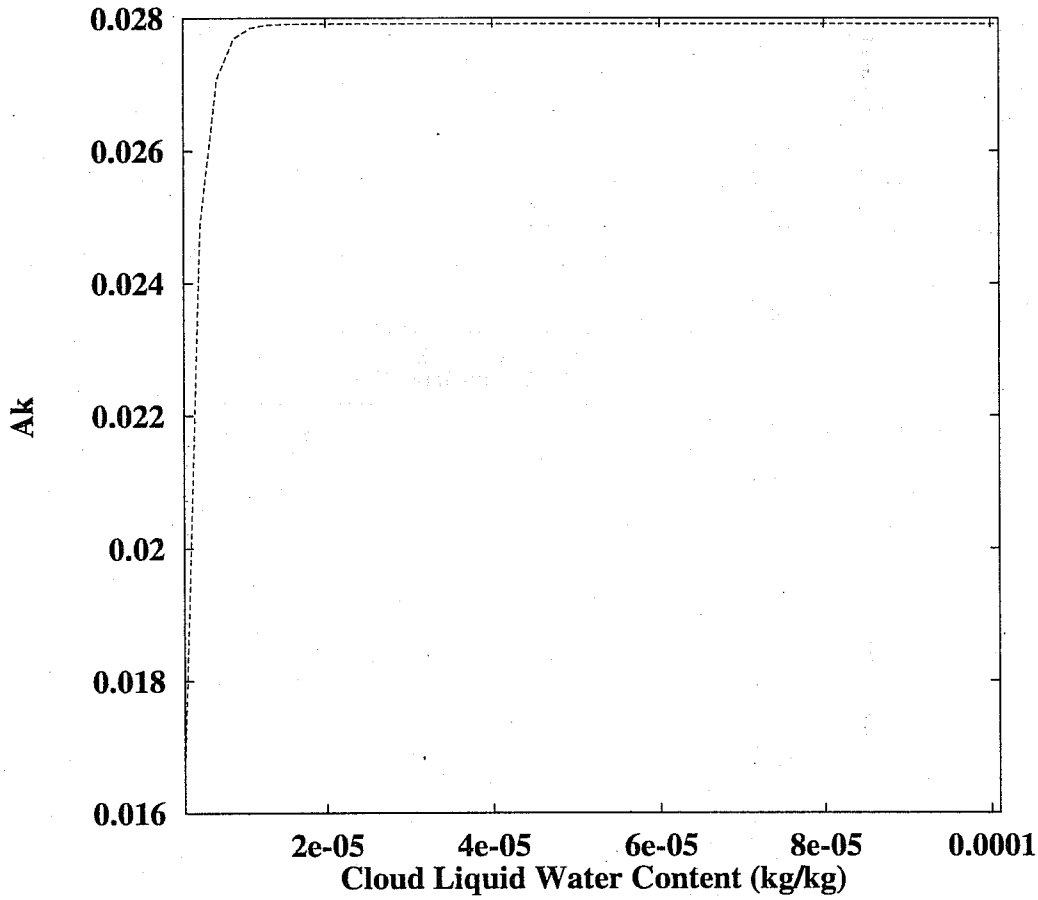

Figure 5: Example of variation of a_k (see Eauqtion (26) in the text) with respect to the cloud liquid water content.

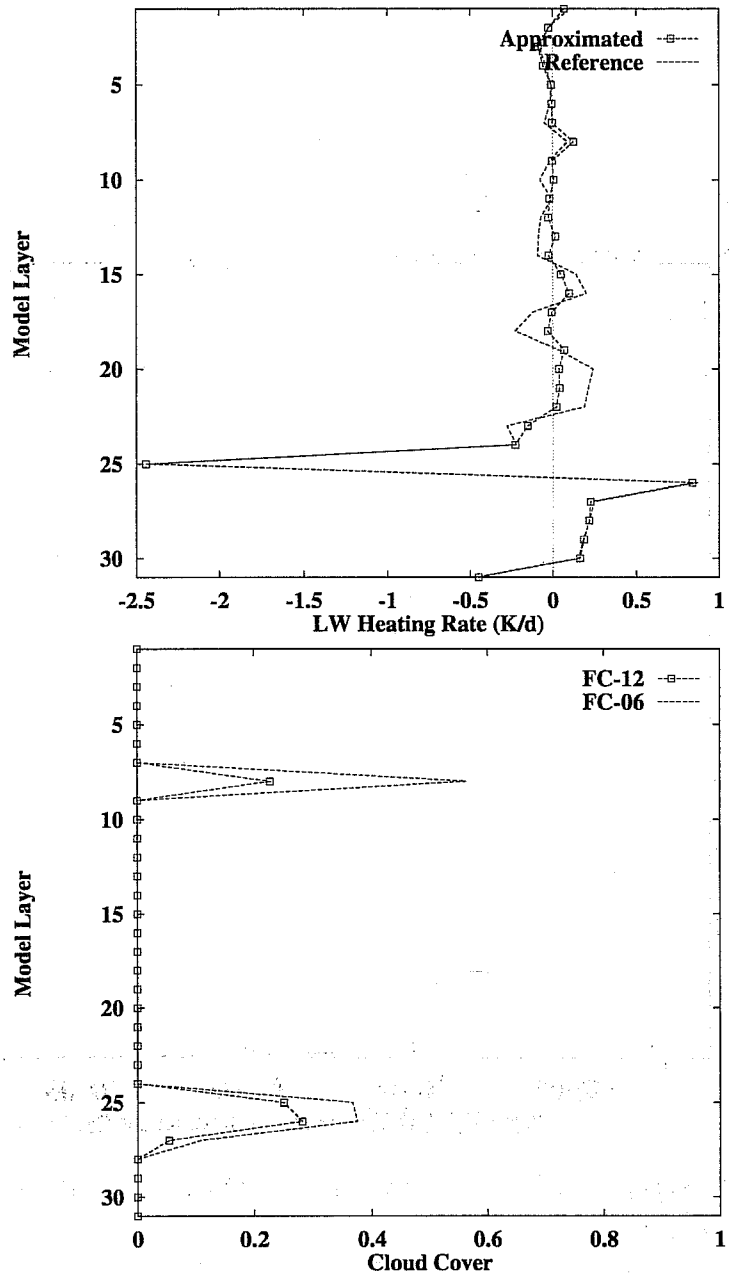

Figure 6: Illustration of the accuracy of the tangent-linear approximation for computing the longwave cooling rate between 12-h and 6-h forecasts. The upper panel shows a comparison between the finite difference perturbation (Reference) and the perturbation computed using an approximated method (as proposed by Equation (29)) The lower panel displays the corresponding forecasts at 6-h and 12-h of the cloud profiles

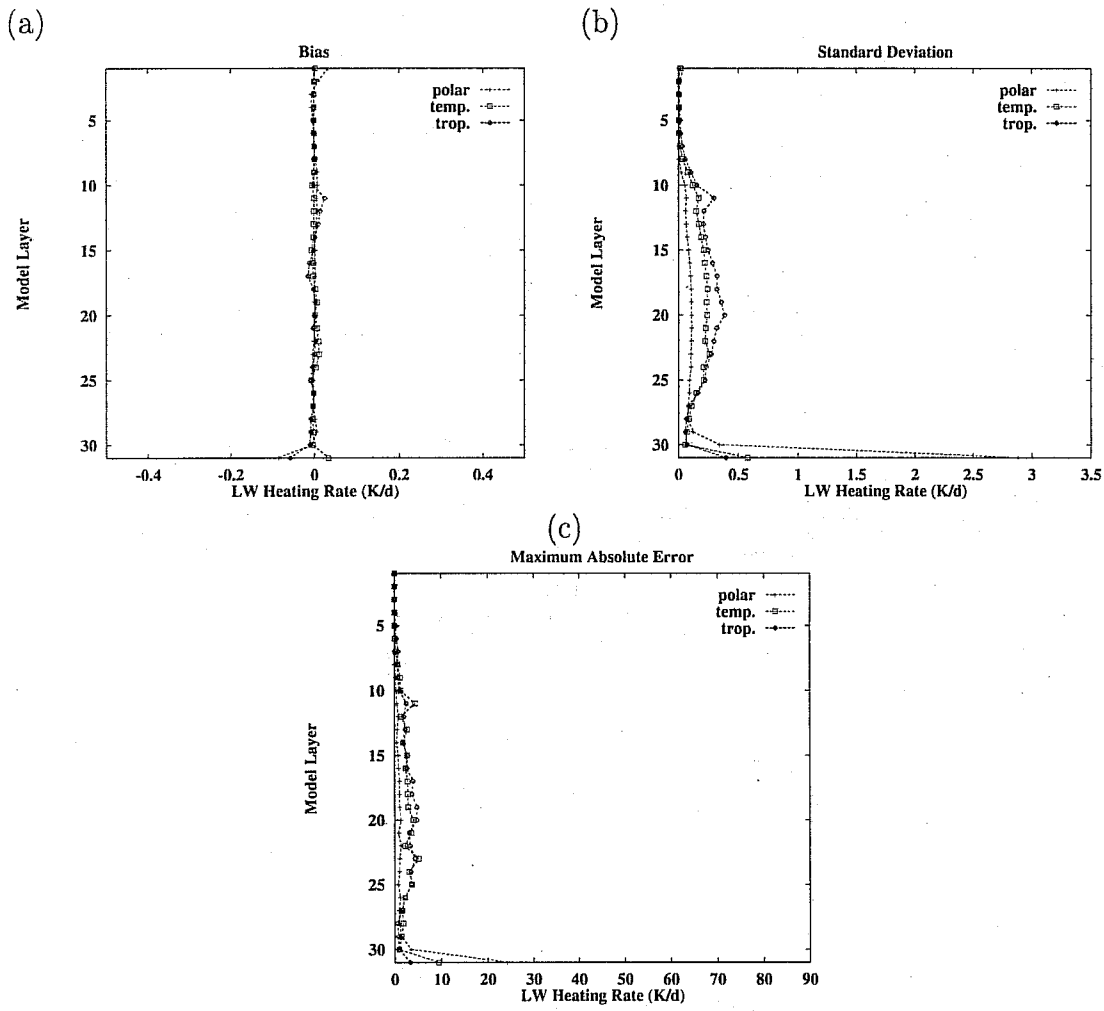

Figure 7: Comparison between the computations of the LW heating rate perturbations by the fast approach using a mean Jacobian matrix (see text) and by the finite difference method. Heating rates in $K.d^{-1}$. 1^{st} July 1998, 00 UTC. $2.5° \times 2.5°$ horizontal resolution. Results are shown for three latitude classes.

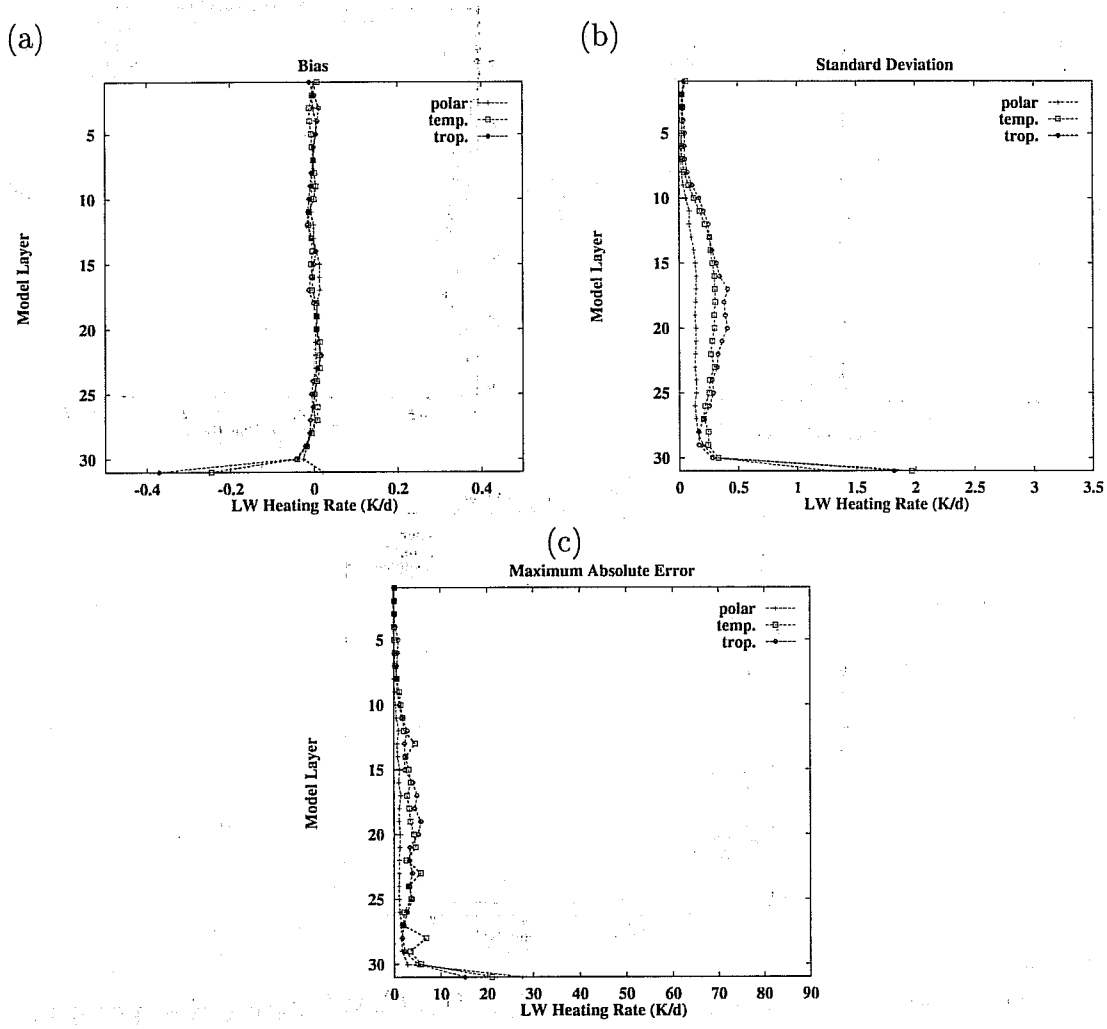

Figure 8: Same as Figure 7 but with Jacobians set to zero.

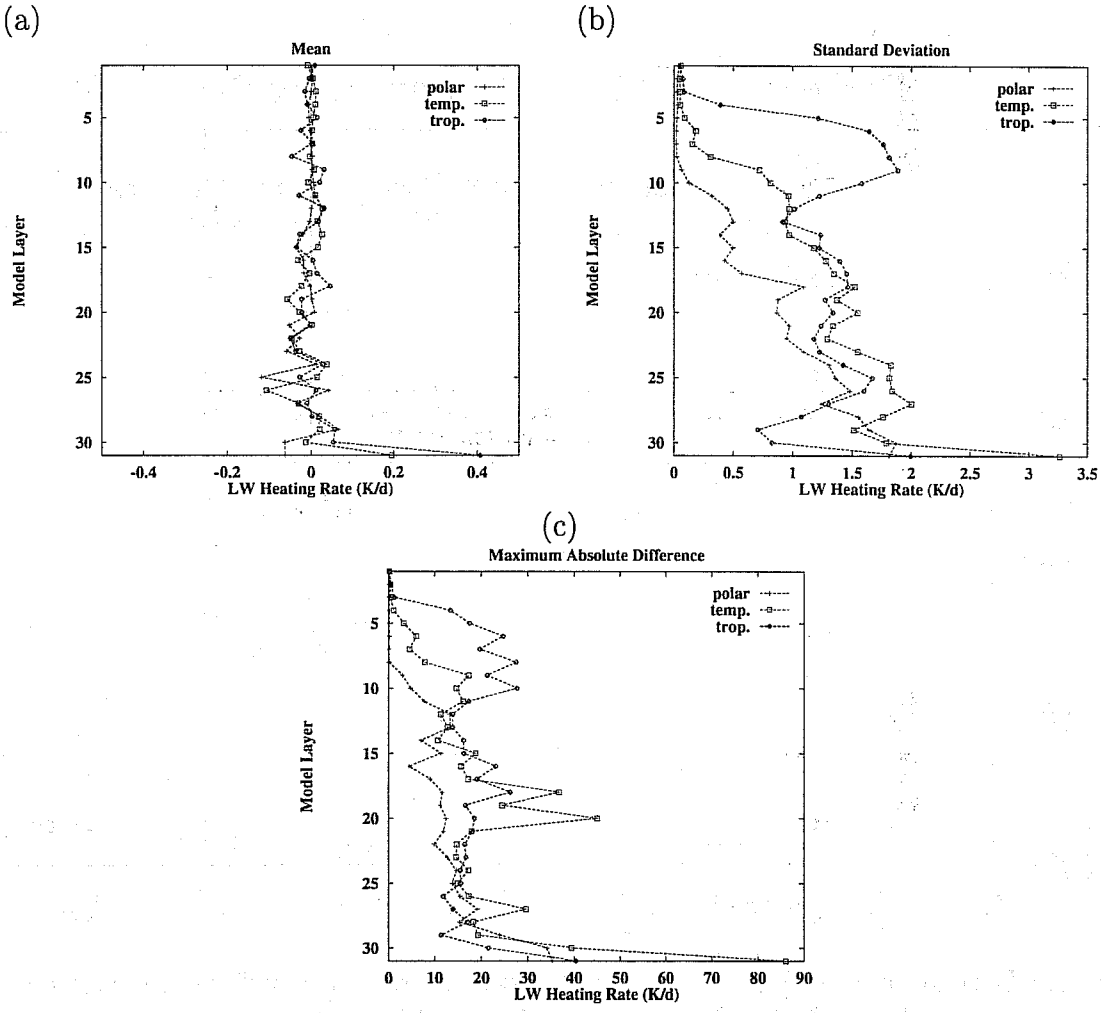

Figure 9: Statistics of LW heating rate perturbations between 6-h and 12-h forecasts. 1^{st} July 1998, 00 UTC. $2.5° \times 2.5°$ horizontal resolution. Results are shown for three latitude classes.

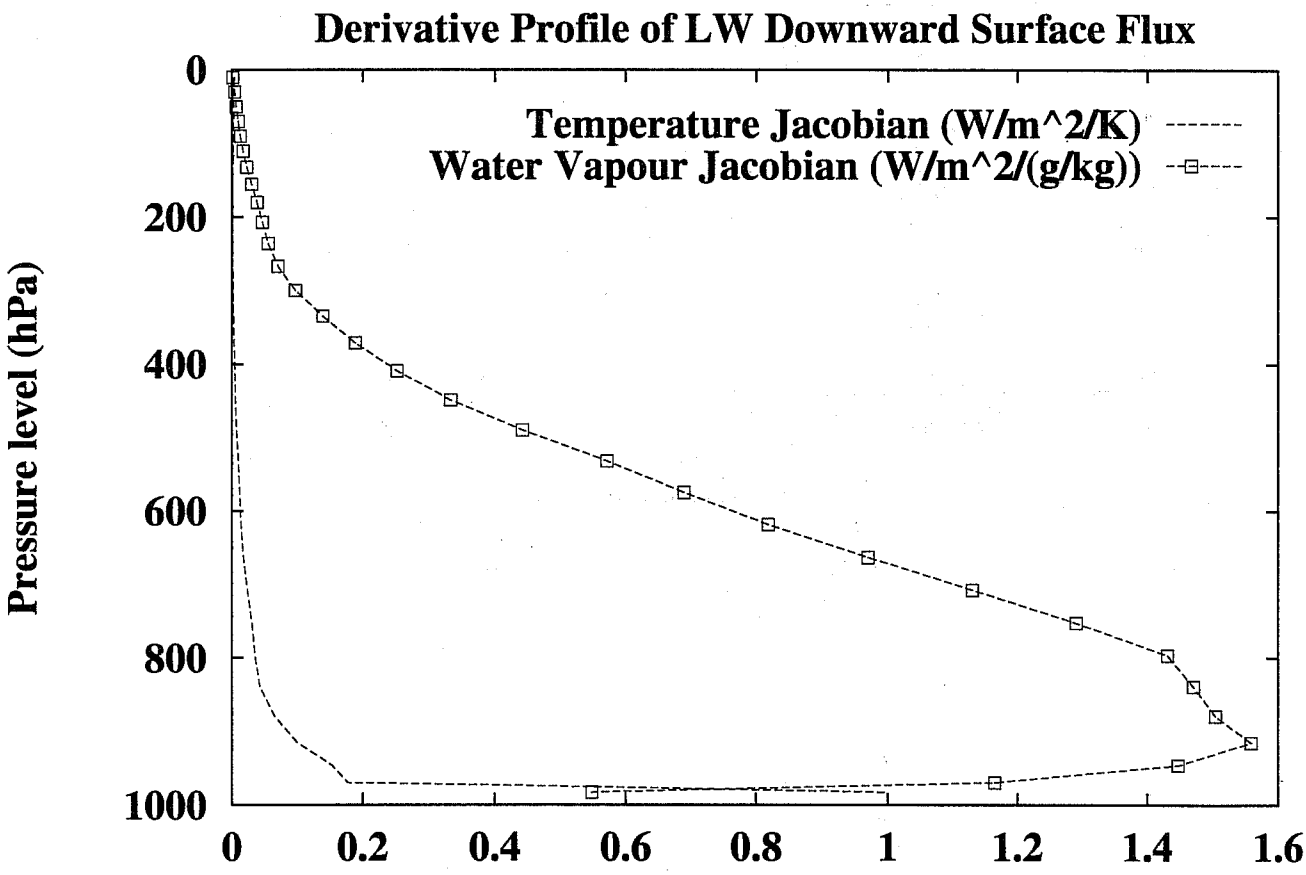

Figure 10: Derivative profiles (Jacobians) of longwave downward surface flux with respect to temperature and specific humidity for a typical mid-latitude profile computed by the ECMWF operational radiation scheme.

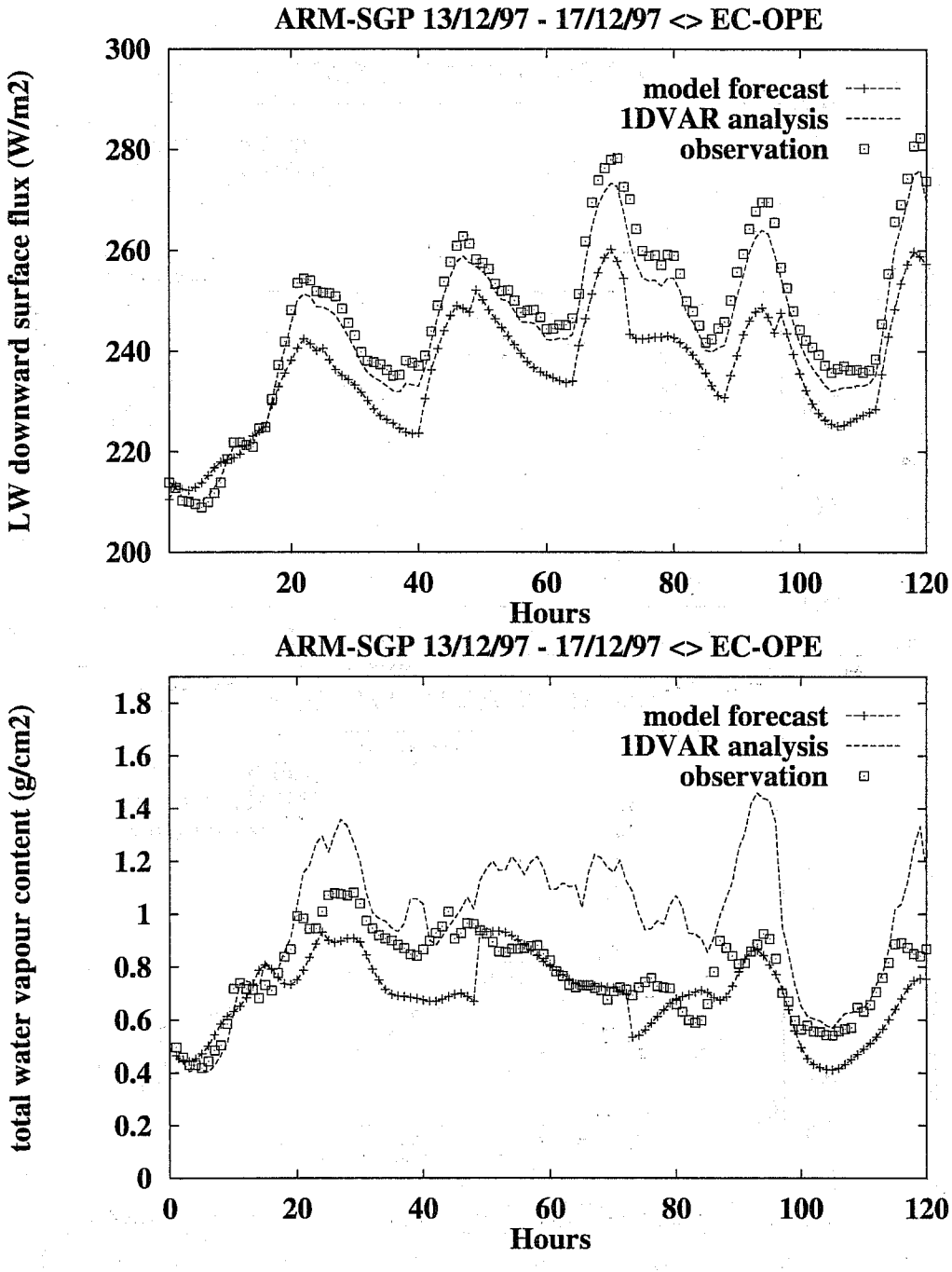

Figure 11: Comparison between the downward longwave flux measured at ARM-SGP site by a pyrgeometer, computed from the ECMWF short-range forecast and estimated from a 1D-Var analysis (upper panel). Comparison between the total column water vapour measured at ARM-SGP site by a microwave radiometer, computed from the ECMWF short-range forecast and estimated from a 1D-Var analysis (lower panel).

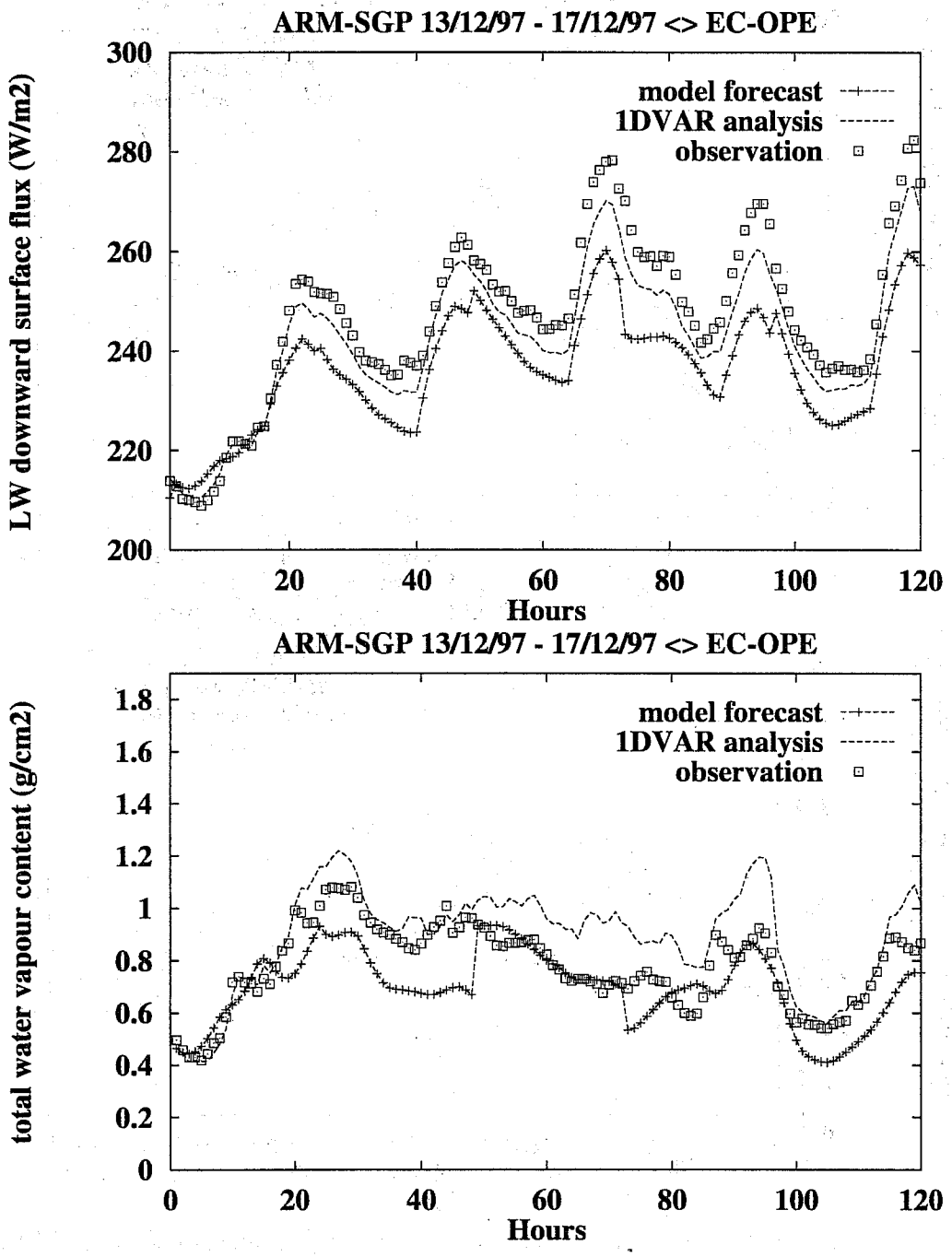

Figure 12: Same as Figure 11, but the 1D-Var analysis includes both longwave flux and total column water vapour observations.

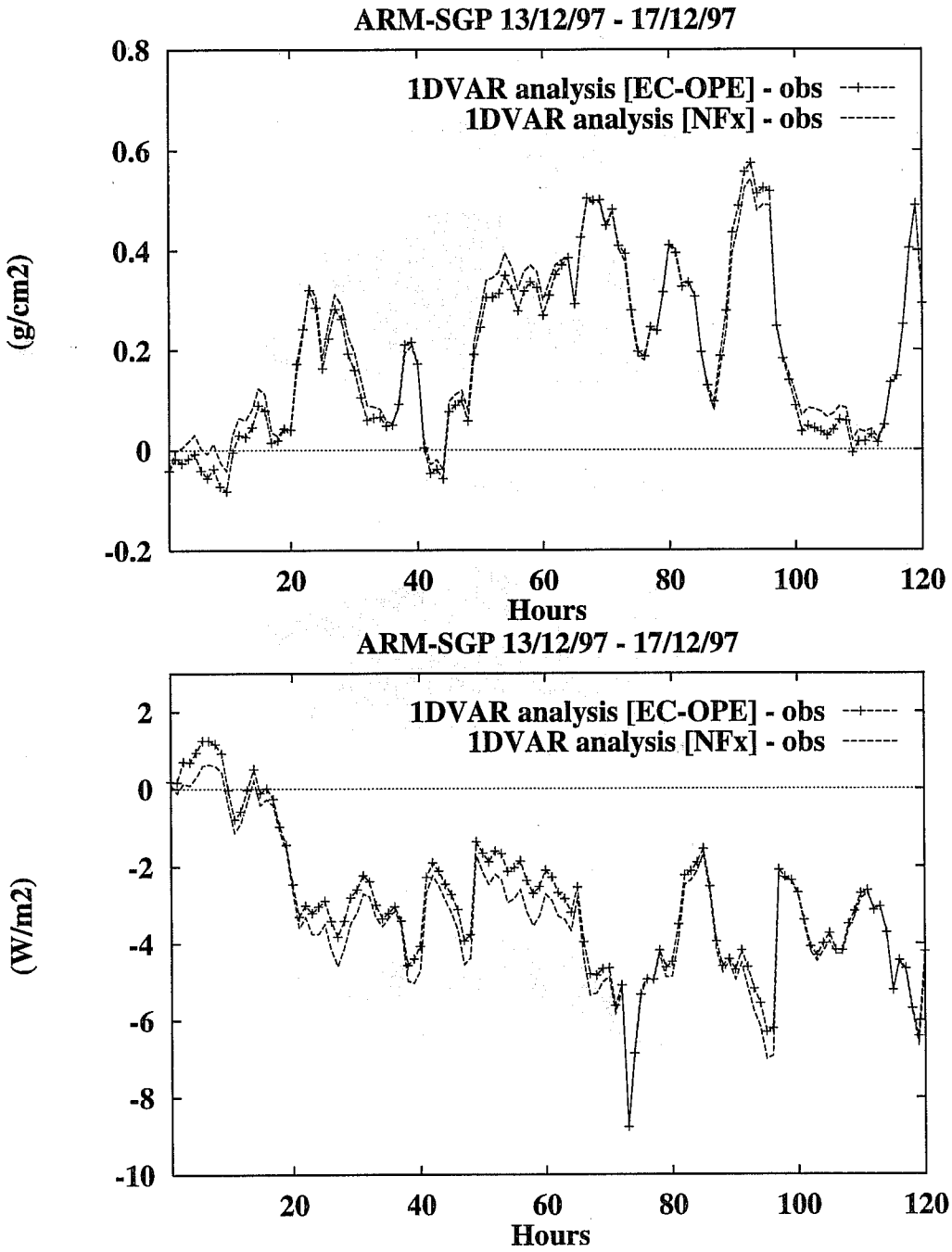

Figure 13: Differences between the result of a 1D-Var analysis for total column water vapour (upper panel) and downward longwave flux (lower panel) using Jacobians computed by the ECMWF longwave radiation scheme and the one using the neural network of it.

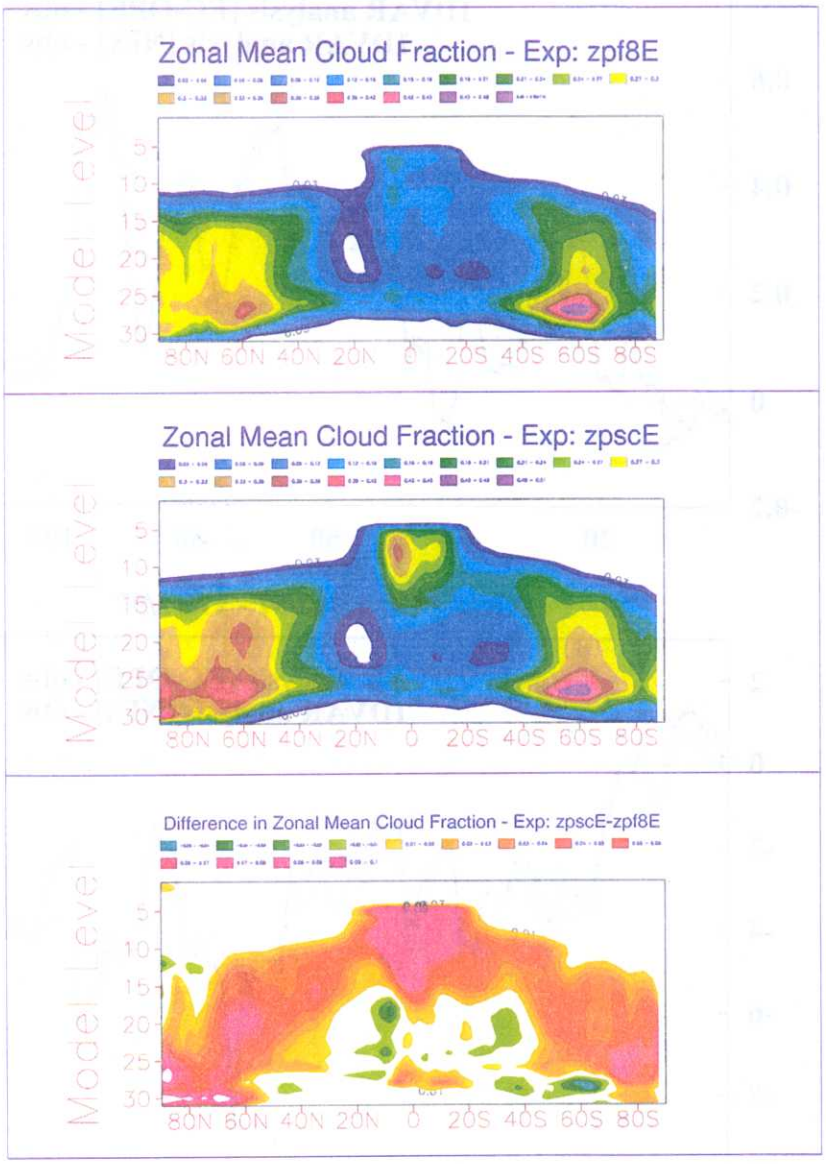

Figure 14: Zonal mean cloud fraction for December/January/February 1987-88 from T63L31 model simulations : control simulation (upper panel), revised physical package (middle panel), differences (lower panel). Model results are an average over an ensemble of three simulations.

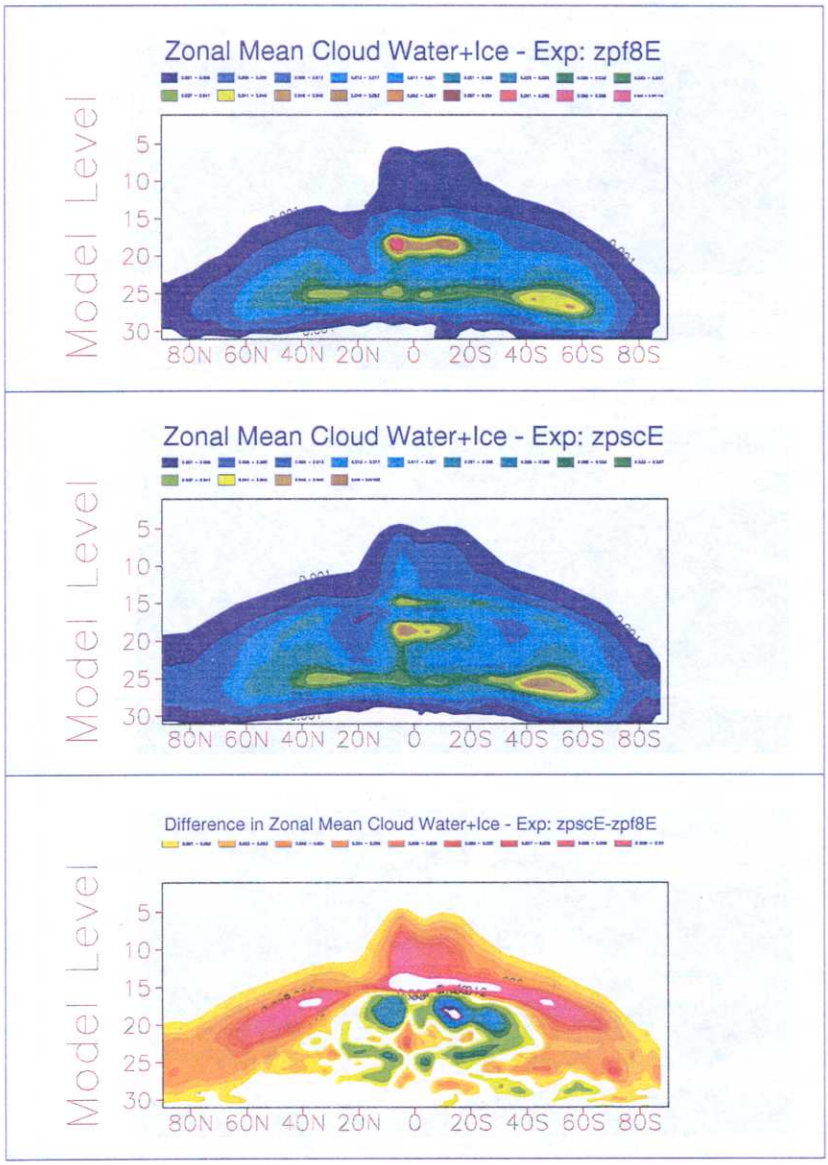

Figure 15: Zonal mean cloud water plus ice content (g/kg) for December/January/February 1987-88 from T63L31 model simulations : control simulation (upper panel), revised physical package (middle panel), differences (lower panel). Model results are an average over an ensemble of three simulations.

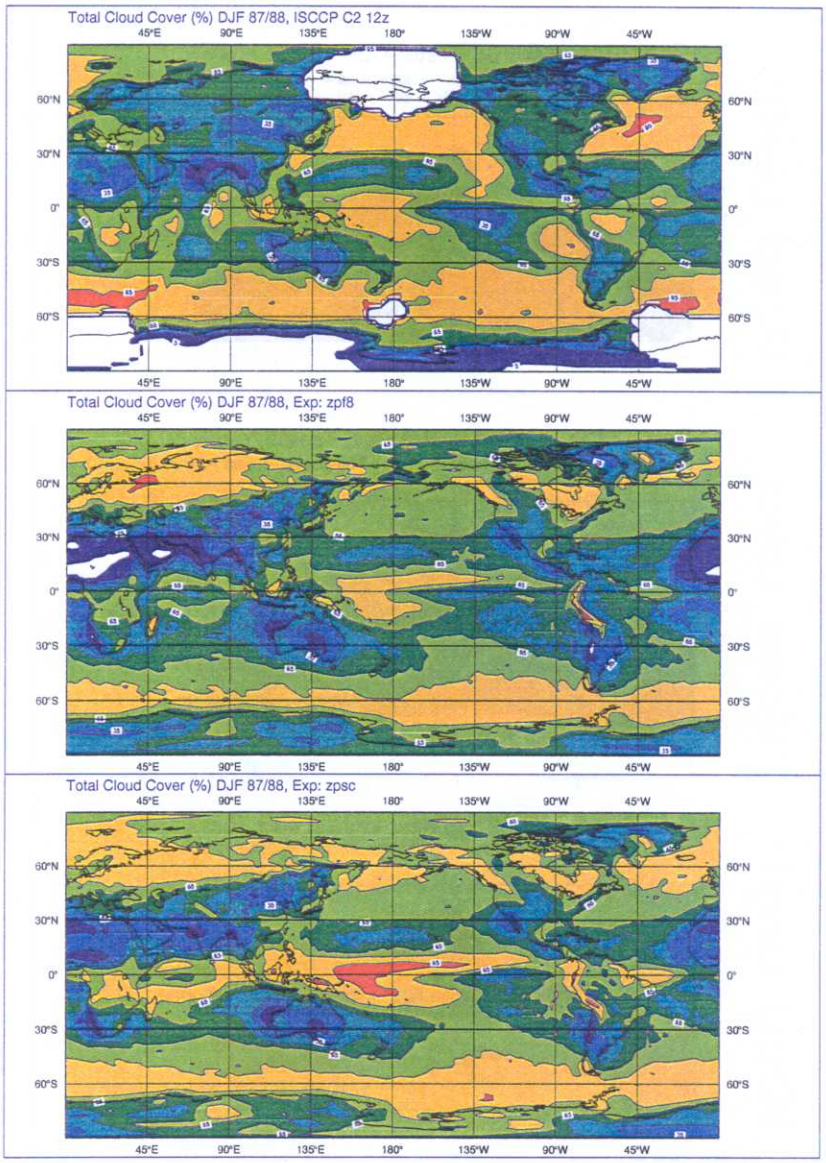

Figure 16: Total cloud cover (%) for December/January/February 1987-88 from T63L31 model simulations : ISCCP climatology (upper), control simulation (middle panel), revised physical package (lower panel). Model results are an average over an ensemble of three simulations. Contours at 5, 20, 35, 50, 65, 80 and 95 %.

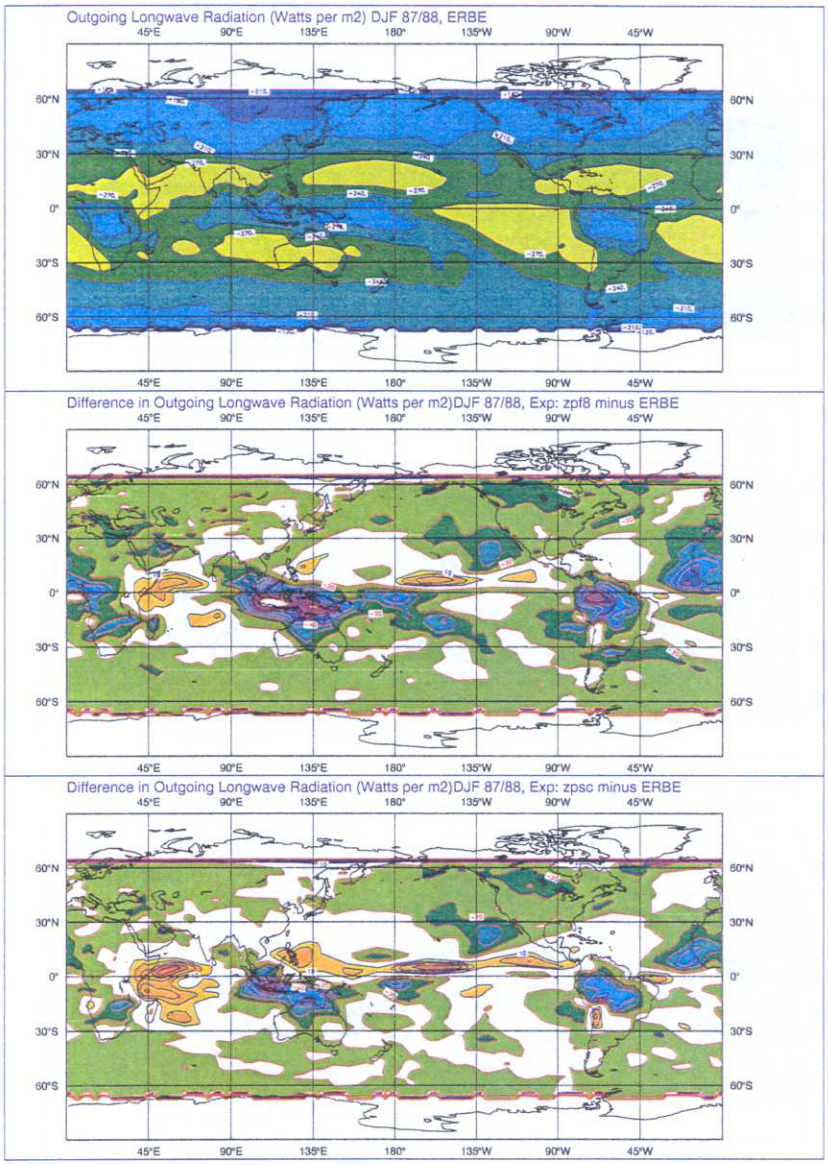

Figure 17: Outgoing Longwave Radiation (OLR - Wm^{-2}) for December/January/February 1987-88 from ERBE (upper panel) and difference of OLR from T63L31 simulations from ERBE : control simulation (middle panel) and revised physical package (lower panel). Model results are an average over an ensemble of three simulations. On OLR plot, contour interval is 30 Wm^{-2}. On plot differences, contour interval is 10 Wm^{-2}.

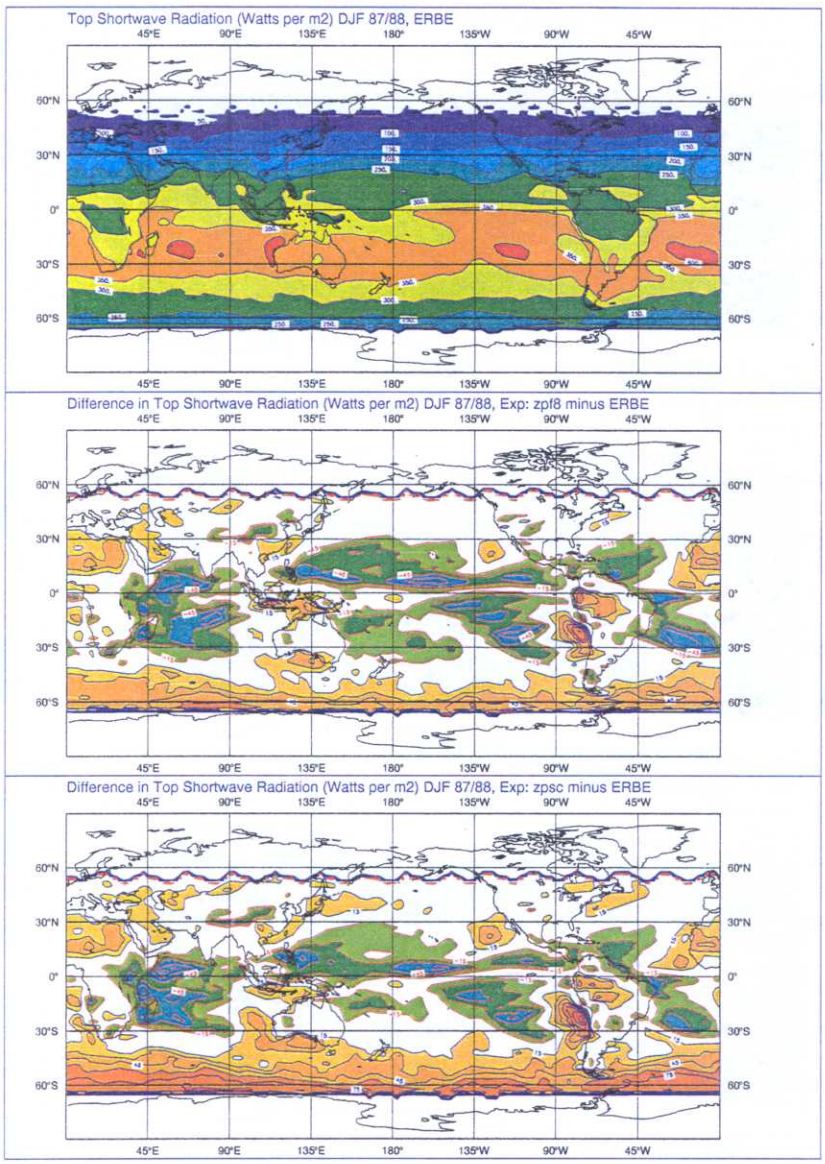

Figure 18: Top of atmosphere absorbed shorwave radiation (ASW - Wm^{-2}) for December/January/February 1987-88 from ERBE (upper panel) and difference of ASW from T63L31 simulations from ERBE : control simulation (middle panel) and revised physical package (lower panel). Model results are an average over an ensemble of three simulations. On ASW plot, contour interval is 50 Wm^{-2}. On plot differences, contour interval is 15 Wm^{-2}.

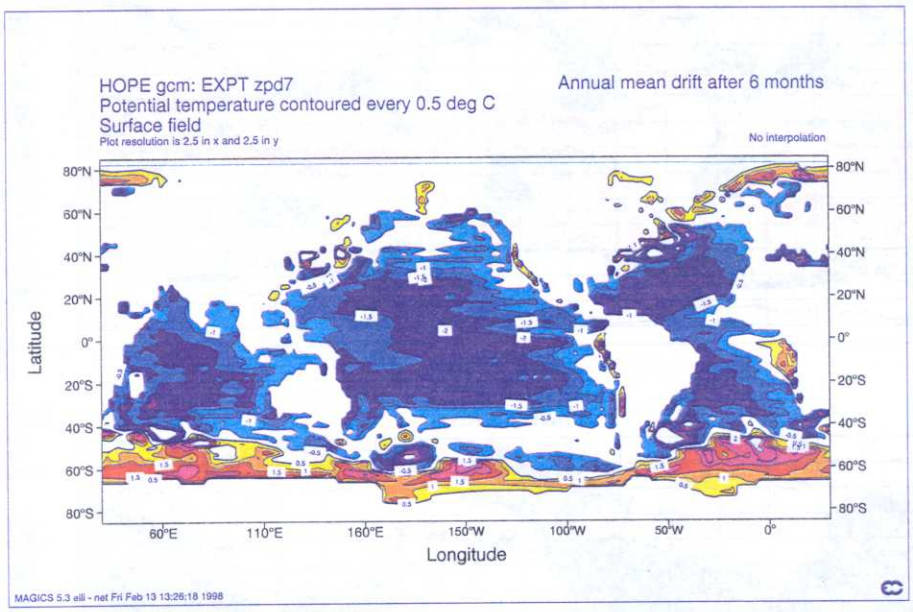

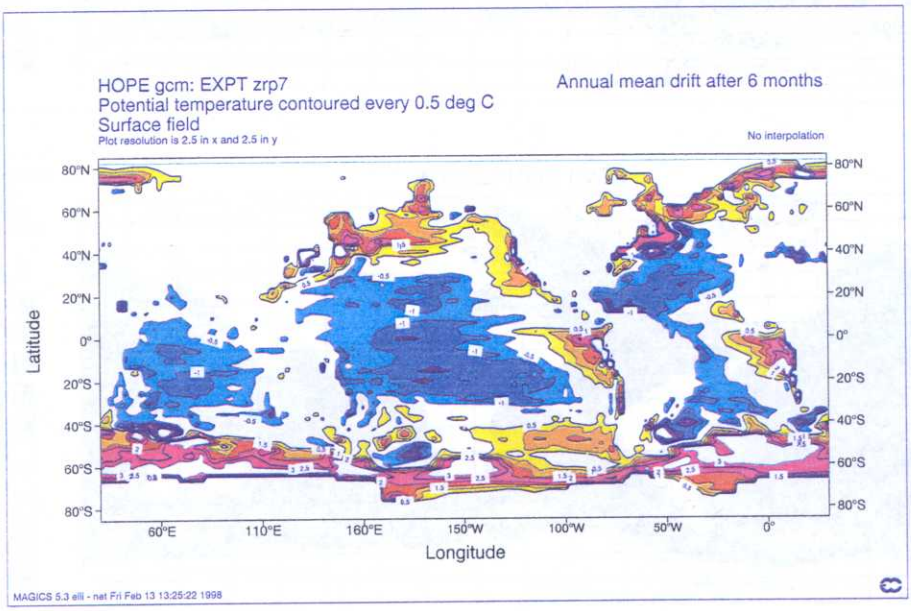

Figure 19: Drifts of sea surface temperature (as compared to obervations) for the last month of a six month forecast at T63 with the ECMWF coupled ocean-atmosphere model, averaged over an ensemble of 24 forecasts (starting for the 1st January, 1st April, 1st July and 1st October for years 1991 to 1996) using a control physical package (upper panel) and a revised physical package (lower panel).

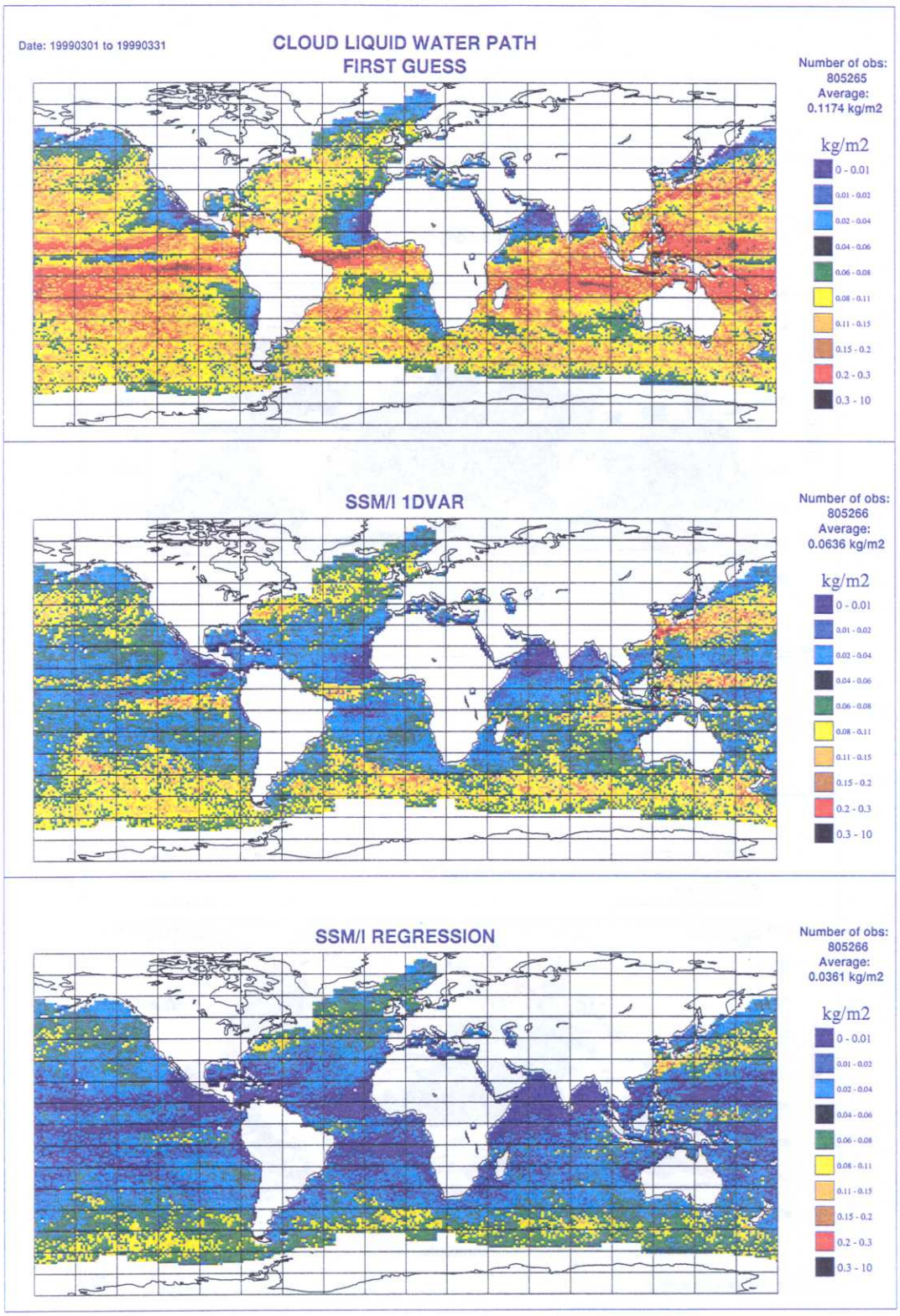

Figure 20: Monthly mean values of cloud liquid water path in kgm^{-2} (March 1999) as produced by the ECMWF model first-guess (6-h forecast), a 1D-Var retrieval (Phalippou, 1996) and a statistical algorithm (Weng and Grody, 1994).

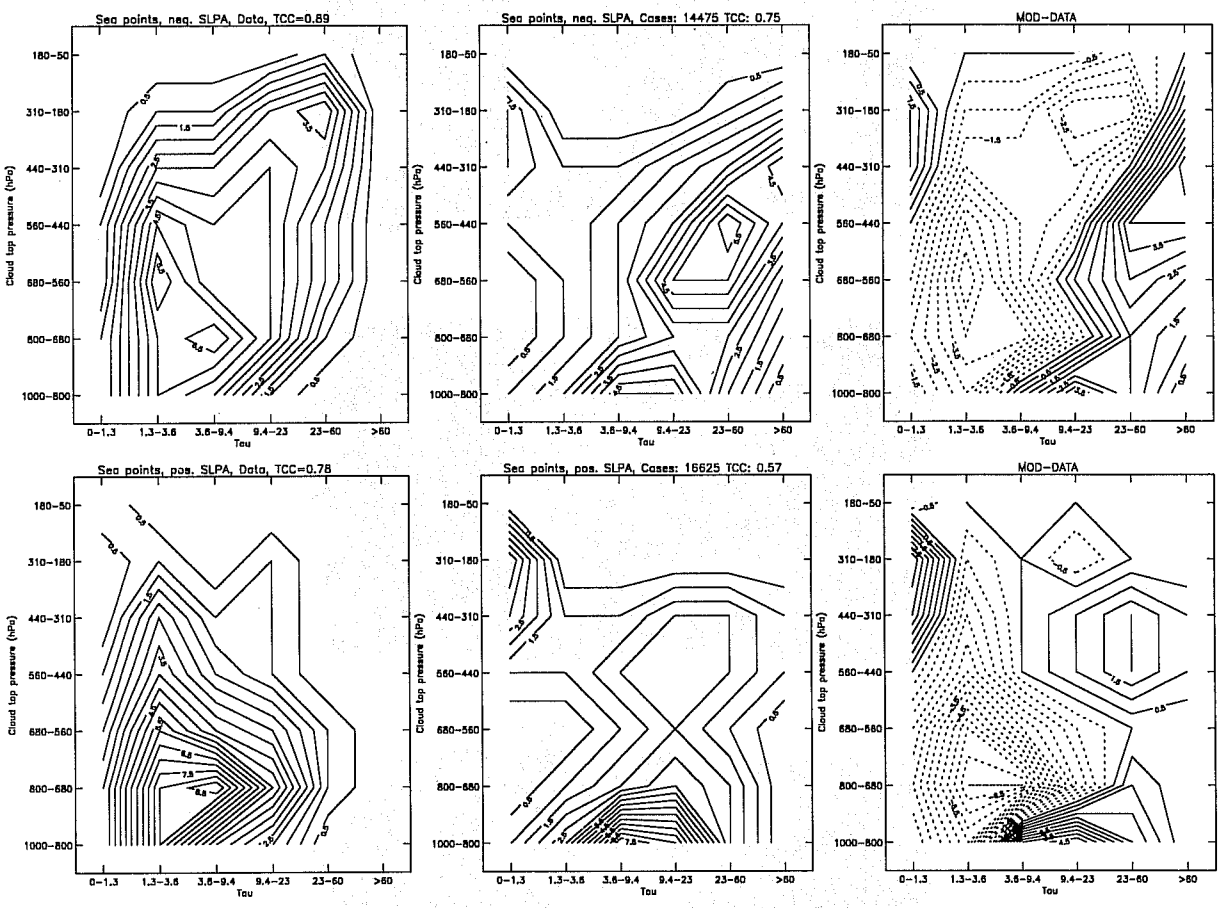

Figure 21: Distribution of cloud top pressure against cloud optical thickness for the ocean areas of 30°N to 60°N in the month of April 1992. The data is stratified into local negative sea level pressure anomalies of more than -5 hPa (top panels) and positive sea level pressure anomalies of more than 5 hPa (bottom panels). Distributions are derived from ISCCP D1 data (left), and ECMWF T106L31 12 and 24 hour forecasts (middle). The right panels show the difference between model and data.

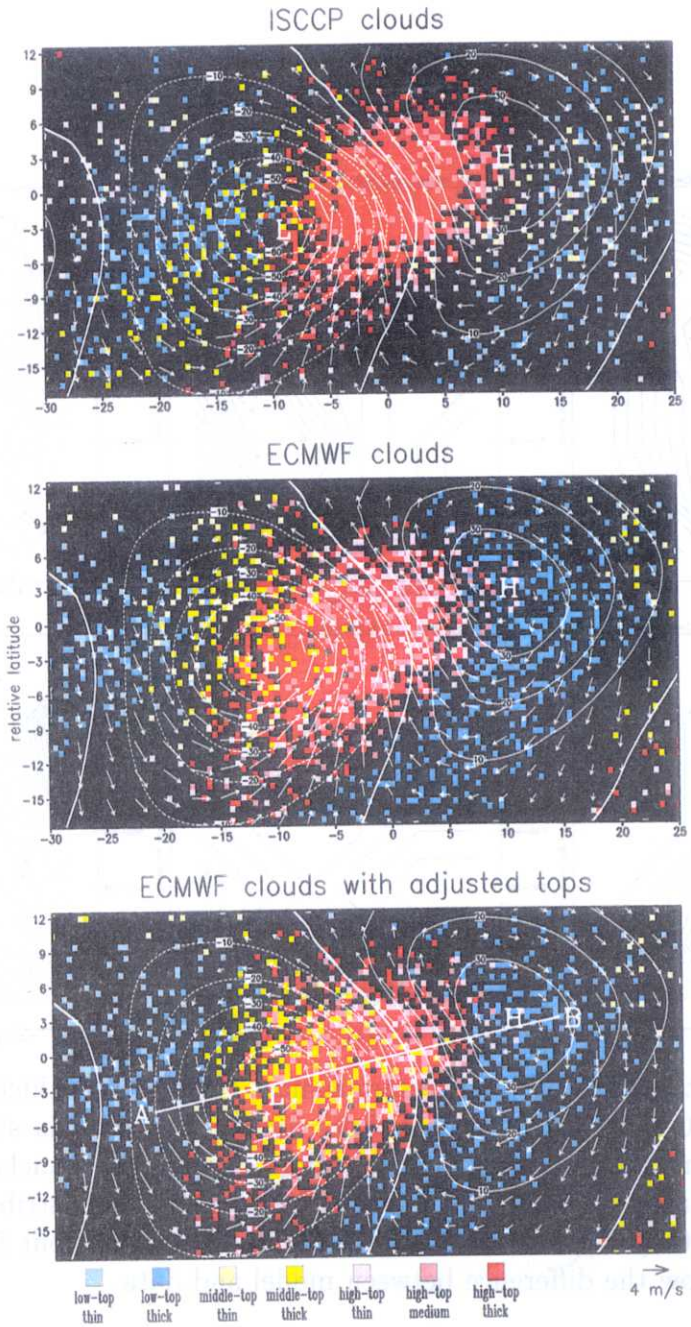

Figure 22: Cloud distribution in a composite cyclone derived from ISCCP C1 data (top), 12 to 36 hour forecasts of the ECMWF T106L31 model using physical cloud top (middle), and from the same forecasts using "radiative" cloud top (bottom).

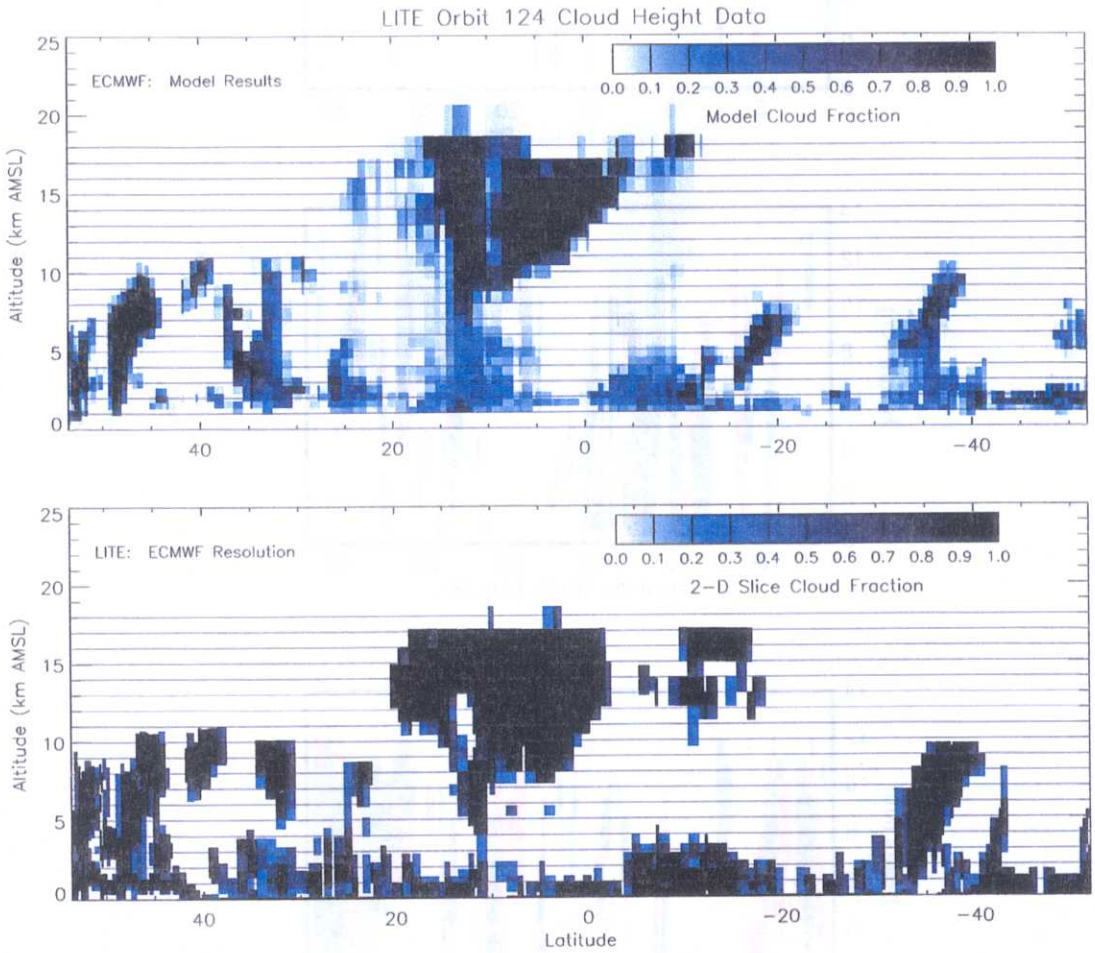

Figure 23: Cloud fraction comparison between ECWMF short-range forecast and LITE orbit 124 (September 16, 1994, 14:25-15:00 UTC, spanning the Western Pacific warm pool).

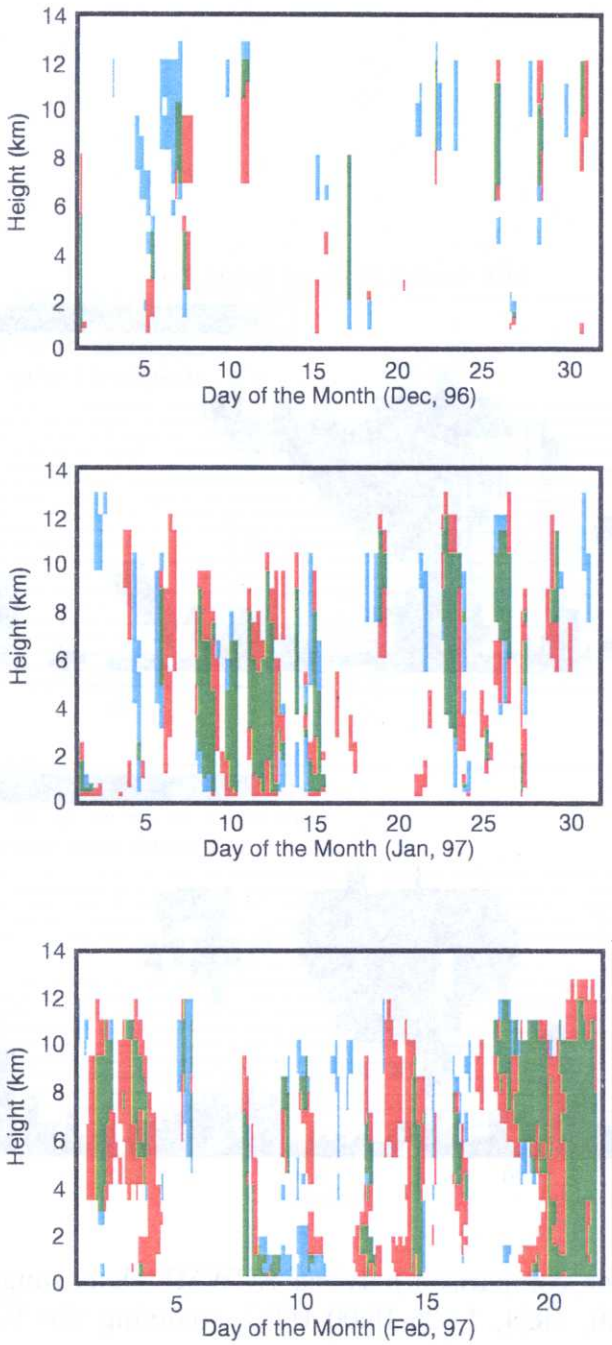

Figure 24: Day to day comparison of the ECMWF model output and a cloud radar-derived hydrometeor mask. The color code is as follows: green indicates both model and radar hydrometeor occurences, red indicates model occurence when no radar occurence was observed and blue indicates radar occurence when no model occurence was predicted. The radar was not operational from 11-15 Dec and 6-7 Jan. Data were only available for 00 UTC-12UTC from 15-31 Dec.

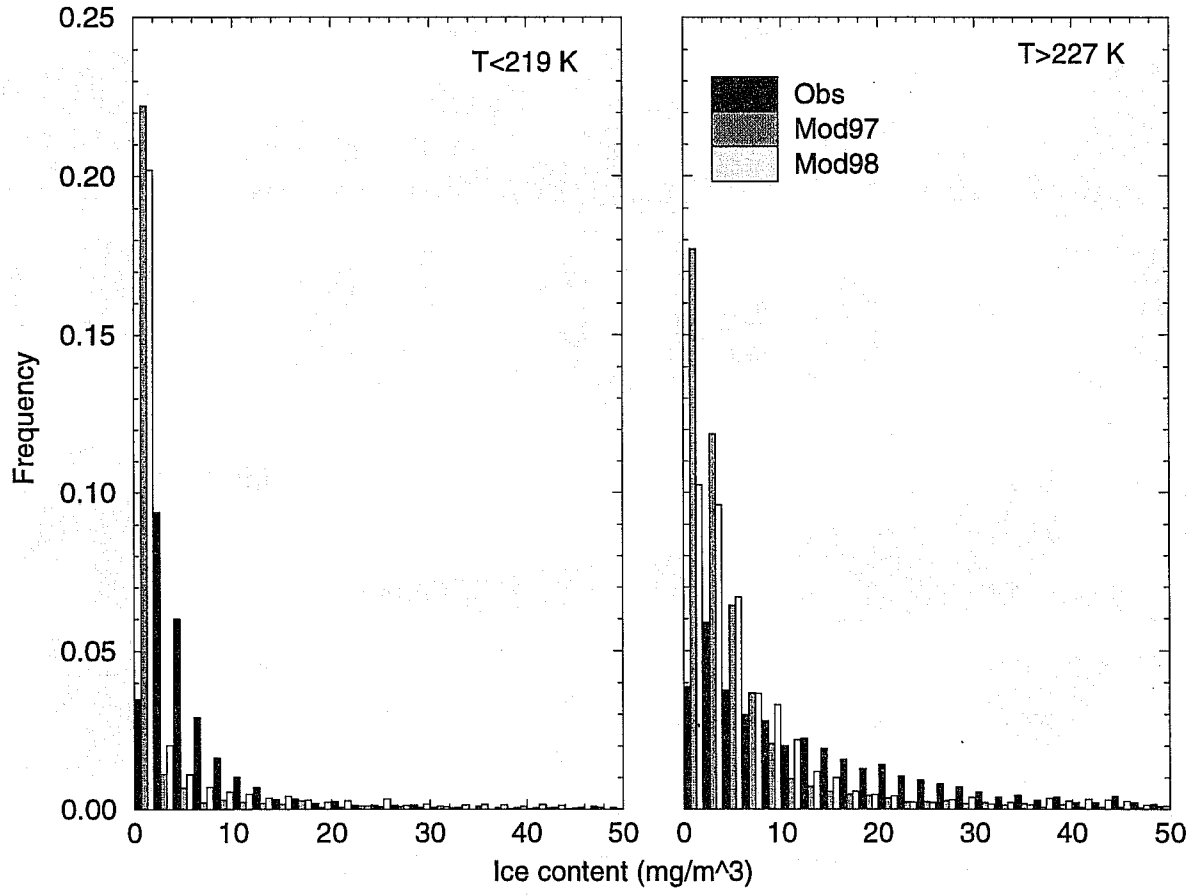

Figure 25: Frequency distributions of cloud ice in isolated cirrus (see Mace et al. 1997 for definition) over the ARM SGP site for two different temperature ranges. Shown are values derived from a combination of radar reflectivity and infrared interferometer data and from two versions of the ECMWF model.

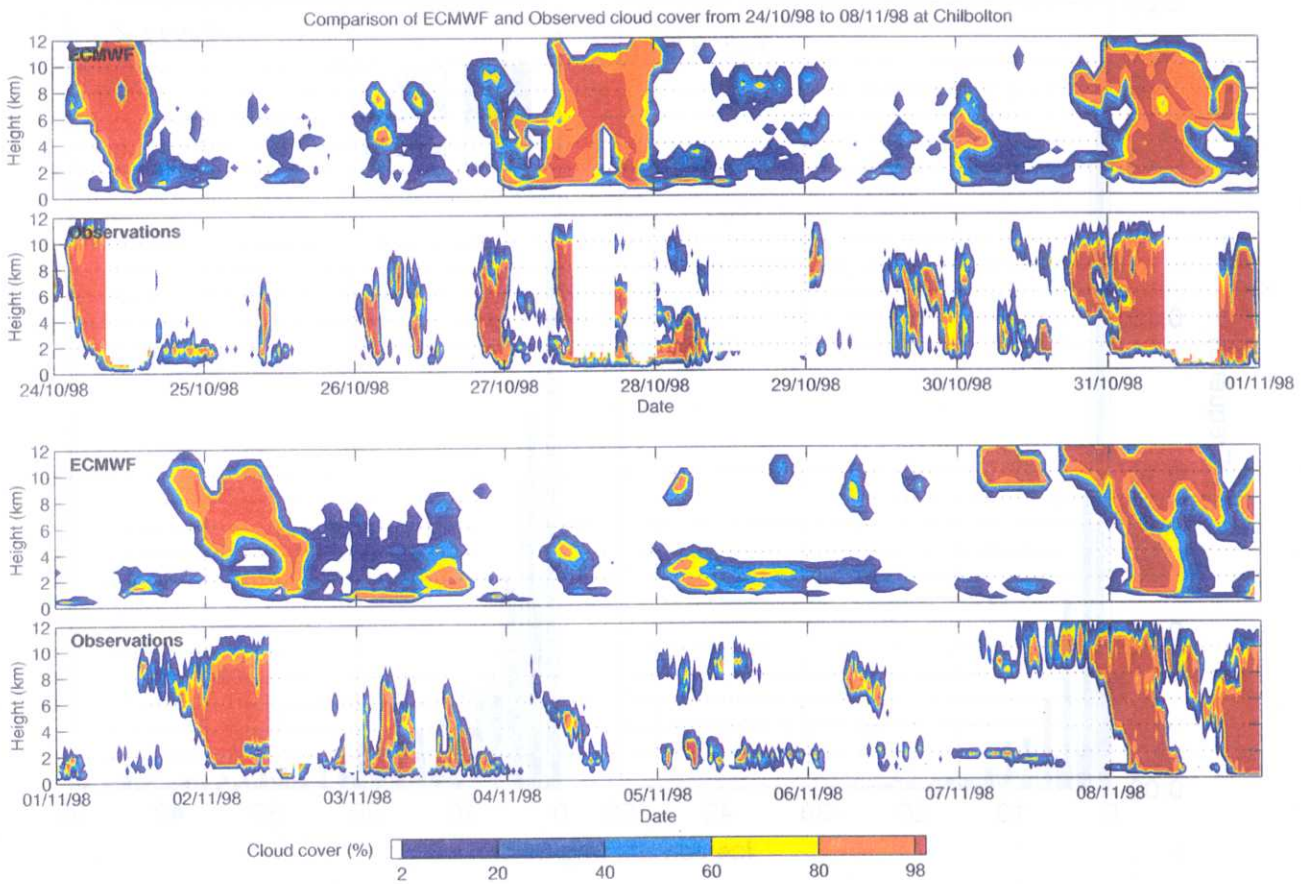

Figure 26: Comparison of ECMWF cloudiness profiles with radar estimates during CLARE experiment (25/10-08/11/98).

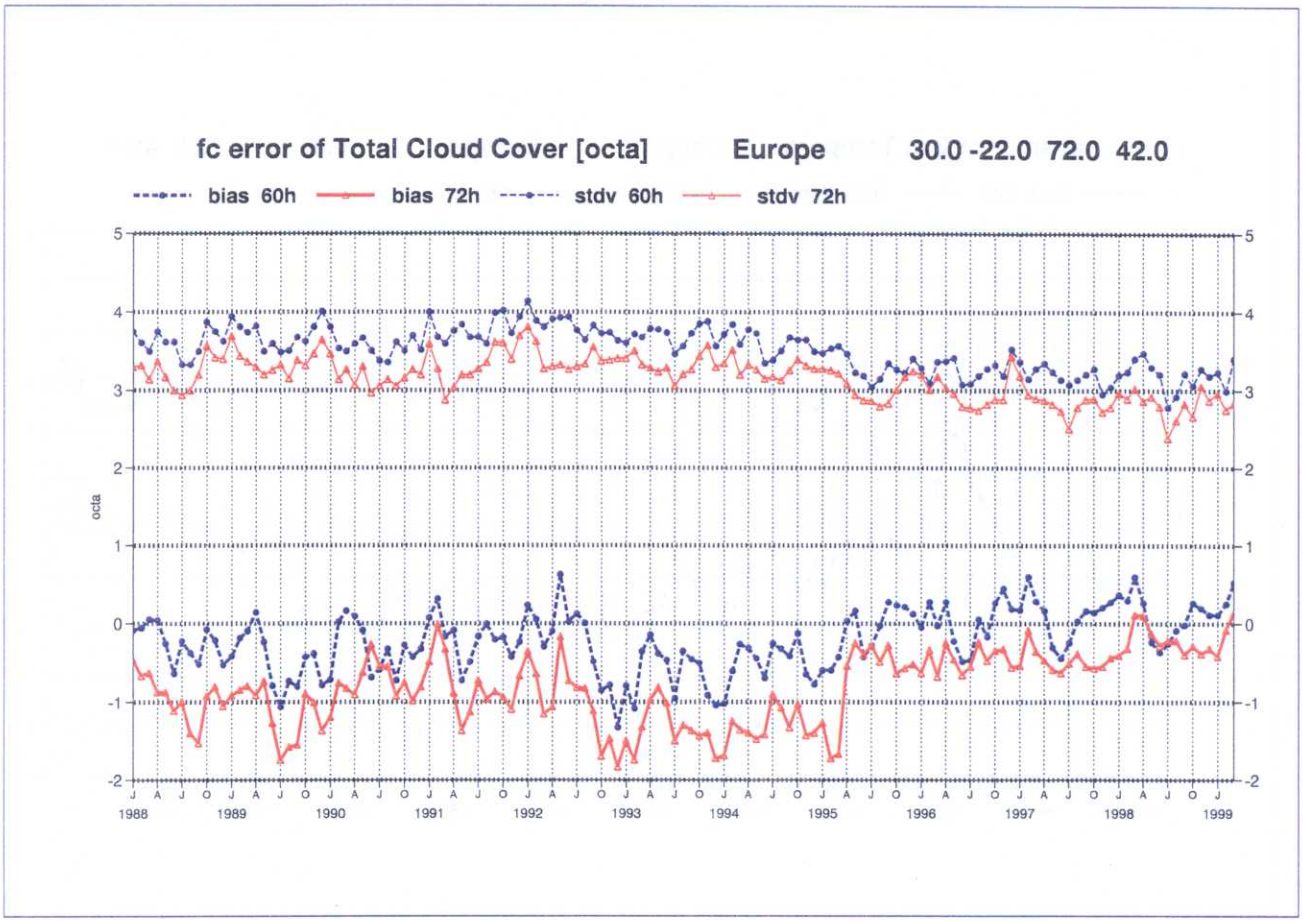

Figure 27: Monthly comparison of 60-hour and 72-hour forecasts of cloud cover from the ECMWF operational model with surface observations over Europe. The top curves represent the standard deviation, the bottom curves show the bias.

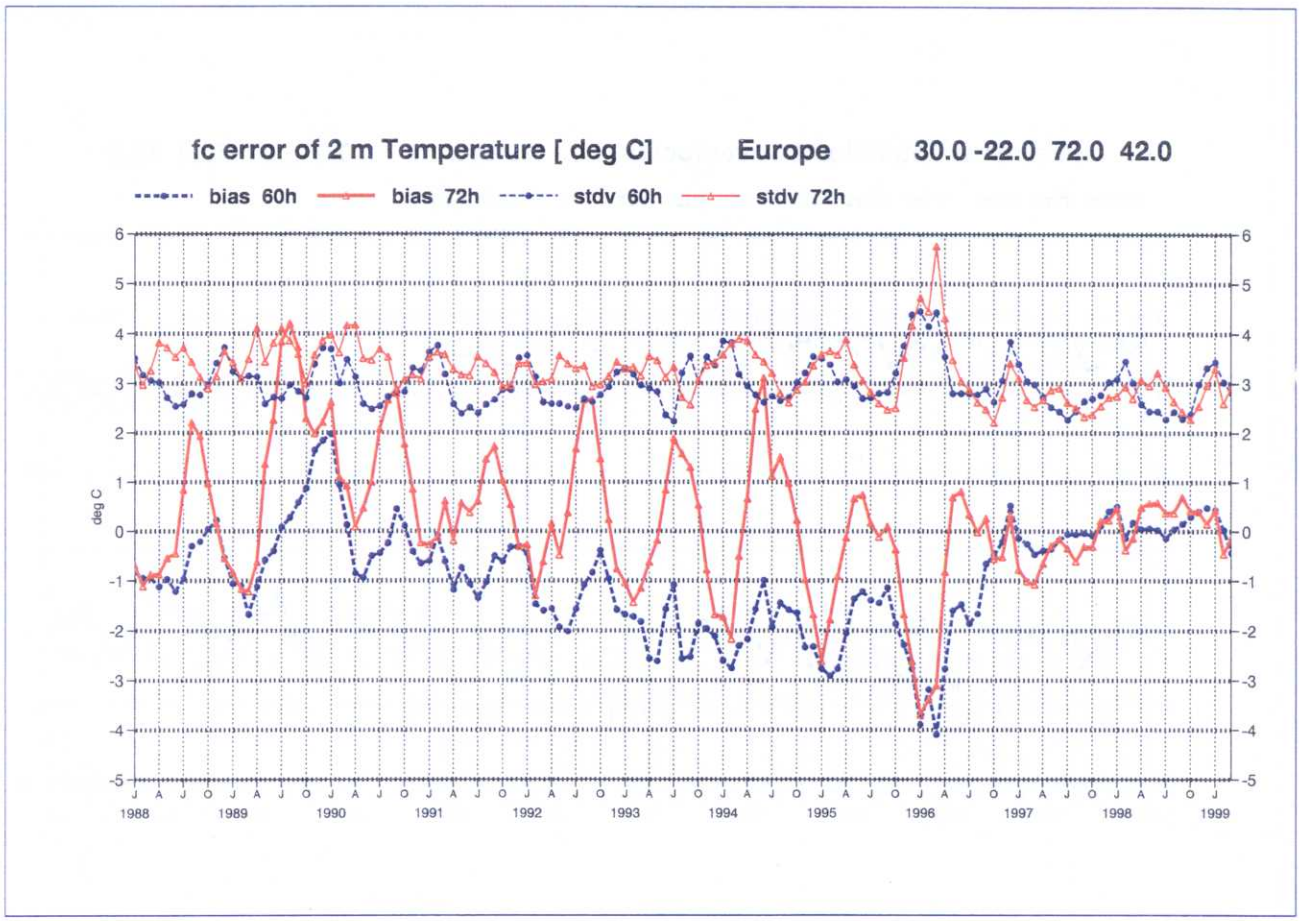

Figure 28: Monthly comparison of 60-hour and 72-hour forecasts of 2m temperature from the ECMWF operational model with surface observations over Europe. The top curves represent the standard deviation, the bottom curves show the bias.

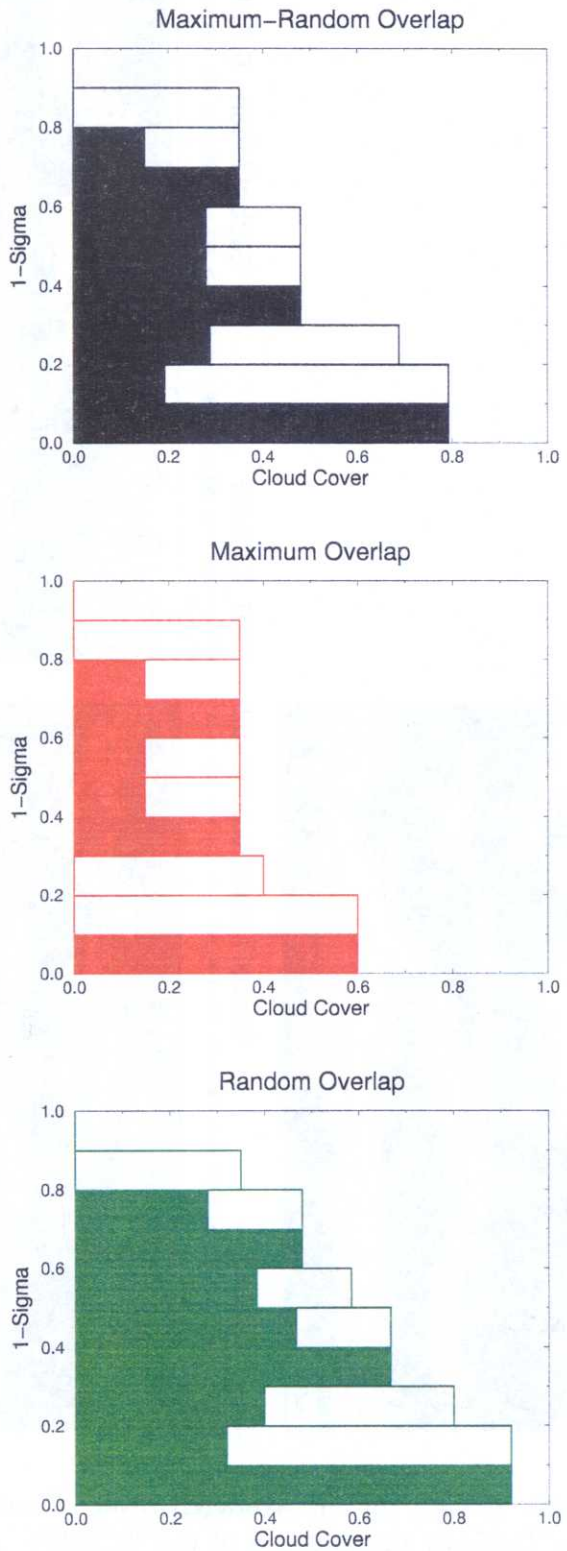

Figure 29: Schematics of various cloud overlap assumptions. The clouds are shown as white rectangular blocks filling the vertical extent of a layer. The total cloud fraction from the top of the atmosphere down to a given level is shown by the line on the right delineating the clouds and the shaded area below

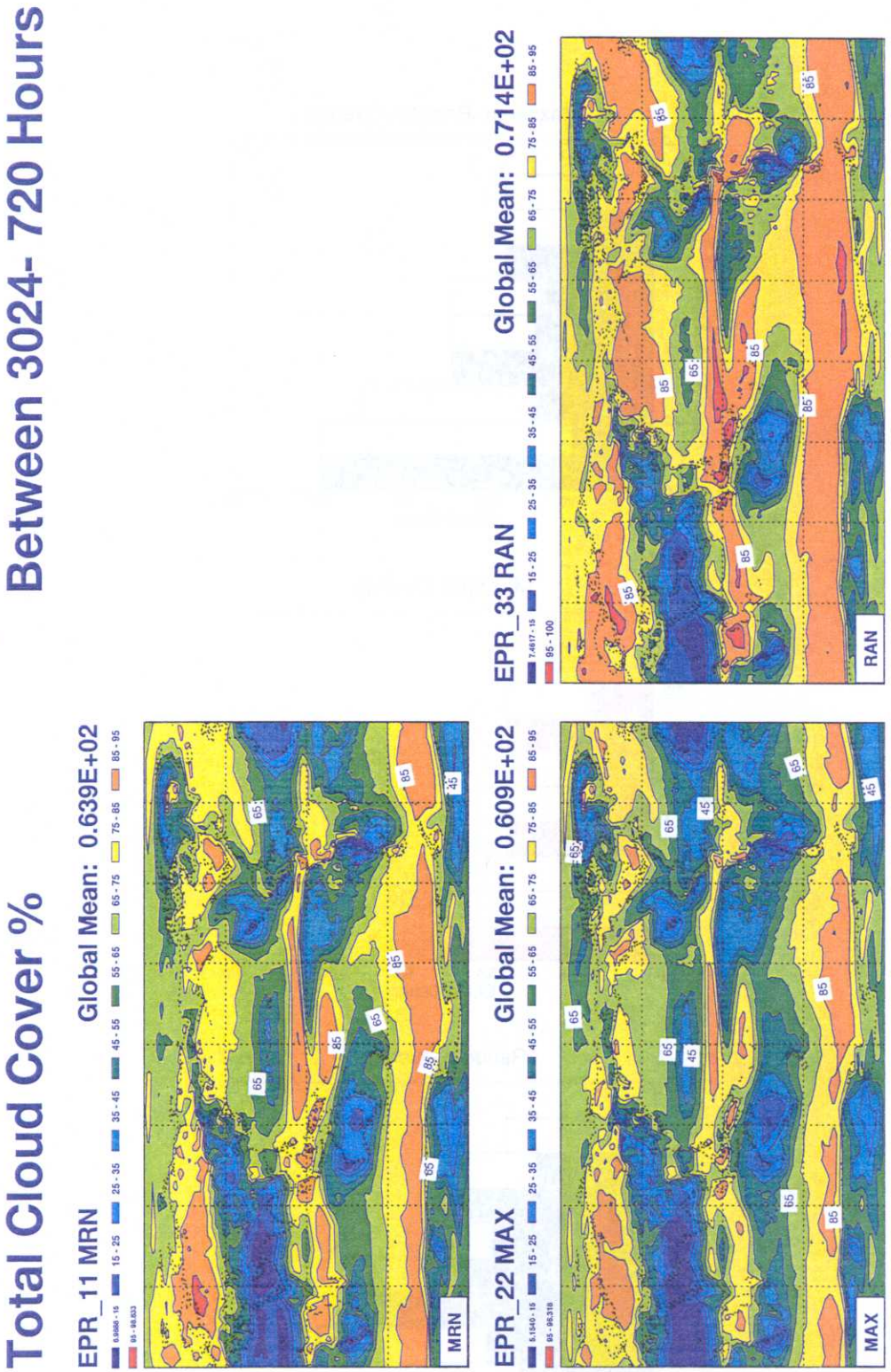

Figure 30: Total cloudiness (TCC) in % averaged over three months (December/January/February) from T_L95L31 integrations of the ECMWF model of EPR simulations with maximum-random (MRN), maximum (MAX) and random (RAN) cloud overlap assumptions.

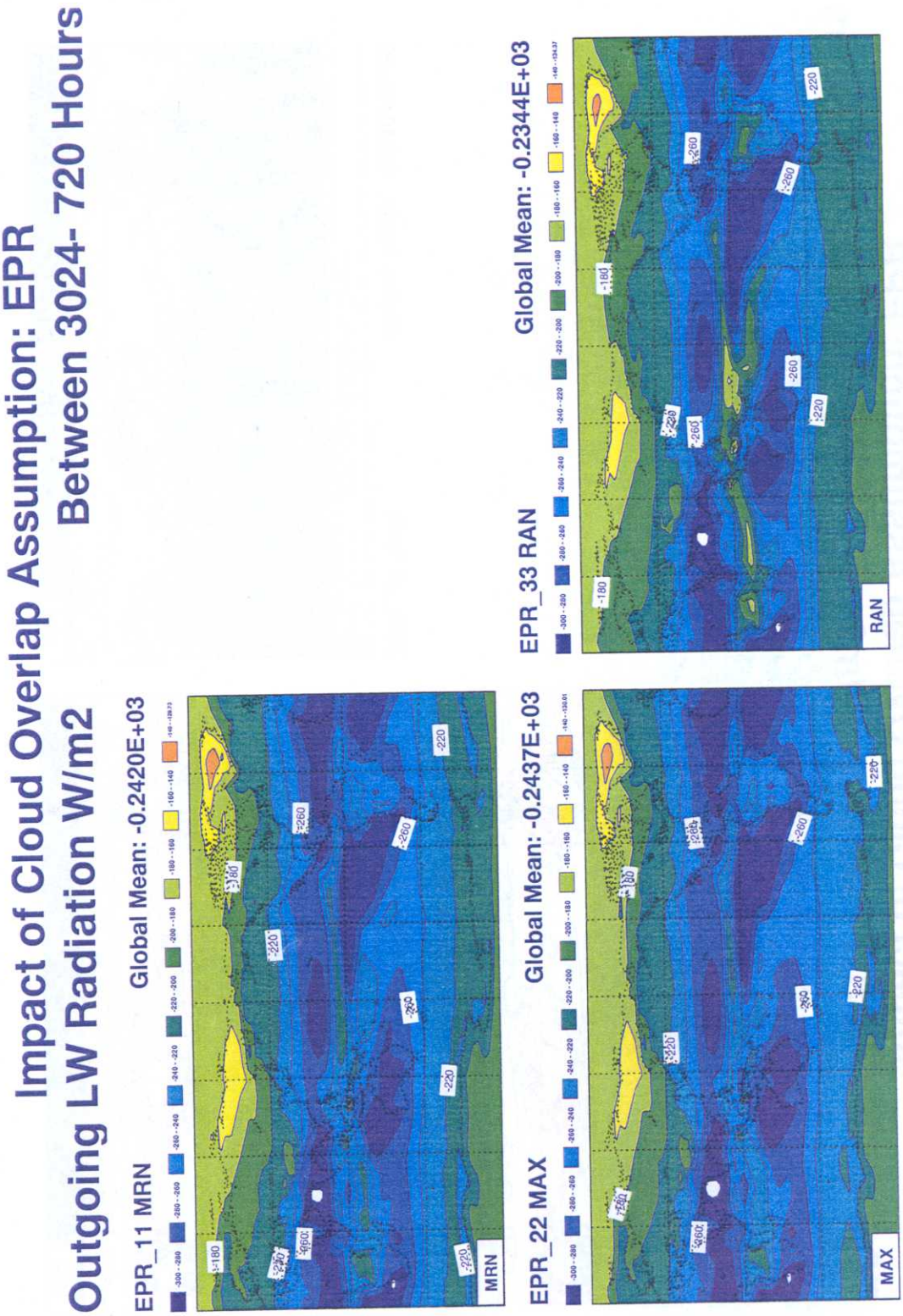

Figure 31: Outgoing longwave radiation (OLR) at the top of the atmosphere in Wm^{-2} averaged over three months (December/January/February) from T_L95L31 integrations of the ECMWF model of EPR simulations with maximum-random (MRN), maximum (MAX) and random (RAN) cloud overlap assumptions.

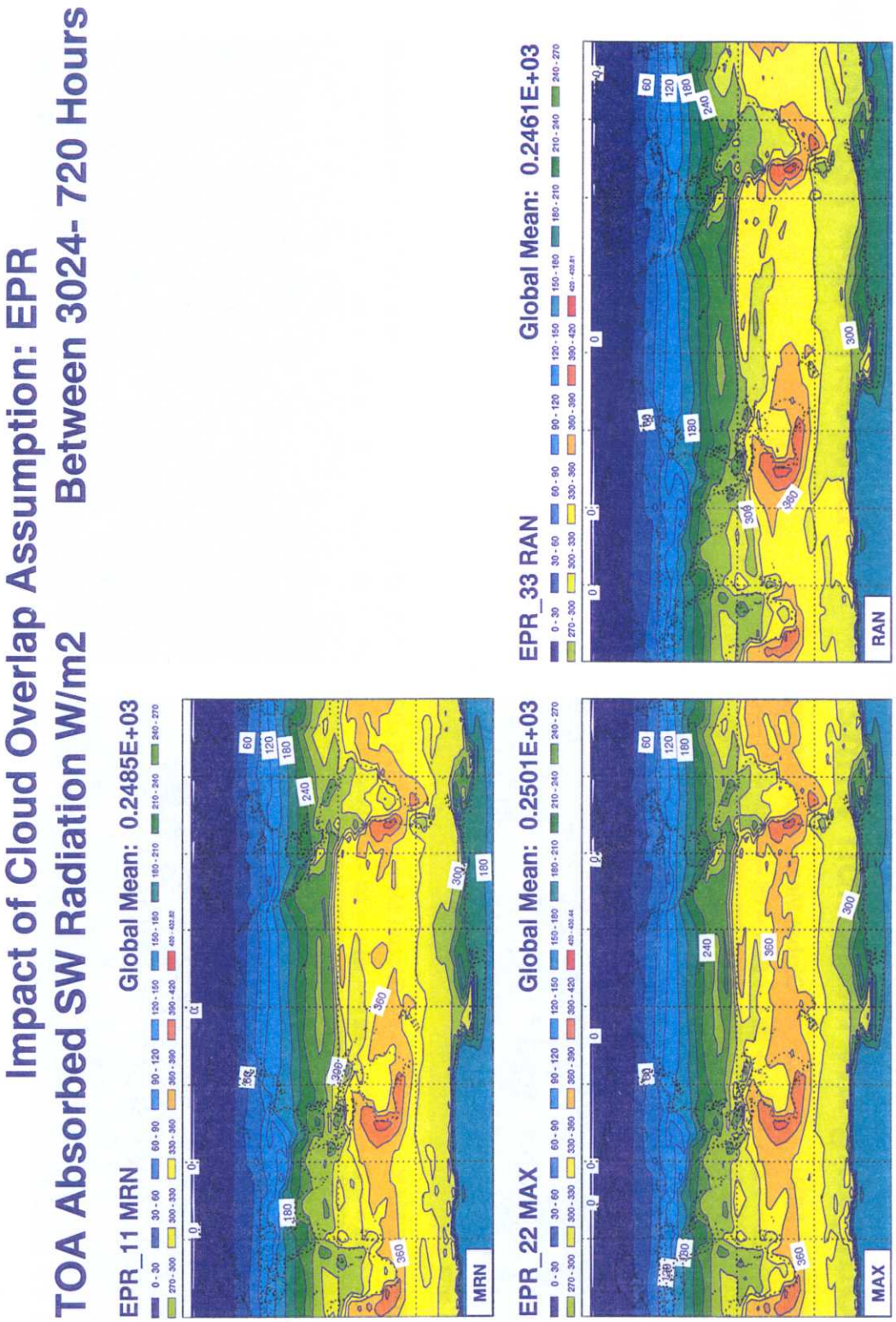

Figure 32: Absorbed shortwave radiation (ASW) at the top of the atmosphere in Wm^{-2} averaged over three months (December/January/February) from T_L95L31 integrations of the ECMWF model of EPR simulations with maximum-random (MRN), maximum (MAX) and random (RAN) cloud overlap assumptions.

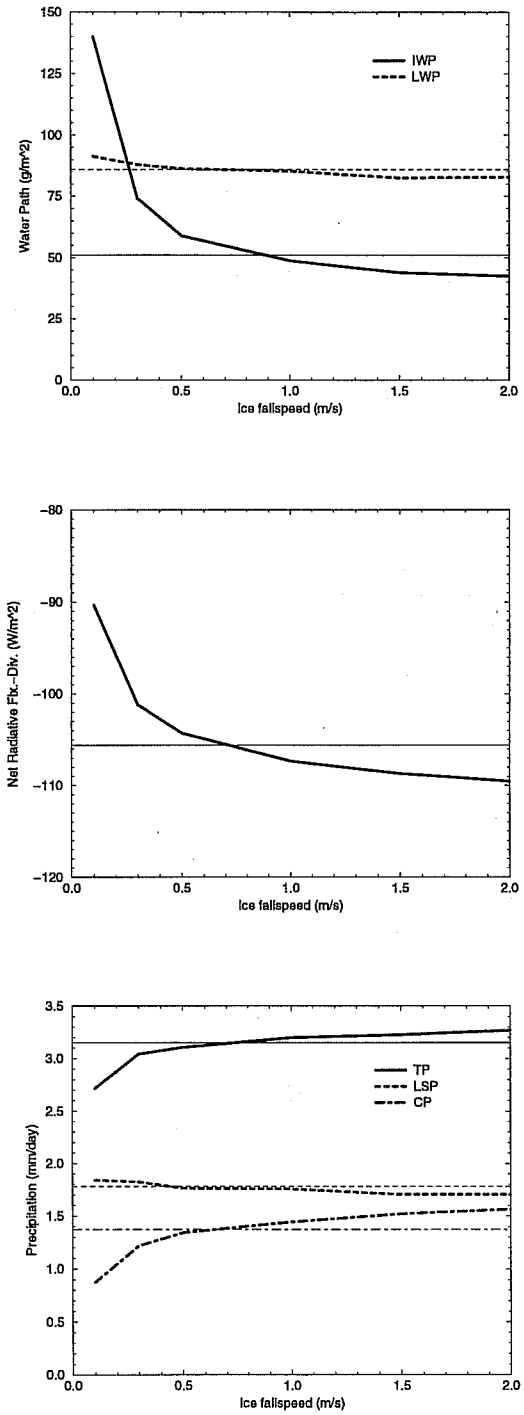

Figure 33: Three-month averages (JJA87) of the global means of IWP/LWP (a), radiative flux divergence (b), and precipitation (c) in a T63L31 version of the ECMWF model as a function of the assumed fall speed for ice. CONTROL model results are shown as horizontal lines. Precipitation is shown as total precipitation (TP), and split into convective (CP) and large-scale (LSP) precipitation.

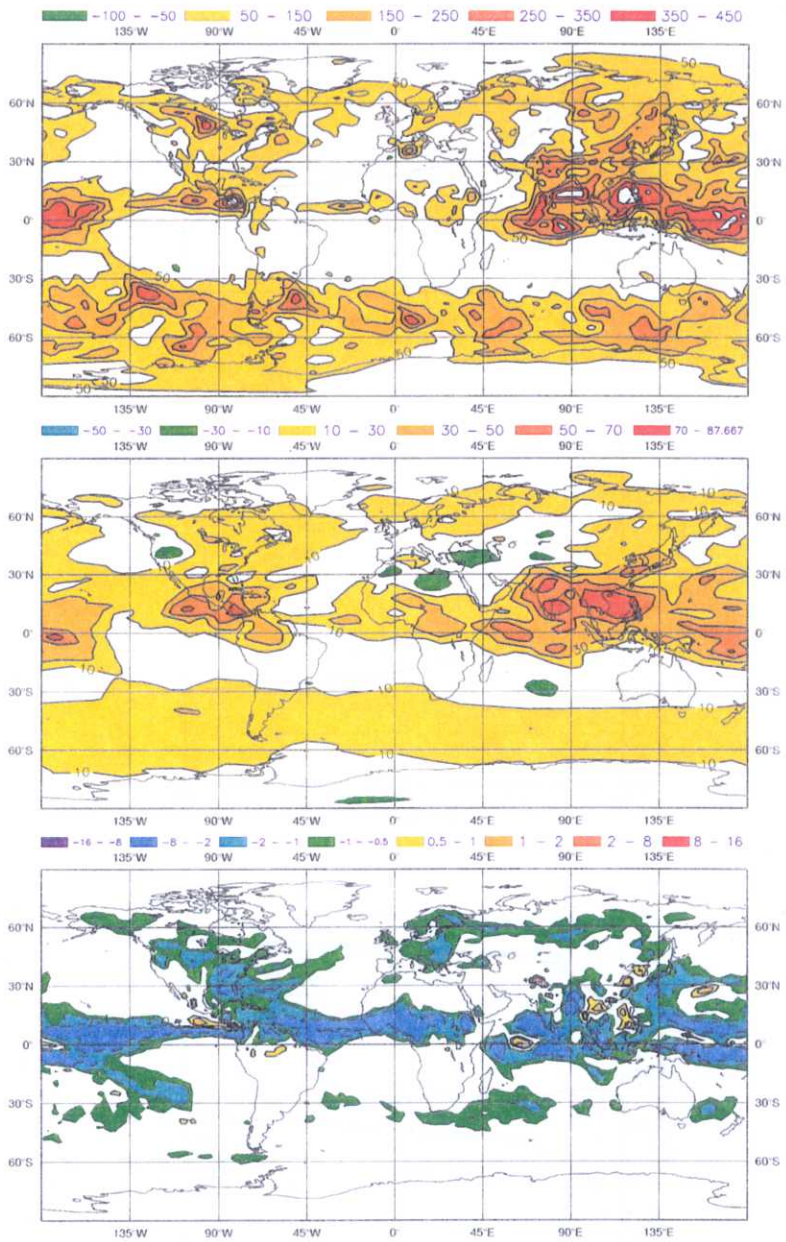

Figure 34: JJA 87 differences between the experiment assuming $w_{ice} = 0.1ms^{-1}$ and the CONTROL simulation for IWP (top), OLR (middle) and convective precipitation (bottom). Units are gm^{-2} for IWP, Wm^{-2} for OLR and mmd^{-1} for precipitation.

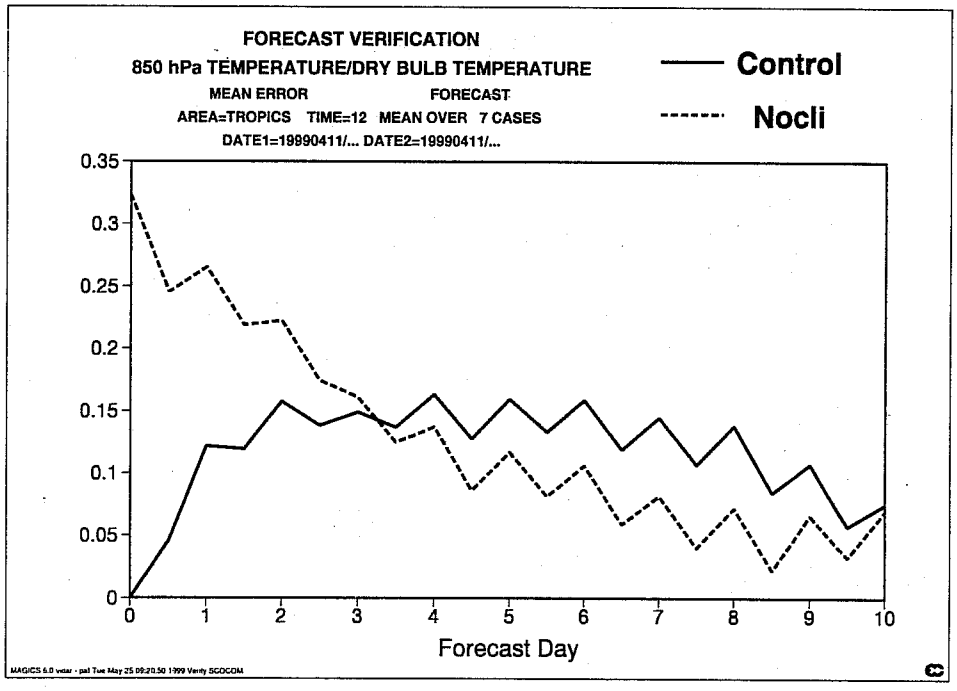

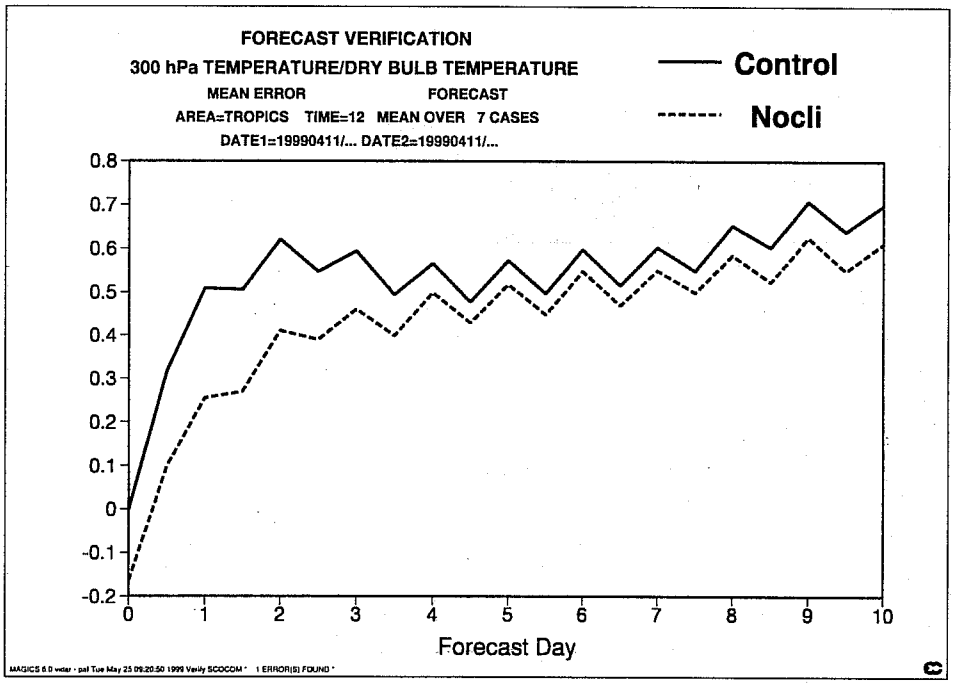

Figure 35: 10-day forecasts of mean temperature errors in the tropics at 850 hPa (upper panel) and 300 hPa (lower panel) for an average of 7 *Control* experiments and experiments with zero initial clouds (*Nocli*).

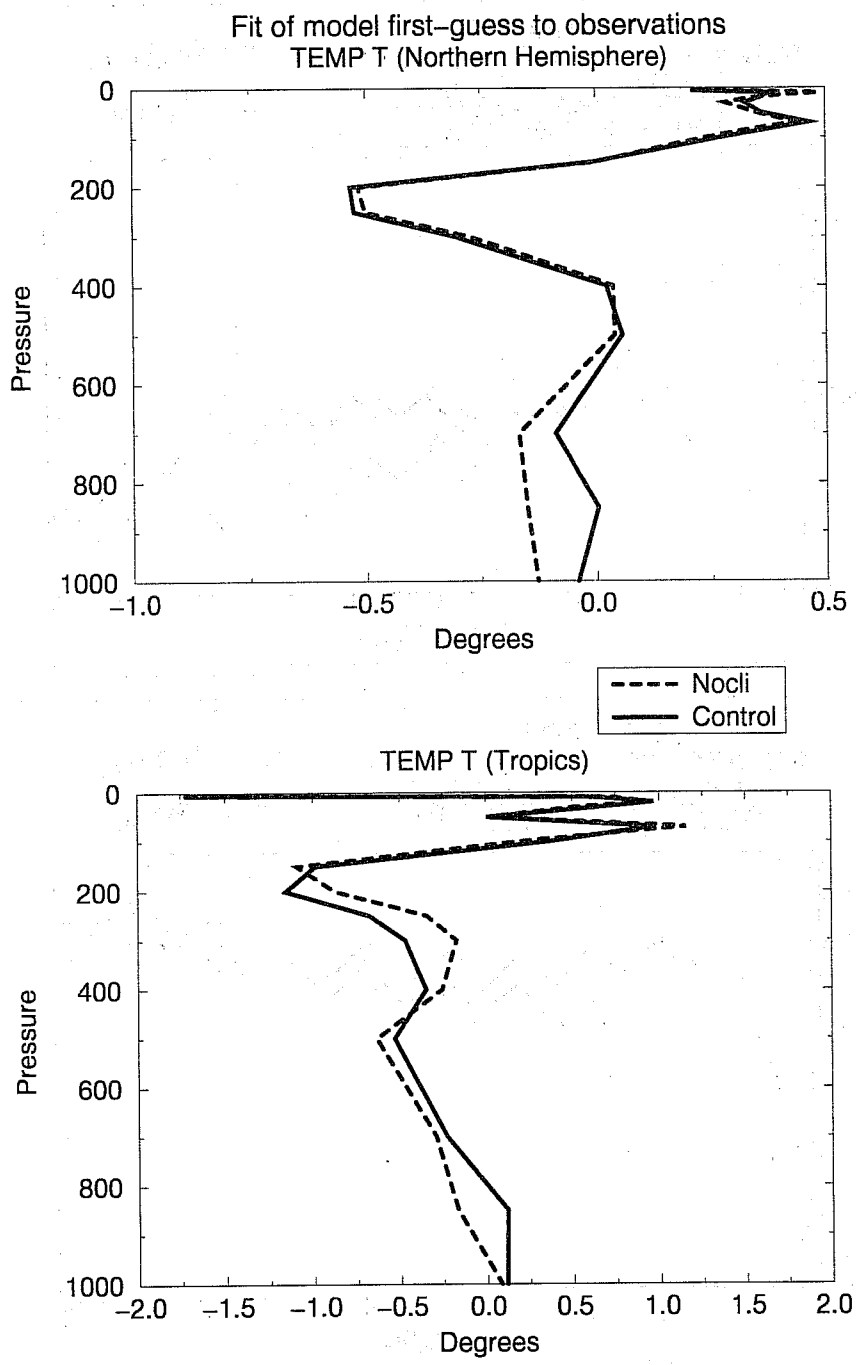

Figure 36: Mean bias of the model first-guess to radiosonde temperature over the Northern Hemisphere and the Tropics averaged over 7 days (11/04/99 - 17/04/99). The solid lines represent the fit for a *Control* 4D-Var assimilation and the dashed fit for a 4D-Var assimilation with zero initial clouds (*Nocli*).

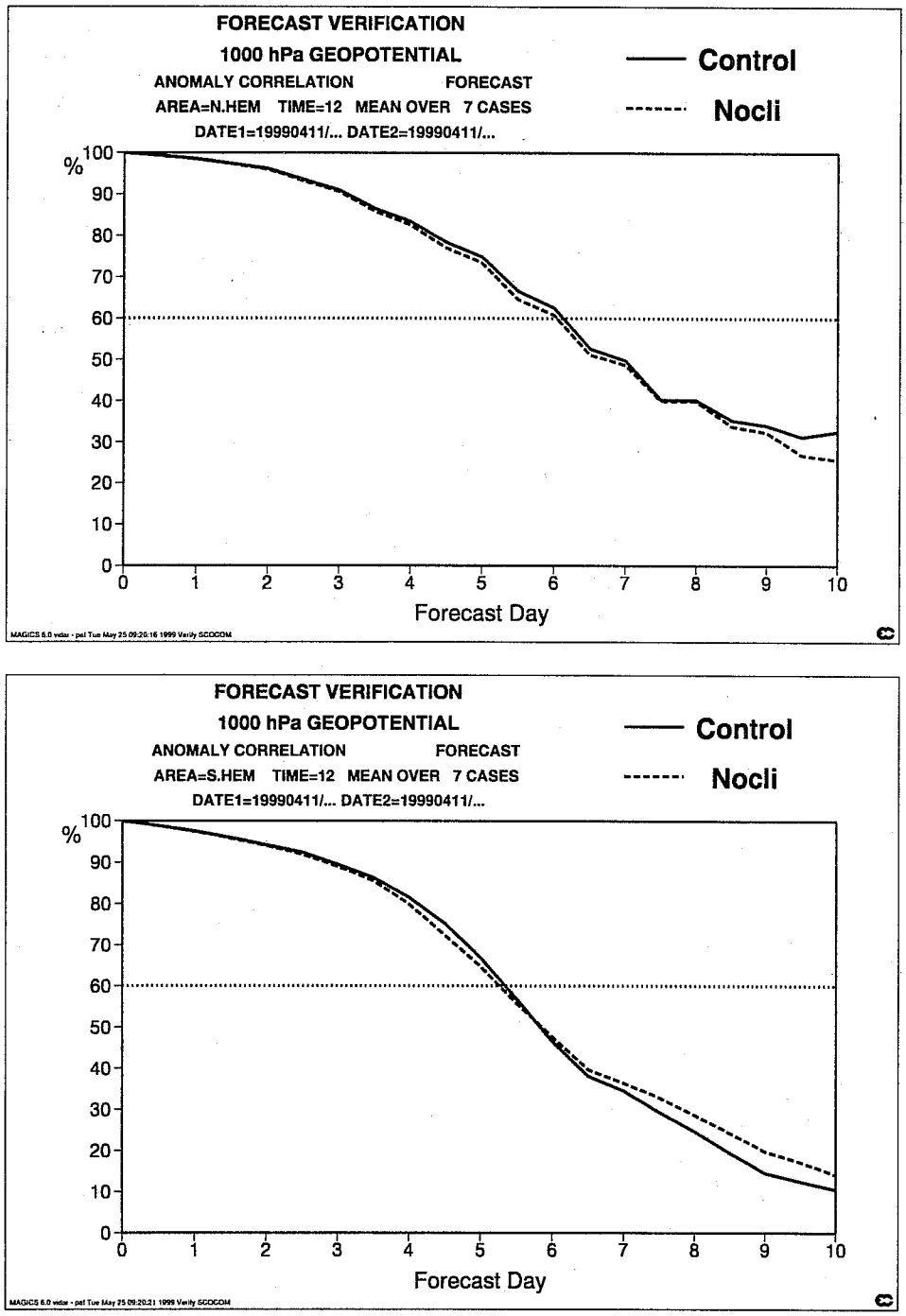

Figure 37: 10-day forecasts of anomaly correlation of the geopotential at 1000 hPa over the Northern (upper panel) and Southern (lower panel) Hemispheres for an average of 7 *Control* experiments and experiments with zero initial clouds (*Nocli*).